University of Stavanger

Faculty of Science and Technology

MASTER'S THESIS

Study program/ Specialization: **Marine- and Offshore Technology**	Autumn Semester, 2020 **Open/~~Restricted access~~**
Author: **Olha Ivanova**	 (Signature of Author)
Faculty supervisor: **Prof. Yihan Xing**	
Title of thesis: **Optimization of the Local Failure Design of Carbon-Fibre Epoxy Composite Curved Plates**	
Credits (ECTS): **30**	
Key words: Composite material, Carbon-fibre Curved plates, Design Variables, Optimization, ANSYS, Correlation and Determination matrix, Response surface, Failure Criteria analysis	Pages: 107 **Stavanger,** **15th January 2021**

Abstract

This thesis presents the optimization of the local failure design of Carbon-Fiber Epoxy Composite used in the manufacturing of the curved plates. As relatively new and reliable material carbon fiber can be used in different industries and fields, for instance oil and gas industry, with aim to optimize the design of the manufactured models and reduce the possibility of failure to occur in curved plate model structures.

Using ANSYS Workbench 2020, a case study of local failure check is investigated. Thus, the thesis meets its main objectives as the simulation of the local failure in curved plate components helps to indicate main parameters which affects the model most and find parts of the model which are influenced by loads with the high risk of failure. This can affect the process of the manufacturing of structure main parts. The dissertation gives the explanation about the correlation and determination study as well as the response surface methodology in order to optimize the local failure design and further design of the curved plate components. The curved plate is subjected to high pressure and force. The engineering properties of used material and models, geometries, boundary conditions, loads and meshes are the input parameters and carried out using Static Structural tool and ACP process in ANSYS software. Output parameters are optimized values of failure criteria. Studies of correlation and determination matrixes are investigated to find parameters which affect the results. The Spearman correlation with different sample sizes is used to define and check the design parameters with the highest correlation and determination coefficients. These parameters are used for further study of the response surface. The result of correlation reflects that thickness of the model and applied pressure are strongly correlated with the predefined failure criteria. Thesis indicates the main design parameters which affect the curved plate and can lead it to the failure with critical values of the failure criteria. The model gives the area where the failure can be observed. With identifying the impact and main correlations, the critical step in design optimization is done. As the next step of the further design optimization process, response surface is investigated.

The response surface methodology provides more accurate results of the failure criteria and gives precise information about the outcome parameters. The quality of the response surface

varies with different response surface types and size of the response surface itself. Comparison studies of different response surface types results are investigated in this dissertation. The conclusion provides information about response surface results with small failure criteria values and optimal design parameters values. This provides the safe design of the curved plate model with the stiffeners.

Key words:

Curved plates, carbon-fiber, composite material, response surface, correlation and determination matrix, failure criteria analysis.

Acknowledgement

I would like to express my sincere gratitude to my supervisor, Prof. Yihan Xing, University of Stavanger. I really appreciate his suggestion and idea of my thesis topic and I would like to thank professor for his support and motivation during the time of my work on thesis. His guidance in software tools, patience in assisting and valuable advices contributed much to my thesis improvements.

Furthermore, I am thankful to all the faculty members and my fellow students for sharing innovative ideas and motivation which helped me to finish my research successfully. Their suggestions and opinions on my work helped to improve my thesis in very efficient way.

Stavanger, January 2021

Olha Ivanova

Table of Contents

List of Figures

List of Tables

Nomenclature

$\sigma_1, \sigma_2, \sigma_3$ – maximum material normal stresses in the lamina, principal stresses in x, y and z directions

σ_1	–	principle stress in x-direction
σ_2	–	principle stress in y-direction
σ_3	–	principle stress in z-direction
P	–	outer pressure on the plate surface
σ_1^T	–	tensile material strength of laminate in longitudinal direction, in x-direction (along fiber direction)
σ_1^C	–	compressive material strength in longitudinal direction, in x-direction
σ_2^T	–	tensile material strength of laminate in transverse direction, in y-direction, (transverse to fiber direction)
σ_2^C	–	compressive strength in transverse direction, in y-direction
σ_3^T	–	tensile strength limit in z-direction
σ_3^T	–	compressive strength in z-direction
τ_{12}^T	–	positive shear strength of laminate
τ_{12}	–	shear stress in the x-y plane, maximum shear stress in the lamina, laminate shear stress
τ_{12}^C	–	negative shear strength of laminate (considers equal to positive)
τ_{12}^F	–	shear stress along to the fiber in x-y plane
τ_{23}	–	shear strength limit in y-z plane
τ_{23}^F	–	shear stress transverse to the fiber in y-z plane
τ_{13}	–	shear strength limit in x-z plane
τ_{13}^F	–	shear stress along to the fiber in x-z plane
τ_{12}^F	–	ultimate shear stress in x-y-plane (shear stress limit in x-y)
τ_{23}^F	–	ultimate shear stress in y-z-plane (shear stress limit in y-z)
τ_{13}^F	–	ultimate shear stress in x-z-plane (shear stress limit in x-z)
t_{total}	–	plate wall thickness
OD	–	curved plate Diameter
ν_{12}	–	major Poisson's ratio

t – ply thickness

E_1 – longitudinal modulus

E_2 – transverse modulus.

G_{12} – shear modulus.

A – axial force

G_f – shear modulus of the fiber.

G_m – shear modulus of the matrix.

$\rho_{rgX,rgY}$ – coefficient of Spearman correlation

$cov(r_{gX}, r_{gY})$ – covariance of the rank variable

1 Introduction and Background

1.1 Curved Plates

General understanding of plate provides its meaning as a planar body which has small thickness. The structure of a thin plate usually bounded with lower and upper surface planes located on a h - distance between each other which is demonstrated in Figure 1. The neutral plane (midplane) of the thin plate with the x-z coordinate axes are presented in Figure 2. It also has a y-axis which is a normal to x-z plane. Therefore, the neutral plane location lies in the middle of the distance h, called midplane. Plates usually have simple structure and can be web of a stiffener or can be more complicated. This thesis provides study of a complicated cylindrically curved stiffened plate under defined loads.

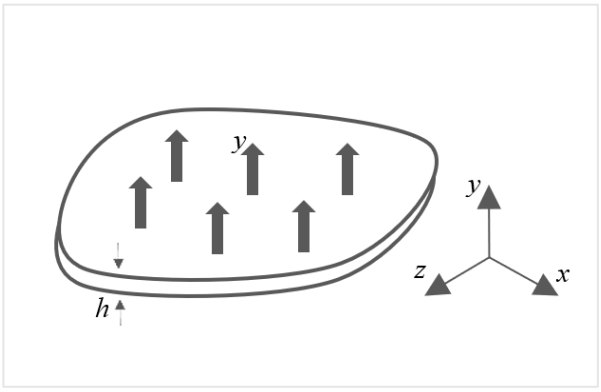

Figure 1: Thin plate structure with axes

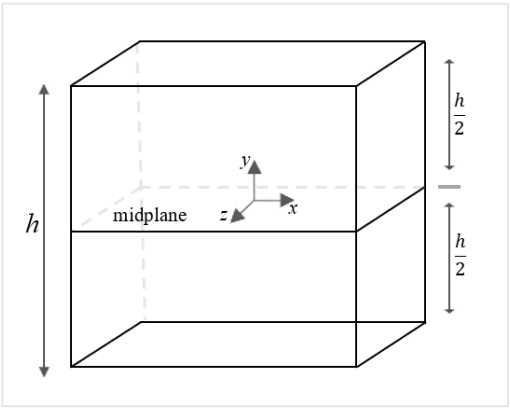

Figure 2: Plate midplane with h and axes

Curved shell plate structures are often used in different industries, i.e., oil and gas, maritime or aerospace industries. Curved plates are frequently used in manufacturing of pressure vessels, aerospace vehicles, ships substructures etc. This thesis proposes a study of the curved plates used in the marine and offshore structures, for instance ship hull design. Example of the curved plate usage can be seen in Figure 3 and Figure 4.

Curved plates for the hull design usually have three dimensional curved surfaces which are very complicated for the whole hull and at the stern and bow part particularly. The research considers curved plate geometry of the middle part of the structure and provides the study of optimal design and critical failure criteria values due to the loads applied on the structure.

Figure 3: Curved plate used in the design of the bridge

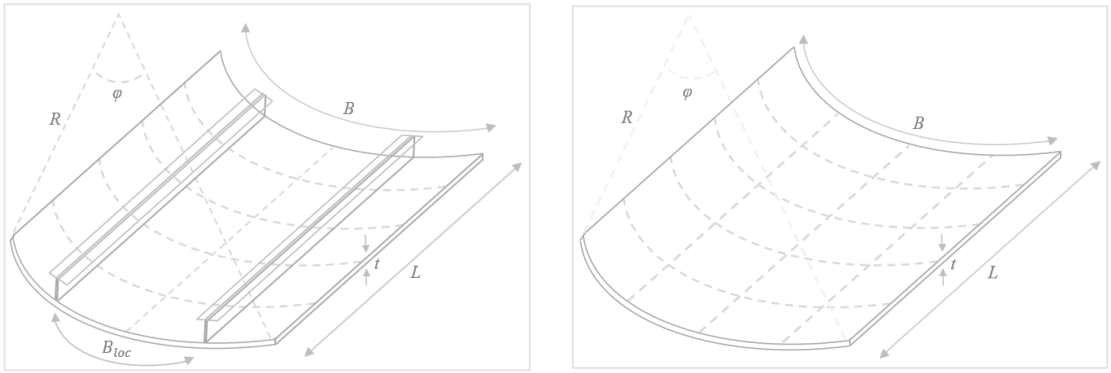

a) b)

Figure 4: Geometry of the curved plate a) with stiffeners and b) without stiffeners

The curvature value of the plate remains constant in the thesis while the load, thickness, and number of stiffeners play the main role in failure criteria study. In the case study, a finite element method is applied to the curves plate geometry with loads which are applied to it. High computational analysis with the ANSYS software is provided for the load due to the main objectives of the research. During the analysis, the curved plate behaviour under plane compression caused by loads is evaluated. The increase in loads can cause plate surface buckling and gives the critical points for the analysis of buckling strength as well as compression and tension due to the boundary conditions of the plate. The increase in load can cause deformations of the plate until the failure occurs. Using finite elements methods, the software gives opportunity to see the nodes where the collapse is most expected.

Studying of the curved plates possible loads and failures in combination with advanced finite elements analysis provides an opportunity for the designers to achieve an effective model of plates and adapt the analysis and structure details to the standardized safety levels.

Increased material quality due to its engineering properties and efficient use of computational facilities lead to sustainable costs in manufacturing of the curved plates. For this aim one of the best materials is composite material which started to be more and more essential in the gas, oil, marine and offshore fields.

1.2 Carbon Fiber Composite Materials

Composite material is a combination of two or more materials with properties which are very efficient in use in different areas and particularly in oil and gas, offshore and subsea industries.

The aerospace industry has been using the composite materials since 1980s. From that time, usage of carbon fiber increases twice every five years. Composites are very important for construction industries, for example in construction of bridge systems or high-voltage electrical towers installations. For offshore industry, many assets, made of composite materials, were installed on platforms, i.e., grids, ladders, or gratings. Subsea industry uses polymer composite materials for the last 30 years for different applications like pipes, pipe protection and coating, hulls of the vessels, subsea units etc. and for repair processes. Due to some engineering properties composite materials can prevent the damage of pipes and structures as well as protect pipes from corrosion for 20 years and more.

Composite materials have a range of advantages compare to other materials. With combination of two or more materials composite becomes stronger and lighter, with the exceptional properties of strength and stiffness. It has high thermal and chemical resistance as well as high resistance to electricity which provides excellent electrical insulation properties. The carbon fiber composite material is used for the curved plate model in ACP process of ANSYS in this research. As example, the strength of this material can be 5 times stronger than 1020 grade steel as well as 5 times lighter than the same steel. So, in addition, carbon fiber composite material has very high strength-to-weight ratio. Besides that, the material can be reinforced which makes it more rigid and prevent further crack propagation. This property specified that thin fibers of the material can be well-attached to each other and form a matrix which increases the strength even more. The research provides usage of continuous category of

fiber-reinforced material, arranged in a laminated structure. Using the software, the epoxy carbon fiber composite material type 230 prepreg is used.

1.3 Epoxy Carbon Fiber UD (230GPa) Curved Plate

Carbon Fiber Material is a good decision for the design of curved plates used in marine industry. Besides main properties of composites, the Epoxy carbon fiber composite (230GPa) prepreg includes more advantages in use. As the material is «prepreg», it is reinforced with the epoxy resin system and have very high strength, little cure time and uses special lamination techniques which includes uniform thickness and identical laminates.

Main mechanical properties of Epoxy Carbon UD (230Gpa) in comparison to steel and aluminum alloy are presented in Table 1 below:

Table 1: Epoxy Carbon UD (230Gpa) prepreg in comparison with Steel and Aluminum

	Epoxy Carbon UD (230Gpa) prepreg	Steel	Aluminium Alloy
Yield Strength (GPa)	3.53	0.25	0,28
Ultimate Tensile Strength (GPa)	2.231	0,46	0,31
Density (g/cm3)	1.49	7.85	2,77

It can be seen that the Epoxy Carbon UD (230Gpa) prepreg is lighter and have higher yield and ultimate tensile strength.

As the material is «prepreg», it is reinforced with the epoxy resin system and have very high strength, little cure time and uses special lamination techniques which includes uniform thickness and identical laminates. The structure of Epoxy Carbon Fiber UD (230GPa) prepreg material can be seen on the Figure. It usually contains carbon fibers and epoxy matrix. Matrix helps to distribute loads to all fibers and protect them from the impact of the external environment. Fibers, in their turn, assure stiffness and strength of the component. Thus, the strength due to needs and applications can be achieved with choosing the laminate layout and setting up the fiber directions which are presented in the Figure 5.

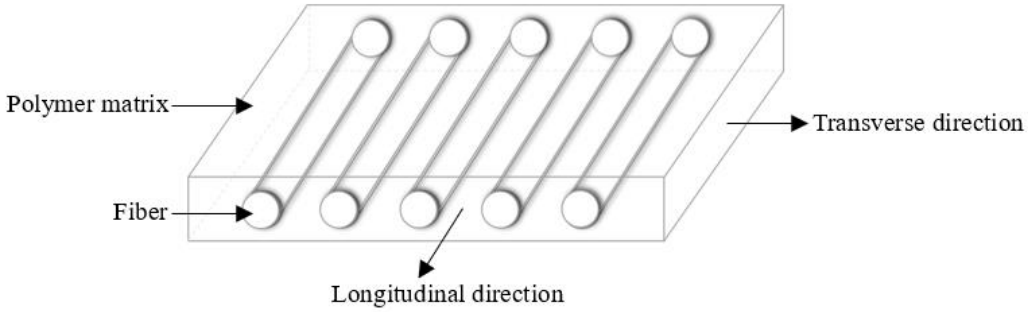

Figure 5: The fiber reinforced lamina structure

With these important engineering properties, carbon fiber composite material is perfect to be used in pipes design, tanks, vessels, and subsea units. These properties make the Epoxy Carbon Fiber UD (230Gpa) Composite material attractive and cost-effective for the engineering design. However, curved plate models and corresponding structures usually subjected to multiple loads and their combinations, i.e., axial forces, external pressure, bending or torsion, which requires detailed stress analysis.

1.4 Design Optimization Procedure

Repeated stresses and loads applied on the curved plate and its laminates which leads to delamination process. This can cause the laminate split in many layers and fibers separation from the matrix. The failures can occur in each individual fiber in compression or tension. To predict and prevent failures, composite structures are usually tested. It happens before and after construction process to have a precise analysis of possible outcomes. Ply-by-ply analysis is investigated in pre-construction testing with the usage of finite element analysis. The non-destructive testing (NDT) is used to test the material during and after construction process i.e., it can implicate thermography, ultrasonic, radiography, X-ray etc.

The thesis research includes many stages of work including usage of carbon-fiber composite materials in design of the plate element, finite element analysis of the curved plate, load application and failure analysis, check and testing of failure criteria. It is required to use the optimized method in order to obtain samples/design points with the optimized failure criteria values. Parametric correlation can be applied to find the parameters that influence the failure criteria most and apply them in response surface (RS) and six sigma analysis. Response

surface methodology is a convenient tool which can be used to calculate optimized failure results and evaluate the sample results with the building a RS model. Response surface requires less time for the simulation of the experiment design in case of large sample size.

However, elements of the simulation as response surface type and size, number of chosen parameters, interpolation methods can influence the accuracy of the values which require detailed and careful study.

The response surface was used in many engineering application and projects which are investigated in works of Jia, Simpson and Gupta. The response surface Kriging type was used in research of Jia who investigated the reliability analysis of the structure [1]. The 2nd order polynomial and Kriging response surfaces were used in works of Simpson [2]. The response surface method was used for the delamination problems studying in works of Gupta [3].

1.5 Thesis Objectives and Outline

The main aim of this dissertation is to study and estimate the optimal method which is used to predict the failure in the design of the curved plate with stiffeners. The thesis suggests the study of several failure criteria and response surface methodology in order to find the most reliable design parameters and values applied in the curved plate design, thus, find the safest design with the small failure rates. All simulations are performed in the ANSYS Workbench 2020 software. The main steps of the thesis are presented in the flowchart below (Figure 6).

The importance and usage of the curved plates and general properties of the Carbon Fiber Composite Materials are discussed in the Chapter 1. This section contains main objectives of the thesis and the discussion of the design optimization procedures.

Classical laminated plate theory is presented in the Chapter 2 of the thesis. It also contains the description and characteristics of the lamina, laminate staking and plies application. Chapter 2 includes information about failure criteria analysis with calculations of the Hashin, Max. Stress and Tsai-Wu failure criteria as well as introduce the finite element analysis of the curved plate. In Chapter 3, the design optimization methods are discussed. The Pearson and Spearman Correlation methods theory and calculations are presented in this section.

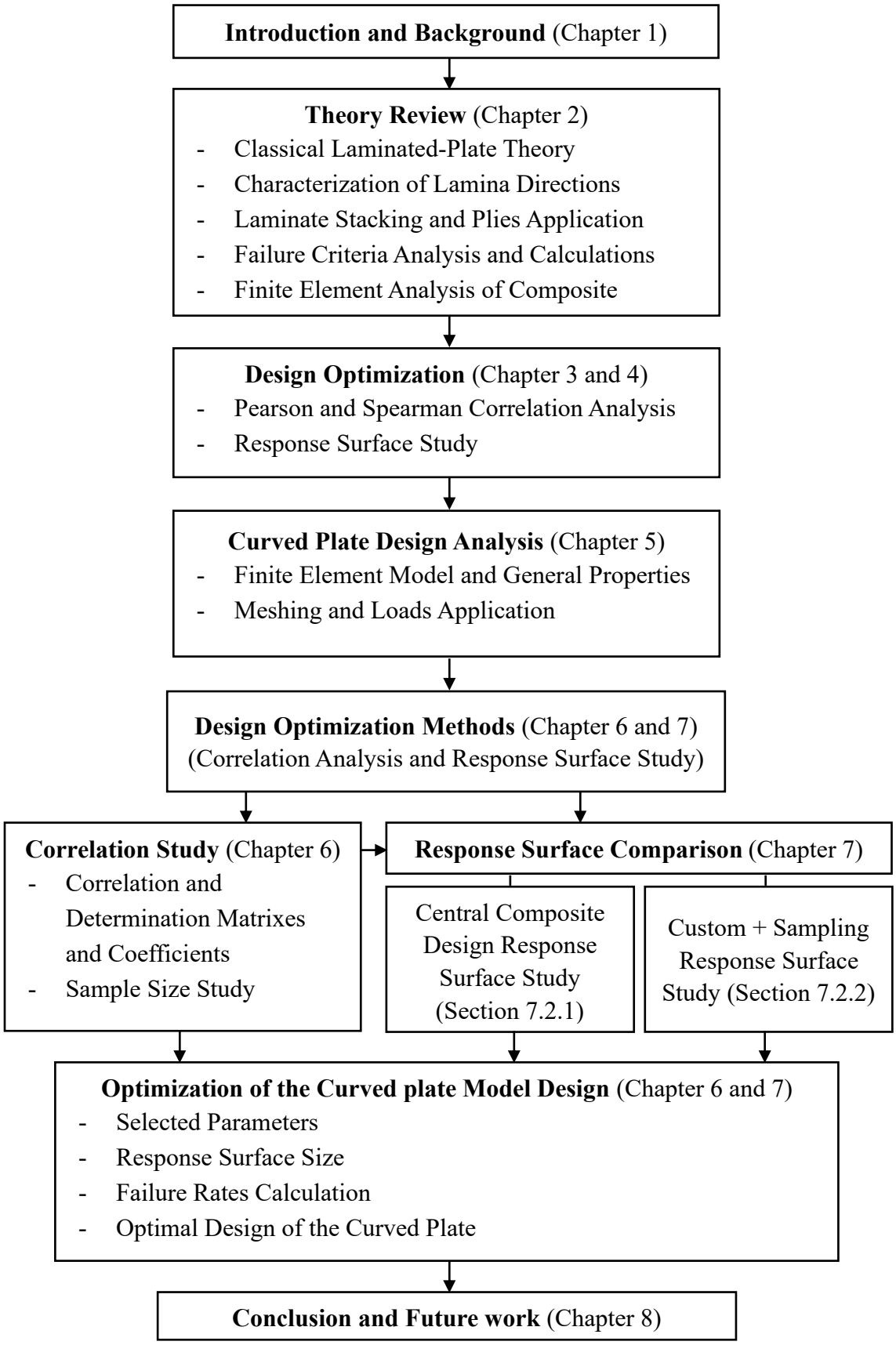

Figure 6: Flowchart of the thesis

The design optimization methods also include the Response Surface methodology which is discussed in the Chapter 4 of the thesis. It contains the information about Central Composite Design and Custom + Sampling Response Surfaces. The Section 4.1 of Central composite design response surface contains theory of its different types as Kriging, Non-parametric, Neural Network, Generic Aggregation and Full 2nd Order Polynomial Response Surfaces.

The case study of curved plate design is presented in the Chapter 5. It contains the information about geometry and material properties of the curved plate with the stiffeners under applied loads with boundary conditions and meshing study as well as the software application steps for the case investigation.

In Chapter 6, the correlation study for the base case is presented. The Spearman correlation matrixes are investigated and analyzed in order to define the parameters which have the largest correlation coefficients, thus, co-related with each other and have significant influence on the model. Selected parameters are used in the further response surface study.

The response surface for the base case is presented in the Chapter 7 of this thesis. It contains the study and results of 2 different types of the response surface calculations: Central Composite Design (CCD) and Custom + Sampling Response Surfaces. Central Composite Design sub-types as Kriging, Non-parametric, Neural Network, Generic Aggregation and Full 2nd Polynomial Response Surfaces are studied. The results of different CCD sub-types and Custom + Sampling Response Surface are compared. The response surface optimal candidate points are presented for the reliable design of the model.

Considering results from the Chapters 6 and 7, the conclusion is made and presented in the Chapter 8 as well as suggested recommendations for future work.

2 Theory

As the laminated composite plates are widely used in different industries, as marine or aerospace, the appropriate theories must be developed in order to analyze and predict theirs dynamical and structural behaviour.

2.1 Classical Laminated-Plate Theory

A fiber-reinforces laminate can be interpreted as a sheet of composite material, which consists of many fibers embedded and bonded together in a matrix material with possible addition of some agents and filters which increase its toughness and achieve desired thickness and stiffness. The composite fibers can be unidirectional, randomly distributed, woven, continuous or discontinuous. Each composite ply in laminate has its own unique direction, which leads to increased strength of plies along the fiber direction with a combination of their light weight. In condition of off-fiber directions, the same plies become weaker. To increase the strength of each lamina and withstand the loads from multiple angles it is essential to use a laminate which consists of a certain number of plies oriented in different directions. The classical lamination theory (CLT) studies coupling effect between bonded laminae in composite materials which leads to different stress and strain distribution (more complicated stress-strain relationships), assuming the common isotropic materials as in the classical plate theory. To study and analyze stresses and strains in composite material and its' laminates of the plate the classical lamination plate theory (CLPT) is used. Noor [4-6] was studying the transverse shear stresses and their accuracy in calculations with the usage of the 3D elasticity theory which had high-cost evaluation. To reduce cost and simplify the analysis from 3D-model to 2D-model, the classical laminated plate theory (CLPT) was used. The CLTP is an extension of classical plate theory which ignores transverse shear stresses and includes study and important assumptions of Kirchhoff- Love [7-8] for CLPT, so called Kirchhoff hypothesis [9]:

1. Transverse normals (perpendicular to the mid-surface) do not bend and remain straight after deformation. The transverse normal strain $\varepsilon_{zz} = 0$.

2. Transverse normals have the same length, and stay unstretched after deformation, so they do not experience elongation. The plate thickness remains unchanged during and after deformation.
3. The transverse normals remain normal as have the right angle to the neutral plane and stays perpendicular to the mid-surface. The transverse shear strains are zero: $\varepsilon_{xz} = 0$, $\varepsilon_{yz} = 0$.

Due to the difference between stress-strain relationships in lamina, classical lamination theory includes few more assumptions which are valid for thin laminates with small displacements and thickness. It is assumed that there is the perfect boding between layers. This assumption considers strong bonding with no gap between plies and no possibility for laminates to slip relative to each other. The stress in thickness direction can be neglected and remain zero ($\gamma_{yz} = \gamma_{xz} = 0$).

With the classical laminate theory and classical laminated plate theory the mathematical method is possible to be used to evaluate the applied loads on the composite material of plates and provide stress and strains deformation calculations.

2.2 Characterization of Lamina Direction

A unidirectional lamina material symmetry planes are transverse and parallel to the fiber direction illustrated in Figure 7.

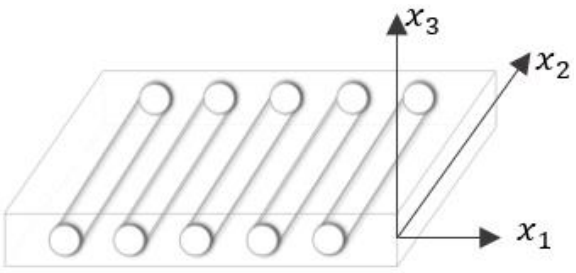

Figure 7: A unidirectional composite layer with coordinate system (x_1, x_2, x_3)

Where: $x_1, x_2, x_3 -$ coordinate axis.

$x_1 -$ parallel to the fiber (oriented along the fiber direction)

$x_2 -$ transverse to the fiber direction in the plane of the lamina

$x_3 -$ perpendicular to the plane of the ply (lamina)

In the study of the unidirectional lamina, such main assumptions can be made: fibers are uniformly distributed and parallel, there is perfect bonding between matrix and fiber, matrix is in stress-free state and has no cracks. Load can be perpendicular or parallel to the fiber direction. Hooke's law can be applied on matrix and fiber which also considered to be isotropic. To characterize the fiber and matrix with some physical properties we can use the modulus, the Poisson ratio of fiber-reinforced material and volume fractions of components:

$E_f -$ modulus of the fiber $E_m -$ modulus of the matrix

$\nu_f -$ Poisson's ration of the fiber $\nu_m -$ Poisson's ration of the matrix

$v_f -$ Fiber volume fraction $v_m -$ Matrix volume fraction

Engineering constants for lamina can be given as:

$$E_1 = E_f v_f + E_m v_m \tag{1}$$

$$\nu_{12} = \nu_f v_f + \nu_m v_m \tag{2}$$

$$E_2 = \frac{E_f E_m}{E_f v_m + E_m v_f} \tag{3}$$

$$G_{12} = \frac{G_f \times G_m}{G_f v_m + G_m v_f} \tag{4}$$

Where: $E_1 -$ longitudinal modulus,

$E_2 -$ transverse modulus,

$\nu_{12} -$ major Poisson's ratio,

$G_{12} -$ shear modulus,

$G_f -$ shear modulus of the fiber,

$G_m -$ shear modulus of the matrix.

$$G_f = \frac{E_f}{2 \times (1 + \nu_f)} \tag{5}$$

$$G_m = \frac{E_m}{2 \times (1 + \nu_m)} \tag{6}$$

The engineering parameters $(E_1 E_2 E_3 G_{12} G_{13} G_{23} \nu_{12} \nu_{13} \nu_{23})$ can also be calculated with measuring applied load and cross-sectional area. Using parameters above it is possible to make calculations of transverse and longitudinal strains and stresses as well as use them in the failure criteria calculations [7].

To improve such material properties as stiffness, strength, weight reduction, corrosion resistance, thermal properties, fatigue life, and wear resistance of any construction, the composite material can be formed. In the direction of the fibers the unidirectional plies have the highest strength and modulus but at the same time in transverse direction to fibers unidirectional plies strength and modulus are very low. To solve this issue, withstand loads applied from multiple angles and increase the strength and modulus of the laminae it is appropriate to use lamination which can be constructed with a certain number of laminae oriented in different directions illustrated in Figure 8.

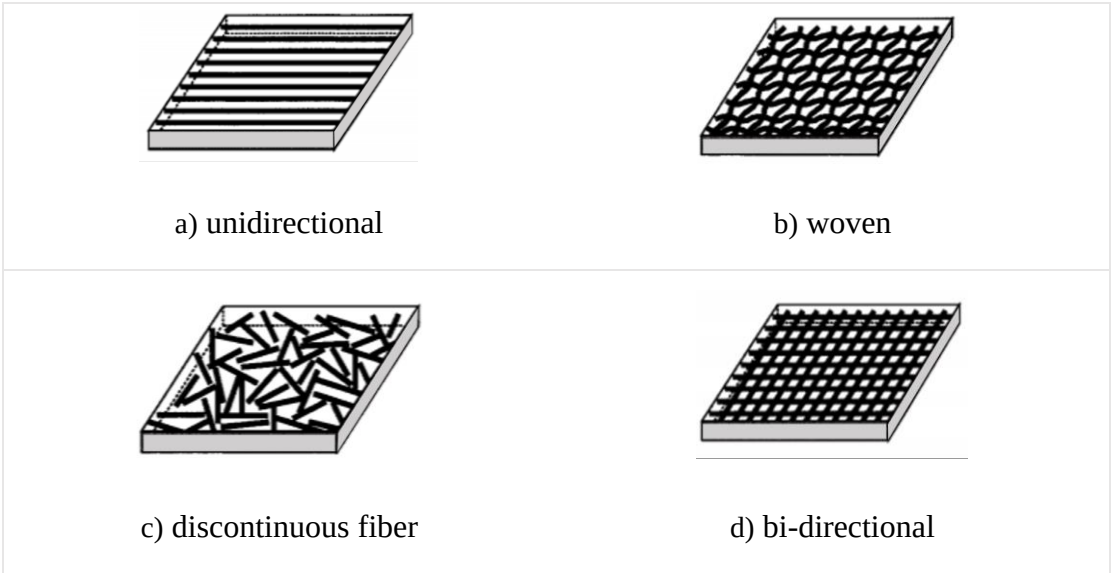

Figure 8: Different types of composite lamina: a) unidirectional, b) woven, c) discontinuous fiber, d) bi-directional

2.3 Laminate Stacking and Plies Application

The epoxy matrix of the composite material is reinforced with the multiple number of carbon-fiber layers which have different fiber directions. The orientation and the angle of the fibers play an important role in the evaluation of the analysis result and influence the failure criteria values. The results can be affected with the change fiber orientation and stacking sequence due to the material properties and changes is stiffness of lamina. The example of the lamination stacking is shown in Figure 9 and Figure 10:

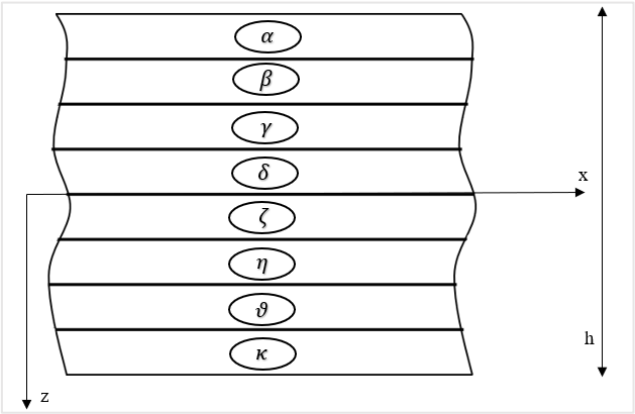

Figure 9: General stacking sequence of the lamina

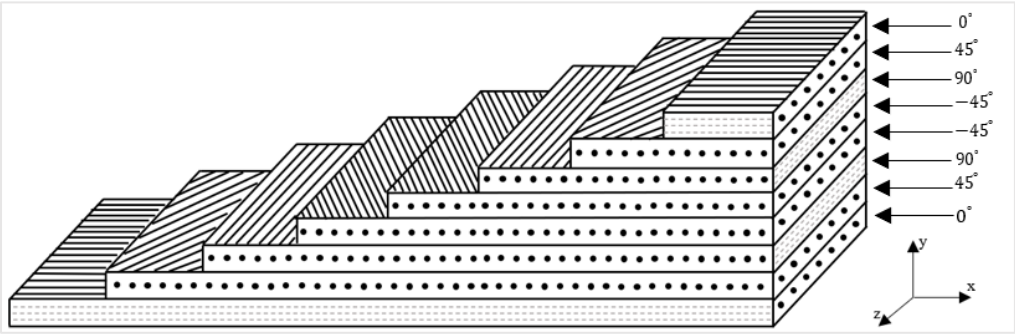

Figure 10: Different fiber orientation of the laminate

Where: $\alpha, \beta \ldots \theta$ are orientations of the plies. The plies are assumed to be in the positive z direction (Figure 9). The layers have different orientations θ with a condition of $-90° < 0 < 90°$. The 0° direction ply is usually oriented in the same direction with x-axis. Each ply can have an angle which can be defined by rotation of the ply clockwise (positive angle) or counterclockwise (negative angle) from the 0°. For instance, as illustrated in figure 10, the laminate consists of 8 plies with different fiver directions.

The laminates can be symmetric and non-symmetric. In non-symmetric laminate the sequence starts from the outmost ply and plies are counted till the bottom with the subscription «T» for the total number of the plies. Symmetric laminate sequence, in its turn, starts from the outermost ply and must be calculated to the middle ply with the subscription "S" as symmetric. The middle ply can be indicated with the bar on the top of the angle. Plies with the same direction can be grouped together and be denoted with the number of plies at the corner. Laminate stacking sequences with these features are shown in Figure 11:

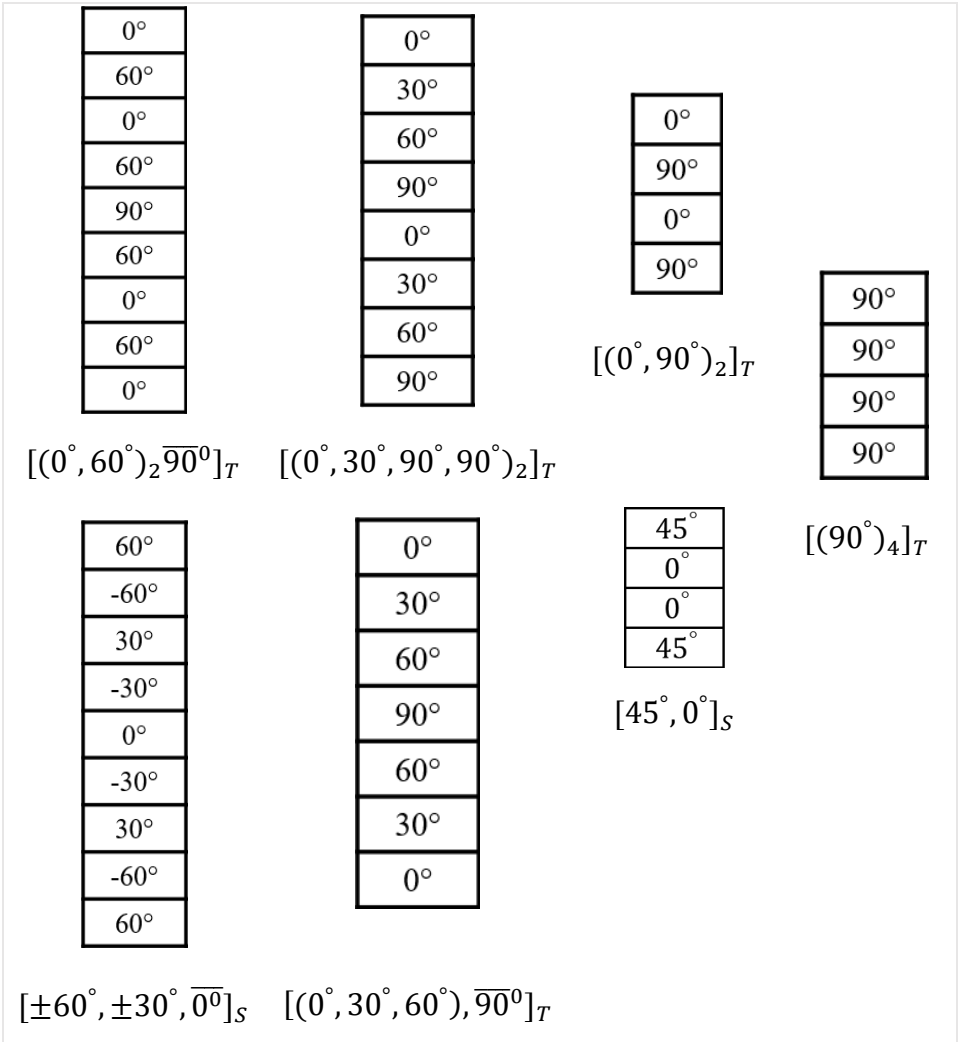

Figure 11: Notations for different stacking sequence of the lamina

The further study of the laminate stacking sequence for applications in different fields were investigated. The influence of fibre orientation was evaluated in works of Hazimeh [10] (influence on the response of composite joints), Strait [11] (influence on the resistance of thermoplastic toughened epoxy laminate) and Hassan [12] (influence on the torsional natural frequencies of laminated composite beams).

2.4 Failure Criteria Analysis

Composite materials of many structures are often exposed to the high loads and tough environmental conditions which lead to appearance of the multi-axial dynamic states of stresses in structures. In these conditions, it is important to figure out the behaviour of the material to prevent failures and damages in structures. To define and evaluate the failure of the structure during the design mode, the failure criteria can be utilized.

The stresses $\sigma_x, \sigma_y, \tau_{xy}$ can be found for each ply of the laminate considering its principal axis with the corresponding loads acts on each ply. The loads must be calculated for each laminate layer. The load-carrying capacity can be estimated with using of strength or failure criterion:

$$f(\sigma_x \sigma_y \tau_{xy}) = 1 \tag{7}$$

When the criterion has the value less than 1 it means no failure. With the value more than 1 which indicates the failure as the stress became larger than the strength limit of the material.

For failure criteria two values are important: the stress that the structure experienced and the material stress limit which is the maximum stress that can be applied to the material without causing deformation. In general, failure criteria can have a simple form of:

$$\sigma_i \leq f \times \sigma_{ui} \tag{8}$$

Where: $\sigma_i -$ actual stress

$f -$ failure ratio

$\sigma_{ui} -$ ultimate strength of the material

To have a stable structure under certain load, the actual stress, applied to the structure must be lower than the ultimate strength of the material. The $f -$ ratio between failure stress and allowable load for the structure.

To evaluate the behaviour of composite material under stress different failure theories and lamina failure criteria groups are investigated.

There are two failure criteria groups used to analyze lamina failure. These are group of failure criteria which are not related to failure modes (e.g., Tensor Polynomial Criterion, Tsai-

Hill, Hoffman etc.) and group of failure criteria associated with failure modes such as fiber fracture or matrix cracking. There are three categories of failure theories related to the second failure criteria group:

1. Limit (non-interactive theories) failure criteria which consider a comparison of independent lamina stresses/strains with corresponding strength/ultimate stresses. Stresses and strain components acting on the lamina do not interact with each other; thus, the failure of the component is defined with the stress or strain only in one direction and not dependent on the strain and stress in any other directions. The most applied Failure criteria of this category are Maximum Stress Failure Criterion and Maximum Strain failure Criterion.
2. Fully interactive theories such as the Hashin, the Tsai-Hill and the Tsai-Wu criteria, where two or more stress and strain components interact with each other, included in one formula (in one failure criterion) and give the expression for the failure value.
3. Partially interactive (failure-mode-based theories), where separate individual fiber failure modes and inter-fiber failure modes are evaluated and considered in failure values. These failure criteria also can consider the interaction between strains/ stresses action on one lamina. They are Hashin-Rotem, Puck, and NU-Daniel failure criteria.

Under of the composite material behaviour and its' response on the load gives the opportunity to evaluate different failure criterions. In this thesis Max. Stress, Tsai-Wu and Hashin failure criteria are investigated.

For further failure criteria investigation, in the classical laminate theory and the classical laminated-plate theory was assumed that the strains and stresses in z-direction can be neglected ($\sigma_3 = \tau_{23} = \tau_{13} = 0$).

2.4.1 Maximum Stress Failure Criterion

All the stresses which are acting on the plies can be resolved into shear and normal stresses in the local axes. If any of these stresses become equal or close to the corresponding ultimate strengths of the lamina, the failure can be predicted. For this purpose, it can be essential to use Maximum Stress failure criterion.

Maximum stress failure criterion is one of the non-interactive failure criteria which is widely used in failure analysis for composite materials. This criterion is stress-based, linear, depends on the failure mode and has no stress interaction. Maximum failure theory assumes that failure of the lamina occurs when any normal or shear stress component become equal or exceeds the value of the corresponding strength. Maximum stress failure criterion indicates likely failure mode, requires separate comparison of resolved stresses with failure stresses and allows for no interaction in situations in non-uniaxial stresses. Thus, the failure occurs when the stresses in principal material direction exceeds the strength in the same direction [13] and can be calculated with the Equation 9 [14]:

$$f = max\left[\left|\frac{\sigma_1}{X}\right|, \left|\frac{\sigma_2}{Y}\right|, \left|\frac{\sigma_3}{Z}\right|, \left|\frac{\tau_{12}}{\tau_{12}^F}\right|, \left|\frac{\tau_{13}}{\tau_{13}^F}\right|, \left|\frac{\tau_{23}}{\tau_{23}^F}\right|\right] \tag{9}$$

$$X = \begin{cases} \sigma_1^C, \sigma_1 < 0 \\ \sigma_1^T, \sigma_1 \geq 0 \end{cases}, \qquad Y = \begin{cases} \sigma_2^C, \sigma_2 < 0 \\ \sigma_2^T, \sigma_2 \geq 0 \end{cases}, \qquad Z = \begin{cases} \sigma_3^C, \sigma_3 < 0 \\ \sigma_3^T, \sigma_3 \geq 0 \end{cases}$$

Where:

$$\sigma_1^C < \sigma_1 < \sigma_1^T \quad \text{for} \quad \left\{ \begin{array}{c} \frac{\sigma_1}{\sigma_1^T} \leq 1 \; if \; \sigma_1 \geq 0 \\ \text{or} \\ \frac{|\sigma_1|}{\sigma_1^C} \leq 1 \; if \; \sigma_1 < 0 \end{array} \right\} \longrightarrow \sigma_1 \geq \begin{cases} \sigma_1^T \; (\sigma_1 > 0) \\ |-\sigma_1^C| \; (\sigma_1 < 0) \end{cases}$$

$$\sigma_2^C < \sigma_2 < \sigma_2^T \quad \text{for} \quad \left\{ \begin{array}{c} \frac{\sigma_2}{\sigma_2^T} \leq 1 \; if \; \sigma_2 \geq 0 \\ \text{or} \\ \frac{|\sigma_2|}{\sigma_2^C} \leq 1 \; if \; \sigma_2 < 0 \end{array} \right\} \longrightarrow \sigma_2 \geq \begin{cases} \sigma_2^T \; (\sigma_2 > 0) \\ |-\sigma_2^C| \; (\sigma_2 < 0) \end{cases}$$

$$\sigma_3^C < \sigma_3 < \sigma_3^T \quad \text{for} \quad \left\{ \begin{array}{c} \frac{\sigma_3}{\sigma_3^T} \leq 1 \; if \; \sigma_3 \geq 0 \\ \text{or} \\ \frac{|\sigma_3|}{\sigma_3^C} \leq 1 \; if \; \sigma_3 < 0 \end{array} \right\} \longrightarrow \sigma_3 \geq \begin{cases} \sigma_3^T \; (\sigma_3 > 0) \\ |-\sigma_3^C| \; (\sigma_3 < 0) \end{cases}$$

And:

$\lvert\tau\rvert_{12} < \lvert\tau\rvert_{12}^{F}$	$\rightarrow$	$\frac{\lvert\tau\rvert_{12}}{\lvert\tau\rvert_{12}^{F}} \leq 1$
$\lvert\tau\rvert_{23} < \lvert\tau\rvert_{23}^{F}$	$\rightarrow$	$\frac{\lvert\tau\rvert_{23}}{\lvert\tau\rvert_{23}^{F}} \leq 1$
$\lvert\tau\rvert_{13} < \lvert\tau\rvert_{13}^{F}$	$\rightarrow$	$\frac{\lvert\tau\rvert_{13}}{\lvert\tau\rvert_{13}^{F}} \leq 1$

Where: σ_1^T – tensile strength in longitudinal direction, in x-direction,

σ_1^C – compressive strength in longitudinal direction, in x-direction,

σ_2^T – tensile strength in transverse direction, in y-direction,

σ_2^C – compressive strength in transverse direction, in y-direction,

σ_3^T – tensile strength limit in z-direction,

σ_3^T – compressive strength in z-direction,

τ_{12} – shear stress in the x-y plane, maximum shear stress in the lamina,

τ_{12}^F – shear stress along to the fiber in x-y plane,

τ_{23} – shear strength limit in y-z plane,

τ_{23}^F – shear stress transverse to the fiber in y-z plane,

τ_{13} – shear strength limit in x-z plane,

τ_{13}^F – shear stress along to the fiber in x-z plane,

$\sigma_1, \sigma_2, \sigma_3$ – maximum material normal stresses in the lamina, principal stresses in x, y and z directions.

If any of the stress ratio which are presented above reach 1, the failure is predicted, the failure mode and failure value will be found with the failure surface which is presented by the plane where the failure occurs and the corresponding stress component. [14]

In Maximum stress failure analysis important value is also the Margin of Safety (MS) which can be calculates as $MS = \left(\frac{1.0}{SF \times F} - 1\right) \times 100$ with SF as a safety factor and F as an applied load or stress as well as strength ratio (SR) which is calculated as $SR = \frac{1}{F}$.

2.4.2 Tsai-Wu Failure Criterion

The Tsai-Wu Tsai Wu failure criterion is based on the total energy failure theory and often

used for anisotropic materials with different compression and tension strength of the lamina which defines Tsai-Wu as more general theory compare to the Thai-Hill [15]. Due to Tsai-Wu failure theory it is possible to predict failure when the failure ration in a laminate exceeds 1. Besides that, Tsai-Wu take in account the total strain energy with the purpose to predict the failure and can be used to determine safety factor of the orthotropic shells. The detailed study and usage of Tsai-Wu failure criterion are explained in the research of Koponov and Gol'denblat [16] and expressed in form of quadratic formulation for 2D state plane stress ($\tau_{23} = 0;\ \tau_{13} = 0;\ \sigma_3 = 0$):

$$F_1\sigma_1 + F_2\sigma_2 + F_{11}\sigma_1^2 + F_{22}\sigma_2^2 + F_6\tau_{12} + F_{66}\tau_{12}^2 + 2F_{12}\sigma_1\sigma_2 \leq 1 \tag{10}$$

Where F_1-F_{66} can be found with help of unidirectional lamina strength parameters:

$$F_{11} = \frac{1}{\sigma_1^T \sigma_1^C} \tag{11}$$

$$F_1 = \frac{1}{\sigma_1^T} - \frac{1}{\sigma_1^C} \tag{12}$$

$$F_{22} = \frac{1}{\sigma_2^T \sigma_2^C} \tag{13}$$

$$F_2 = \frac{1}{\sigma_2^T} - \frac{1}{\sigma_2^C} \tag{14}$$

$$F_6 = \frac{1}{\sigma_{12}^T} - \frac{1}{\sigma_{12}^C} \tag{15}$$

$$F_{66} = \frac{1}{(\tau_{12}^F)^2} = \frac{1}{\sigma_{12}^T \sigma_{12}^C} \tag{16}$$

Which transforms the general Equation 9 into:

$$\frac{\sigma_1^2}{\sigma_1^T \sigma_1^C} + \frac{\sigma_2^2}{\sigma_2^T \sigma_2^C} + \frac{\tau_{12}^2}{(\tau_{12}^F)^2} + \sigma_1\left(\frac{1}{\sigma_1^T} - \frac{1}{\sigma_1^C}\right) + \sigma_2\left(\frac{1}{\sigma_2^T} - \frac{1}{\sigma_2^C}\right) + 2F_{12}\sigma_1\sigma_2 \tag{17}$$

Where F_{12} – coefficient, which is related to principal stresses σ_1, σ_2 and can be found experimentally, with bi-axial tests and must be in range of -1 to 1 [16]. If the data is not available, value of F_{12} can be found with the formula:

$$F_{12} \approx -\frac{1}{2} \times \sqrt{F_{11}F_{22}} = -\frac{1}{2} \times \frac{1}{\sqrt{\sigma_1^T \sigma_1^C \sigma_2^T \sigma_2^C}} \tag{18}$$

For 3D state plane stress, the Tsai-Wu criterion changes to:

$$\frac{\sigma_1^2}{\sigma_1^T\sigma_1^C}+\frac{\sigma_2^2}{\sigma_2^T\sigma_2^C}+\frac{\tau_{12}^2}{(\tau_{12}^F)^2}+\frac{\tau_{13}^2}{(\tau_{13}^F)^2}+\frac{\tau_{23}^2}{(\tau_{23}^F)^2}+\sigma_1\left(\frac{1}{\sigma_1^T}-\frac{1}{\sigma_1^C}\right)+\sigma_2\left(\frac{1}{\sigma_2^T}-\frac{1}{\sigma_2^C}\right)-\frac{\sigma_1\sigma_2}{(\sigma_1^T\sigma_1^C\sigma_2^T\sigma_2^C)^{1/2}}\leq 1 \quad (19)$$

Where: σ_1^T – tensile material strength of laminate in longitudinal direction, in x-direction (along fiber direction),

σ_1^C – compressive material strength in longitudinal direction, in x-direction

σ_2^T – tensile material strength of laminate in transverse direction, in y-direction, tensile material strength of laminate transverse to fiber direction,

σ_2^C – compressive strength in transverse direction, in y-direction,

σ_3^T – tensile strength limit in z-direction,

σ_3^T – compressive strength in z-direction,

τ_{12}^T – positive shear strength of laminate,

τ_{12}^C – negative shear strength of laminate (considers equal to positive),

τ_{12} – shear stress in the x-y plane, laminate shear stress,

τ_{12}^F – shear stress along to the fiber in x-y plane,

τ_{23} – shear strength limit in y-z plane,

τ_{23}^F – shear stress transverse to the fiber in y-z plane,

τ_{13} – shear strength limit in x-z plane,

τ_{13}^F – shear stress along to the fiber in x-z plane,

$\sigma_1, \sigma_2, \sigma_3$ – maximum material normal stresses in the lamina, principal stresses in x, y and z directions,

τ_{12}^F – shear stress limit in x-y plane corresponds to ultimate shear stress in x-y-plane,

τ_{23}^F – shear stress limit in y-z plane corresponds to ultimate shear stress in y-z-plane,

τ_{13}^F – shear stress limit in x-z plane corresponds to ultimate shear stress in x-z-plane.

In Tsai-Wu failure analysis the Margin of Safety also play important role and can be defined with the help of proportionality factor α (strength ratio) which is used in equation:

$$F_1\alpha\sigma_1+F_2\alpha\sigma_2+F_{11}(\alpha\sigma_1)^2+F_{22}(\alpha\sigma_2)^2+F_{66}(\alpha\tau_{12})^2+2F_{12}\alpha^2\sigma_1\sigma_2=1, \quad (20)$$

which was rewritten from the main Equation 9 and considered as a quadratic equation: $A\alpha^2+B\alpha+C=0$.

It can be seen that $A = F_{11}(\alpha\sigma_1)^2 + F_{22}(\alpha\sigma_2)^2 + F_{66}(\alpha\tau_{12})^2 + 2F_{12}\alpha^2\sigma_1\sigma_2$; $B = F_1\alpha\sigma_1 + F_2\alpha\sigma_2$ and $C = -1$. For the real roots of the quadratic equation, the software will use α which has the lowest positive root, thus the rest α will be 0. So, the Margin of Safety in Tsai-Wu will be calculated as MS = ($\frac{\alpha}{SF}$ -1) ×100.

2.4.3 Hashin Failure Criterion

Hashin failure criterion was initially used for the unidirectional polymeric composite materials. Thus, application of Hashin in other non-polymeric composite materials and different types of laminates can have significant approximations. For stress calculations the Hashin can be implemented with 2D classical lamination approach considering degradation of the material and its plies [17]. To evaluate failure modes with the Hashin failure criterion more than one stress components are usually used. Hashin criterion specifies several failure modes which can be defined as [18]:

1. Fibre failures:
   1) Tensile fibre failure ($\sigma_1 \geq 0$) with the following criterion:

$$\left(\frac{\sigma_1}{\sigma_1^T}\right)^2 + \left(\frac{\tau_{12}}{\tau_{12}^F}\right)^2 \quad , \sigma_1 \geq 0 \tag{21}$$

   The strength on the fibre direction is considered in calculations. There is no failure in case the criterion is < 1 and failure if the criterion is ≥ 1.

   2) Compressive fibre failure ($\sigma_1 < 0$) with the following criterion: $-\frac{\sigma_1}{\sigma_1^T}$ which indicates no failure with value of criterion < 1 and failure if the criterion is ≥ 1.

2. Matrix failures:
   1) Tensile matrix failures with the criterion:

$$\left(\frac{\sigma_2}{\sigma_2^T}\right)^2 + \left(\frac{\tau_{23}}{\tau_{23}^F}\right)^2 + \left(\frac{\tau_{12}}{\tau_{12}^F}\right)^2 + \left(\frac{\tau_{13}}{\tau_{13}^F}\right)^2 \text{ where } \sigma_2 > 0 \quad \text{or} \tag{22}$$

$$\left(\frac{\sigma_2 + \sigma_3}{\sigma_2^T}\right)^2 + \frac{{\sigma_{23}}^2 - \sigma_2\sigma_3}{(\tau_{23}^F)^2} + \frac{{\sigma_{12}}^2 + {\sigma_{13}}^2}{(\tau_{12}^F)^2} \text{ where } \sigma_2 + \sigma_3 > 0$$

In the matrix failure the transverse stress is perpendicular to fibre direction.

2) Compressive matrix failure with criterion:

$$\left(\frac{\sigma_2}{2\tau_{23}^F}\right)^2 + \left(\frac{\tau_{23}}{\tau_{23}^F}\right)^2 + \left(\frac{\tau_{12}}{\tau_{12}^F}\right)^2 + \left[\left(\frac{\sigma_2^C}{2\tau_{23}^F}\right)^2 - 1\right]\frac{\sigma_2}{\sigma_2^C}, \quad (23)$$

where $\sigma_2 < 0$ or

$$\left(\frac{\sigma_2 + \sigma_3}{2\tau_{23}^F}\right)^2 + \frac{{\sigma_{23}}^2 - \sigma_2\sigma_3}{(\tau_{23}^F)^2} + \frac{{\sigma_{12}}^2 + {\sigma_{13}}^2}{(\tau_{12}^F)^2} + \left[\left(\frac{\sigma_2^C}{2\tau_{23}^F}\right)^2 - 1\right]\frac{\sigma_2 + \sigma_3}{\sigma_2^C}$$

where $\sigma_2 + \sigma_3 > 0$

For both modes of matrix failures there is no failure in case the criterion is < 1 and failure if the criterion is ≥ 1.

3. Interlaminar failure:

1) Interlaminar tensile failure:

$$\left(\frac{\sigma_3}{\sigma_3^C}\right)^2 + \left(\frac{\tau_{13}}{\tau_{13}^F}\right)^2 + \left(\frac{\tau_{23}}{\tau_{23}^F}\right)^2, \text{ where } \sigma_3 < 0 \text{ or simply } \left(\frac{\sigma_3}{\sigma_3^T}\right)^2 \quad (24)$$

2) Interlaminar compression failure:

$$\left(\frac{\sigma_3}{\sigma_3^T}\right)^2 + \left(\frac{\tau_{13}}{\tau_{13}^F}\right)^2 + \left(\frac{\tau_{23}}{\tau_{23}^F}\right)^2, \text{ where } \sigma_3 \geq 0 \text{ or simply } \left(\frac{\sigma_3}{\sigma_3^C}\right)^2 \quad (25)$$

The stress which is normal to the lamina is estimated with interlaminate failure criterion. For both modes of interlaminar failures there is no failure in case the criterion is < 1 and failure if the criterion is ≥ 1.

Maximum failure values in Hashin failure criterion are considered for further calculations and evaluation of the failures.

2.5 Failure Criteria Calculation

Failure criterions are calculated using Pre/Post ACP solution process in ANSYS Workbench 2020. All the failure modes and results are presented in a post process of ACP

solution tool. On the figure below results of different failure criteria evaluations are presented. In Figure 12 the Maximum failure criterion, Hashin and Tsai-Wu failure criteria results are shown. Maximum failure criterion simulation indicates the failure modes related to stresses acting in different directions. In its turn Hashin failure criterion simulation shows the differences in fibre, matrix and interlaminate failures and corresponding failure modes [19-20]. Tsai Wu failure criterion results are presented on figure 12 showing the failure modes in the middle section of the model.

The highest values of the failure criterions are observed next to the connections between stiffeners and the plate. The highest values of the failure criterions are observed next to the connections between stiffeners and the plate.

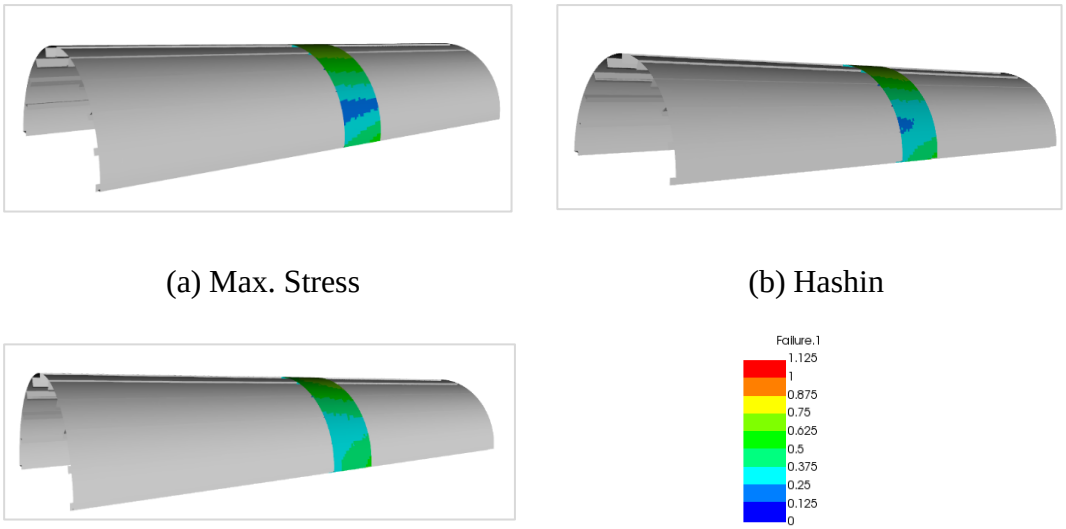

(a) Max. Stress (b) Hashin

(c) Tsai-Wu (d) Range of values

Figure 12: Failure criteria results in the middle section of the model: a) Max. Stress, b) Hashin, c) Tsai-Wu with the d) range of the values

2.6 Finite Element Analysis of Composite Plates

Finite element methods are widely used for representation and analysis of displacement fields of the body elements within applied boundary conditions as well as used for solution of differential and integral equations of these displacement fields. The finite element analysis considers dividing complicated body into different individual and simple geometrical shapes - finite elements with further studying of each element. Example of the finite elements of the

curved plates is presented in Figure 13. All finite elements are connected by global nodes and have various behaviour which depends on the boundary conditions and applied load. Finite elements can be arranged in a set of discrete cells which are called mesh. Number of elements in the mesh defines the accuracy of the numerical model [21]. Process of meshing which considers increasing of the element number gives more accurate result in a model analysis Major steps in Finite element analyses can be defined as [22]:

1. Dividing the model into set of simple finite elements (mesh generation).
2. Integral and differential equations formulation for each finite element.
3. Development and studying these equations of the finite element model with rearranging them in a set of algebraic equations of finite elements model.
4. Assembly of finite elements to obtain the global system of algebraic equations and imposition of boundary conditions.
5. Solution of equations and post-computation and defining the values of interest.

These steps can be applied using software independent of the shape of the body, boundary conditions and applied load. The study of each element connected with global nodes with its boundary conditions and applied loads are presented in works of Chakrabarty [23]. The analysis of laminate with the large number of lamina (i.e., high thickness value) leads to be complicated and expensive due to number of finite elements. To overcome these issues, many analyses were proposed for different models [24-27]. Finite element analysis of the laminated composites plates using ANSYS 2020 ACP tool is presented in Chapter 5 of this thesis.

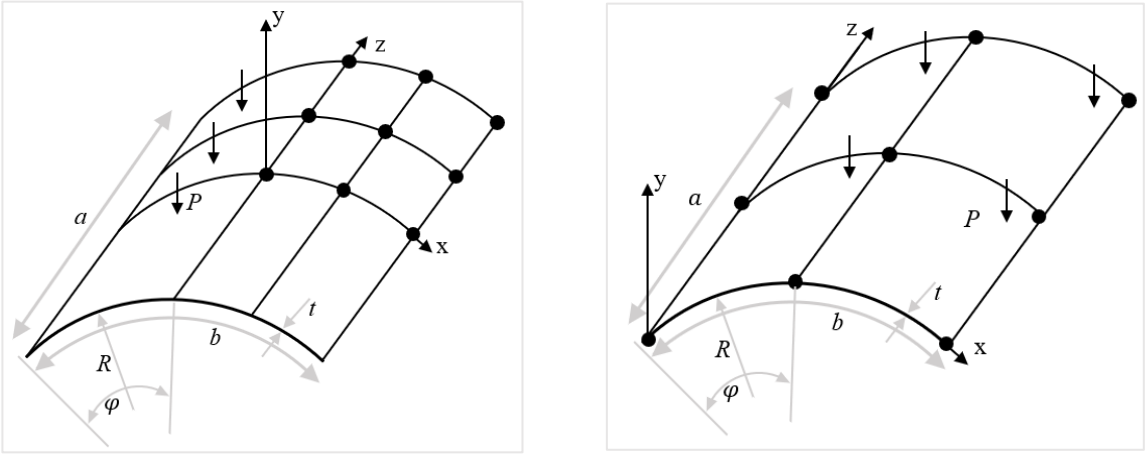

Figure 13: Geometry of the curved plate shell under applied load

3 Design Optimization Methods

3.1 Correlation Analysis Preview

In statistical studies, the correlation or dependence shows the relationship between two or more variables to predict future possible outcomes. To have a correlation between two random variables, the property of probabilistic independence must not be satisfied, so they will be dependent. Correlation gives a degree or value to which two different variables have linear relationship. The degree of correlation or correlation coefficients are usually in range from -1 to 1. If the variables are not correlated, the correlation coefficient is close to 0. Variables with strong correlation have a coefficient close to -1 or close to 1. If one variable value increases with the increasing of other variable value, the coefficient of correlation remains positive. At the same time, increasing of one variable with corresponding decreasing of other variable has negative correlation. Strong positive and negative correlation coefficient values are useful in analysis and can be used to predict the most important and correlated parameters which can influence the model most and use them in practice for further model studying. Approximate values for the correlation coefficients are presented in the table and can be interpreted as [28-29]:

Table 2: Correlation coefficients

Correlation coefficient ρ	0.0~0.2	0.2~0.4	0.4~0.6	0.6~0.8	0.8~1.0
Correlation characteristic	Slight	Low	Moderate	Hight	Very high
Relationship between variables	Almost negligible	Definite	Stable	Noticeable	Very dependent

There are many different methods which are used to compute correlation coefficients. In this thesis the Pearson and Spearman correlation methods to find most correlated parameters in curved plates analysis are discussed and the Spearman correlation is mainly used for computational analysis. The results are presented in the Figures 29, 30, 32, 33 and 45 in the Section 6 of this thesis.

3.2 Pearson and Spearman Correlation

The Pearson correlation measures the strength of the linear dependence between two random variables, which population correlation coefficient can be calculated with the formula:

$$\rho_{X,Y} = corr(X,Y) = \frac{E[(X-\mu_X)\times(Y-\mu_Y)]}{\sqrt{\mathrm{E}(X^2)-\mathrm{E}(\mathrm{X})^2}\times\sqrt{\mathrm{E}(Y^2)-\mathrm{E}(\mathrm{Y})^2}} = \frac{cov(X,Y)}{\sigma_X\sigma_Y} \quad (26)$$

Where X and Y — two random variables

E – expected value operator, expectation

μ_i – expected value of i-variable

σ_i – standard deviation of i-variable and $\sigma_i > 0$.

$\sigma_X\sigma_Y$ – product of standard deviations of two variables.

The correlation is usually symmetric and $corr(X,Y) = corr(Y,X)$. Pearson correlation is most used to find the dependence of two variables.

Spearman correlation coefficient or “grade correlation” coefficient is based on the rank-order correlation as dependence between two variables and rankings [28-30]. Rank-order also can be called “grade-order” and rank itself represents the measure dependence of ranks of 2 variables. The Spearman correlation is «nonparametric» as its coefficient can describe correlation of two variables with the help of monotonic function. To define the Spearman correlation coefficients, Person correlation between rank values of two variables should be calculated. Spearman’s correlation is equal to defined correlation for rank values in Pearson correlation. Spearman’s coefficients calculation formula is [29, 30]:

$$r_s = \rho_{rg_X,rg_Y}\frac{cov(rg_X,rg_Y)}{\sqrt{\mathrm{E}(rg_X{}^2)-\mathrm{E}(rg_X)^2}\times\sqrt{\mathrm{E}(rg_Y{}^2)-\mathrm{E}(rg_Y)^2}} = \frac{cov(rg_X,rg_Y)}{\sigma_{rg_X}\sigma_{rg_Y}} \quad (27)$$

Where random variables X and Y were transformed into ranks (rank variables) rg_X and rg_Y and ρ is applied to the rank variables Pearson correlation coefficient.

Spearman correlation coefficient can be applied for discrete random variables as well as for continuous. In case where two variables got the similar rank, the Spearman coefficients will get higher values [30].

In both Spearman and Pearson correlations when the Y variable increases with the increasing of X variable value, the correlation is defined to be positive. Negative correlation is observed when the Y variable value decreases with the increasing of X variable value. Zero correlation coefficient in Pearson correlation indicated no dependence between X and Y variable. At the same time, zero correlation in Spearman correlation type indicates that Y is not increasing or decreasing with the increasing in X value.

3.3 Correlation and Determination Analysis

Calculation results of the of correlation coefficient and dependencies of the variables can be interpreted and presented in Correlation and Determination matrixes. Engineering model can have n design parameters. The correlation matrix contains all the correlation coefficient values of n design parameters. This can help to identify the most significant parameters which can influence the result and prevent failures. The correlation matrix is symmetric and consists of $n \times n$ - matrix with the n random variables $X_1 \dots X_n$. Determination matrixes show a square value of correlation coefficients and define the percentage of variation in Y variable which is explained by all X variables [31-32]. Coefficient of determination is always positive due to the squared values and ranges from 0 to 1. Simplest line of correlation can be presented with the Person correlation matrixes as the correlation values are defined with the actual values of variables.

For this thesis research rank-order Spearman correlation was used, correlation and determination matrixes explanation and results are presented in Section 6.

4 Response Surface Methodology

The response surface method (RSM) is mainly used in many applications for engineering field with the aim to define structural reliability of the elements of systems in combination with the finite element models analysis. It is well studies by Wilson and Box [33]. In statistics, the response surface methodology defines the relationship between two or more response variables. The main purpose of the RSM is to find the optimal response of the system with the sequence of designed experiments, so it reflects moving the process to the optimum considering all possible constrains.

The RSM is main method to explore the influence of factors and constrains on the model or structure, thus, the effect of the operation conditions on the response variables. [34]. With the usage of proper Design of experiments (DoE) the RSM is extensively used for optimization of factors which influence the structure or model most. So, with advanced DoE the response surface method helps in better understanding and response optimization. RS can be also used for refining models with determined important factors.

RSM are relevant when the relatively accurate prediction of input-output model parameters relationship is needed, or the optimization of the model should be designed. The response surface considers the 'approximate function' between output and input parameters, containing the error which is possible between actual measured values and response surface values:

$$\text{Output1, Output 2, …Output n} = f\,(\text{Input1, Input2, …Input n}) \tag{28}$$

Or can be defined as:

$$Y = f\,(x_1, x_2, x_3 \ldots x_k) \tag{29}$$

Where f is the response surface or performance function, Y - the performance characteristics of the system, the output and x_i −independent parameter i with the k-number of parameters.

These equations with output results show the changes in response due to changes in variables. Further step is the selection of specified operating conditions in order to meet

desired specifications for response surface.

In mathematics and statistics, the response surface methods are used in analysing problems with the fitting of models and defining the independent variables which control dependent variables.

For the proper calculation of the required values and increasing of the response surface accuracy the large sample size (Design of Experiments - DoE size) and response surface type are important. It can be used for the next fittings of the simulated data and graphical demonstration of the parameter interaction.

For generating the response surface in ANSYS, the parameters with the strongest correlation coefficients were used. The DoE as a certain number of sample results was generated. The response surface considers the 'approximate function' between output and input parameters, containing the error which is possible between actual measured values and response surface values. ANSYS allow to use different solutions for response surface with a certain size of samples and response surface type. The larger amount of DoE will show less error in calculations of values of interest.

To study the influence of different factors on the response surface result, five response surfaces types are studied in this thesis: Standard response surface (2^{nd} order polynomial), Generic Aggregation, Neural network, Kriging and Non-Parametric Regression response surface types.

4.1 Central Composite Design Response Surface

The standard response surface methods are based on the design of experiments types and their matrices. In the thesis Central composite design (CCD) analysis as one of the main DoE types with the corresponding CCD's matrixes are used to describe the response surface [33].

CCD is most used method, and it considers fractional factorial (with axial "star" points and center points) or simple factorial design. The number of center points depends on the properties used in the design. Additional axial "star" points are used in order to estimate the curvature (see Figure 14). The number of full factorial design simulations in the CCD can grow

by 2×n “star” points and with n number of factors or basic variables, which means two “star” points per one input variable. New axial and central points can be added to improve the experiment in previously done simple factorial design. [35]. The first and second-order terms can be estimated using CCD.

With the DoE the CCD simulations transform into regression analysis which is used to estimate the unknown coefficients values of the approximation models. Further application of statistical test gives the ability to validate the regression analysis and approve the results of the simulations. Determination coefficients and residual plots are used for this purpose. [36]. After regression model analysis, considering large number of simulations and expected probability of failure, the Monte Carlo method is usually implemented. The number of simulations depend on the probability of failure value. With the lower probability the number of simulations is increasing. Combining Monte Carlo method and RSM the process of stresses and strain calculations is done with easier and faster procedure. Stress, strain, and other values are defined for each point in the design.

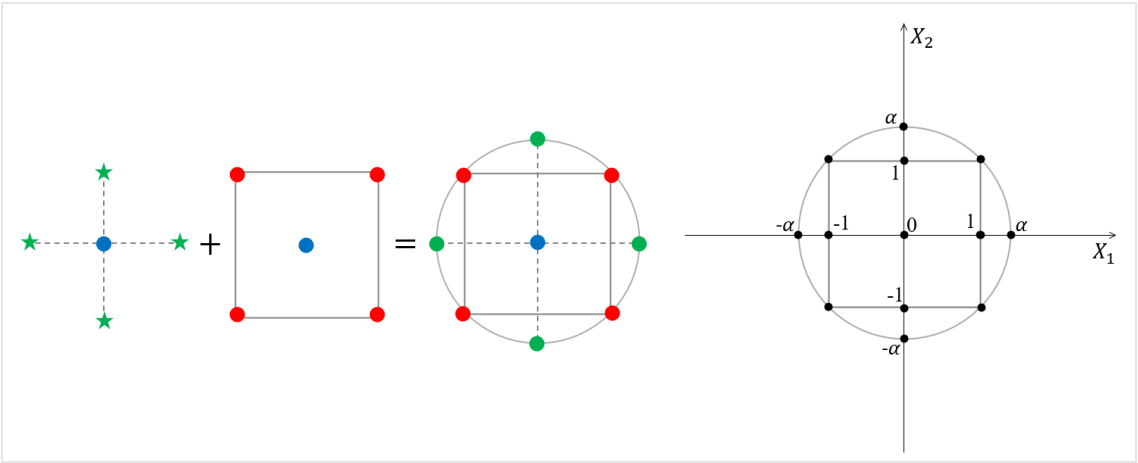

Figure 14: Generation of a Central Composite Design for two factors

Where: red -the corner points (edges),

blue - the center points,

green - extra circumscribed (from the sides) points, axial “star” points.

This array of points is used in CCD response surface analysis. Each “star” point has low or high extreme values for each factor/variable in the design. Figure above illustrates the relationship among the variables in CCD. The distance from factorial point to the center of the

design space is [-1;1] unit for each factor or variable. The distance from axial "star" point to the center of the design space is more than one, $|\alpha| \in (1; +\infty)$ and depends on the number of factors and defined deign properties.

4.1.1 Full 2nd Order Polynomial Response Surface

In general, for the RSM, the response variable y depends on set of corresponding variables $x_1, x_2 \dots x_k$. The appropriate model and equation that describes RSM process is: $y = f(x_1, x_2 \dots x_k) + \varepsilon$ as was in the Equation 29, where ε is the error in the system.

Usually, f is the first order or second-order polynomial. As it was explained above, the easy way to calculate the first-degree polynomial model is to use fractional factorial design or simple factorial design. This is effective methods to define how different variables and factors affect the response surface and its variables of interest. When the most significant variables were calculated, the CCD can be implemented to define the second-degree polynomial model. This is usually used to optimize the variables of interest in response surface, thus, maximize, minimize them, or find a specific target value for the response surface. The analysis of the full 2nd order polynomial model considers fitting the full quadratic polynomial model. Detailed study of the full quadratic polynomial model is proposed by Box and Wilson in their works [33]. The model was defined as easy to apply and estimate even with the lack of process information. The second order polynomial model as function of input-output parameters is determined with the formula [37-39]:

$$y = b_0 + \sum_{j=1}^{k} b_j X_j + \sum_{j=1}^{k} \sum_{j=1}^{k} b_{ij} X_i X_j \tag{30}$$

where b_0, b_j, b_{ij} – regression coefficients with i, j = 1,2…k

X_i – the k input variables.

Or simple:

$$y = b_0 + x_j b_j + x_j b_{ij} x \tag{31}$$

where b_0, – intercept coefficient,

$b_j -$ linear coefficient, i, j = 1,2…k

$b_{ij} -$ second order coefficient,

$x, x_j -$ the k input variables.

One of the most important parts which are considered in the analysis using the 2nd order polynomial response surface is goodness of fit charts.

4.1.2 Kriging Response Surface

Kriging modeling (Gaussian process regression) is interpolation method which estimates the best linear unbiased prediction of the intermediate values with the known sample information and suitable assumptions on the priors' data. Kriging allows to evaluate the dynamics and trends of known samples. The semi parametric Kriging method is more convenient and flexible as it does not need to choose the mathematical model as in traditional fitting methods. It is advanced and flexible method which considers automatic refinement. The Kriging predicts and estimates the result value of a function by computing the weighted average of known measured values at certain location of the design. Simply, the kriging estimates a single realization of random field using simple mathematical model. The practical application of kriging assumes stationary random field with known expectation (zero everywhere μ(x)=0 and relies on known covariance function $(x, y) = Cov(Z(x), Z(y))$. General Kriging modeling is based on the measured sum of two surface components and corresponding error:

$$y(x) = g(x) + Z(x) + \varepsilon(x) \tag{32}$$

or

$$\widehat{N}(s_0) = \sum_{i=1}^{n} WF_i \times \widehat{N}(s_i) \tag{33}$$

Where: g(x)- deterministic polynomial function, the "global" approximation of the design space,

$Z(x) -$ correction to a global approximation; it is a realization of a stationary gaussian random process with $\mu = 0$, variance of $\sigma^2$and stationary non-negative covariance that represents the "local" deviations of the surface from the polynomial,

$g(x) + Z(x)$ – true physical surface,

$\varepsilon(x)$ – random error with zero mean and covariance, which corresponds exactly to the error assumed in the quadratic polynomial model,

$\widehat{N}(s_i)$ – the measured value at the i-location,

WF_i – weight factor of the measured value at the i^{th}-location,

s_0 – predicted location,

n – measured values number.

Without $Z(x)$ the model will be simple polynomial regression model.

In the ANSYS Workbench 2020 the Kriging response surface considers the auto refinement tool. The refinement points are updated with the updating of the response surface itself. At each iteration of refinement process the predicted relative error is estimated. The Predicted relative error is calculated with the formula:

$$PRE = \frac{PE}{V_{max} - V_{min}} \times 100\% = \frac{MV \times (V_{max} - V_{min})}{PV - MV} \times 100\% \quad (34)$$

$$PE = \frac{MV}{PV - MV} \quad (35)$$

Where: PRE – Predicted relative error,

PE – Predicted error,

MV – Measured value,

PV – Predicted value,

V_{max} – the maximum known value,

V_{min} – the minimum known value.

The known maximum and minimum values of the generated data for each design point are considered in predicted relative error calculation. This allows to compare the results easily. In Kriging response surface simulation for the thesis, the maximum predicted relative error is established as 10 %.

Kriging can be used for many applications and for the large problems using different approximation methods. It is commonly used in design optimization of engineering systems and structures. During studying the application of kriging in design optimization for this thesis, many works, and papers were considered. For instance, kriging was discussed in the works of Sacks [40] and Lu [41]. The usage of kriging method in multidisciplinary design optimization eliminated by Simpson [42]. One of the main sources of information for this thesis dynamic kriging response surface application study is a structural design optimization problem studied by Zhao [43]. The kriging surface process and models are accurate and efficiently estimated.

4.1.3 Non-Parametric Regression Response Surface

The estimation of the expected form of non-linear function can be parameterized and relies on the data and basis function. The regression, based on the models which provide estimated finite number of parameters, is known as parametric regression. For instance, polynomial regression which includes multiple regression with different variables $(x_1, x_2 \dots x_k.)$ used in order to find the unknown polynomial parameters (coefficients). In statistics, most of the tools are parametric and are using the data information with data distributions. On other hand, as an alternative tool, the non-parametric techniques are available. They do not rely on assumptions about the data and cannot provide parameterized results for the function in terms of any basis function. In this case, the function can be evaluated using non-parametric regression.

Non-Parametric regression (NRP) is a type of regression analysis which does not consider predetermined model. The result will be derived and estimated from the available data. To provide the effective result in nonparametric regression analysis the large sample size must be used. The non-parametric regression uses many algorithms in the problem-solving process, for instance nearest-neighbor interpolation, regression trees, kernel regression, local regression, neural networks etc. Most commonly used are kernel regression and smoothing splines (both consider weighted filter for data and approaches to optimize the sample size and effective use of data). With the large, complicated datasets and more time, non-parametric algorithms will give more accurate result compare to the parametric one. The constants in NRP remain fixed and cannot be optimized due to ensured compromise between the computational speed for calculations and the accuracy of the result.

In non-parametric regression approach the main goal is to provide a reasonable analysis to the unknown response surface function f with N data points:

$$Y_i = m(x_i) + \varepsilon_i \qquad i = 1, \dots, N, \tag{36}$$

Considering relationship of random variables X and Y:

$$E[Y|X = x] = m(x) \tag{37}$$

Where: $N -$ data points (x_i, y_i).

$m(x) -$ deterministic function (flexible, smooth but usually unknown).

$\varepsilon_i -$ relative error.

With the Nonparametric regression method, the effective, accurate response surface for nonlinear behaviour of the response surface results can be estimated. However, some oscillations in the results of response surface can be possible for case with lower order polynomials.

4.1.4 Neural Network Response Surface

A neural network response surface type is series of algorithms based on the neural network of human brain work. The neural network is represented by the system of artificial/biological neuron connections which depend on the input. For each neuron network the mathematical function can be established. The function contains, collects, and classifies important data for response surface which will be simulated within specific design. The neural network includes input, output, and hidden layers (levels) as well as certain number of interconnected neurons (nodes) which are used in activation of the function. The levels are built in order to interpolate the function and connections are modeled as weights which define the relationship between layers. Examples of neural network are illustrated in Figure 15 and 16.

The weight function between levels can have positive (connection is excitatory) and negative values (connection is inhibitory). Weights are the parameters of the neural network. The neural network can have large number of input parameters as well as several levels of hidden functions.

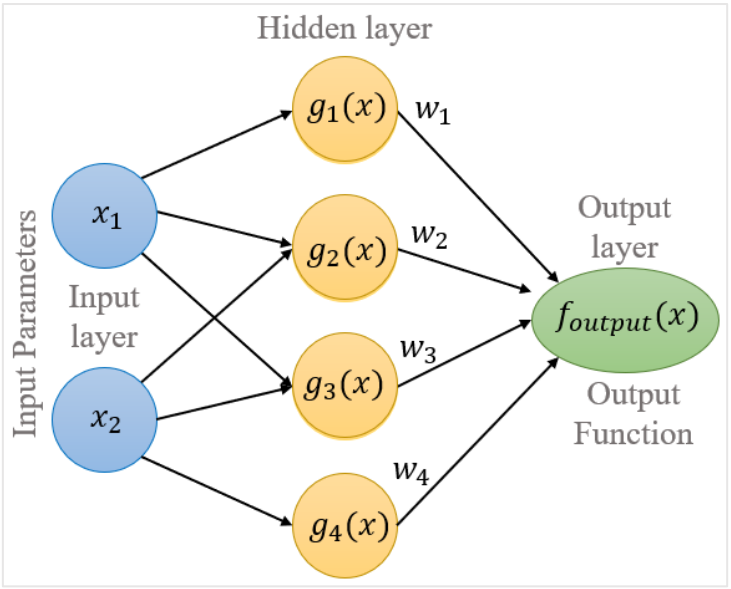

Figure 15: Example №1 of simple Neural Network with one hidden layer

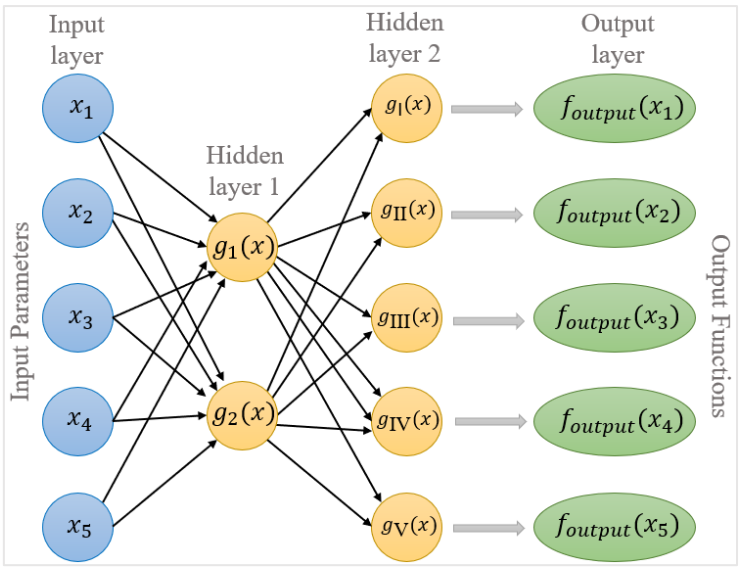

Figure 16: Example №2 of simple Neural Network with two hidden layers

All the input layers are influenced and modified by a weight and usually summed up. Thus, the input patterns are collected. The Input example of logistic regression neural network can be seen in the Figure 17:

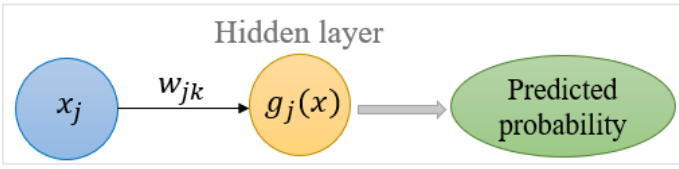

Figure 17: Logistic regression (with only one feature)

The model has one input variable X. To calculate the predicted probability for one input parameter in the neural network this formula can be used:

$$sig(v_k) = predicted\ probability \tag{38}$$

$$sig = \frac{1}{1 + e^{-x}}\ (for\ logistic\ function) \tag{39}$$

$$v_k = \sum_{j=1}^{m} w_{jk} \times x_j + b_k \tag{40}$$

Where: sig – sigmoid activation function,

w_{jk} – weight of the input,

x_j – input signals,

b_k – bias of the neuron,

k – neuron number,

v – summing junction.

The weights can be tuned in the hidden layers until the margin of the predicted error reach its minimum. The arrows between output layers and hidden layers also have weights. Output function has the form of:

$$f_{output}(x_i) = f_{exp}(\sum w_{jk} g_j(x)) \tag{41}$$

Where: $g_j(x)$ – hidden function

f_{exp} – predefined (exponential based) function

Usually the neural network is “feed-forward”. This means that the process is moving from the inputs to the outputs. So, the signal flow will move through all the neutral networks. Reverse process is also possible: the error will move backwards through the model. Examples of feed forward and backward neural networks are given in the Figures 18:

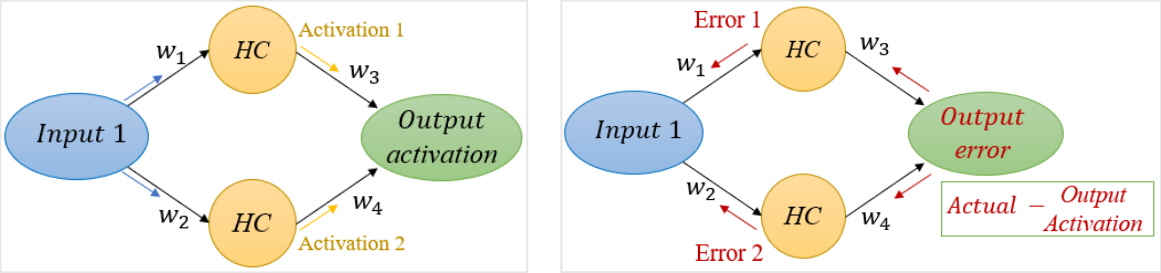

a) Feed forward b) Backward

Figure 18: A) feed forward and b) backward Neural Networks

The feed-forward neural network considers calculations of the activations at each node for each successful hidden layer till it reaches the output. During the backward process, the error magnitude of a specific node will be calculated. The error value is proportional to the impact of that node's output in the function. The neuron (node) with the highest signal of output is studied as critical and deserves most attention.

Some other types of the of Neural Network Topologies are presented in the Figure 19.

The perceptron model type has no hidden layers. It is single-layer neural network with the weighted input for each node. Radial basis type solves approximation problems with the faster learning rate using radial basis function. This type is close to feed-forward neural network. An auto encoder (AE) type of neural network is a machine learning algorithm which contains equal amount of input and output nodes. The Auto encoder generalizes the smaller amount of input data, the results in output will be close or same to input. Long- or short-term memory (LSTM) algorithm use a memory cell and create memory gaps to process the data. The LSTM can be next step after the recurrent natural network (RNN) was used. RNN can use the relevant information from LSTM in case the RNN fails with big amount of data. The probabilistic methods are used in a variational auto encoder (VAR). VAR defines the probability distribution for each neuron/node. For sparse autoencoder (SAE) network the loss function can be defined with a single sample inserted in the network with few activated nodes. The transition of the signal from one state to another is presented in mathematical system called Markov chain. This network is memoryless, so the probability of transition from one state to another one depends only on the current state. In Boltzmann machine (BM) network the original dataset is used for finding the probability distribution with the available data and, thus, understanding the unseen

data. In case all the hidden nodes in BM change their state, the input nodes become output nodes. The variant of BM is restricted Boltzmann machine. It assumes symmetric connections of nodes in hidden and input layers with no internal connections inside each of the layer (differs from simple BM).

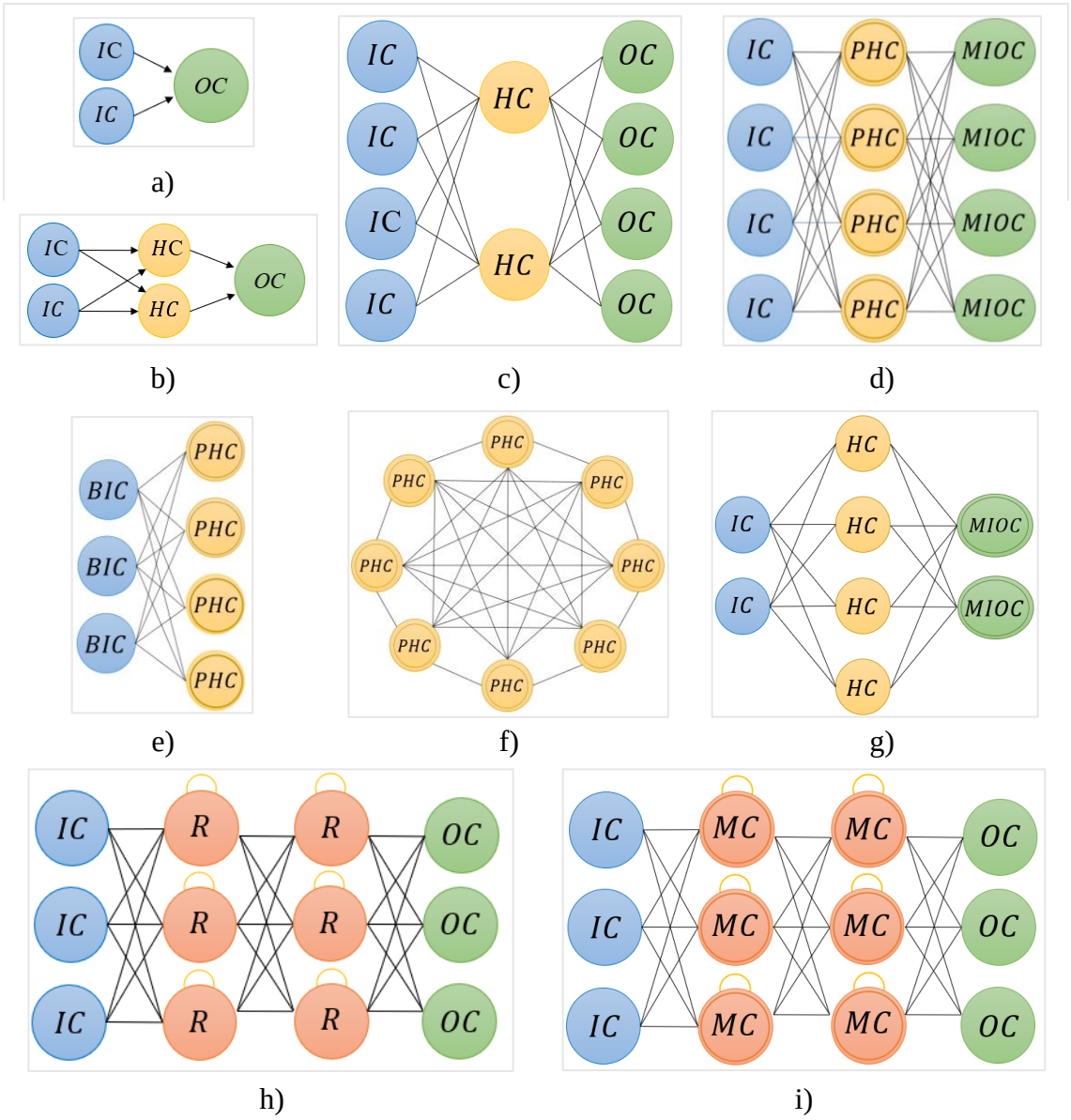

Figure 19: A) perceptron, b) radial basis network, c) auto encoder, d) variational auto encoder, e) restricted Boltzmann machine, f) Markov chain, g) sparse auto encoder, h) recurrent, i) long/short term memory

Where: I – input cell,

H – hidden cell,

O – output cell,

$MIOC$ – match input output cell,

HPC – probabilistic hidden cell,

BIC – back fed input cell.

So, the neural network is a method which is widely used to construct a proper response surface of the design. From the practical side, neural networks are an excellent tool for decision making, data modeling and analyzing. It reflects the complex input-output parameters relationship, used to find a pattern in data, classify it and make predictions to prevent possible errors.

For this thesis, the neural network response surface in ANSYS 2020 is used with the certain number of design of experiments (DoE) to investigate the hidden layer values. The performance can be improved with the larger number of DoE. The Neural networks response surface was studied for the thesis with the help of book by T. Hastie, R. Tibshirani and J. Friedman [44] and Sandy Balkin's [45] publication. Steps to obtain the neural networks nonlinear statistical models and their characteristics are specified and studied in the works of Trevor Hastie et al.,[44].

4.1.5 Generic Aggregation Response Surface

The Generic Aggregation Response Surface (GARS) is an effective response surface type which uses the algorithm that allows population of different response surfaces be solved simultaneously. In general, the GARS is the combination of several different response surfaces types. Considering different types of response surfaces, the GA allows to select, configure, and automatically generate the appropriate type of response surface which is the best for each output parameter. The GARS can be presented by a single response surface as well as by the combination of different response surfaces. Compare to other response surfaces GARS is more reliable and takes more time.

The GARS is usually presented with the Convergence Curves chart which reflect the automatic refinement process of the response surface for chosen parameters. ANSYS 2020 presents the charts when the GARS Type and one or more output parameters are chosen for auto-refinement. The charts are generated and updated automatically when the Generic Aggregation refinement runs. The tolerance value can be defined for each chosen output

parameter. The process of auto-refinement continues till RS accuracy meets user requirements thus till the previously defined stopping criteria is reached. Axis of the charts reflect number of refinement points and ratio between tolerance and maximum predicted error. This is defined for each selected output parameter. Each parameter represented by its own separate curve in the chart which corresponds to the ratio, calculated for each of these parameters.

In general, all the response surfaces such as Non-parametric regression, Kriging, Neural network, and others can be efficiently replaced with the GARS method for most of applications.

4.2 Custom + Sampling Response Surface

One of the most convenient Response Surface method is Custom + sampling. The main advantage of this model is the ability to change and generate design of experiments (DoE) according to the user decisions and goals. This can be reached with usage of simple custom model with the custom model with the samples, which together is called Custom + sampling.

When the Custom + Sampling model is in use, the DoE input is replaced with manually created table of values of the input parameters. The table and values can be changed by the used. If the other model as Central composite design was selected before Custom + Sampling, the same table of values of parameters remains same but the user can change values manually and complete the table with adding new points or deleting some of values.

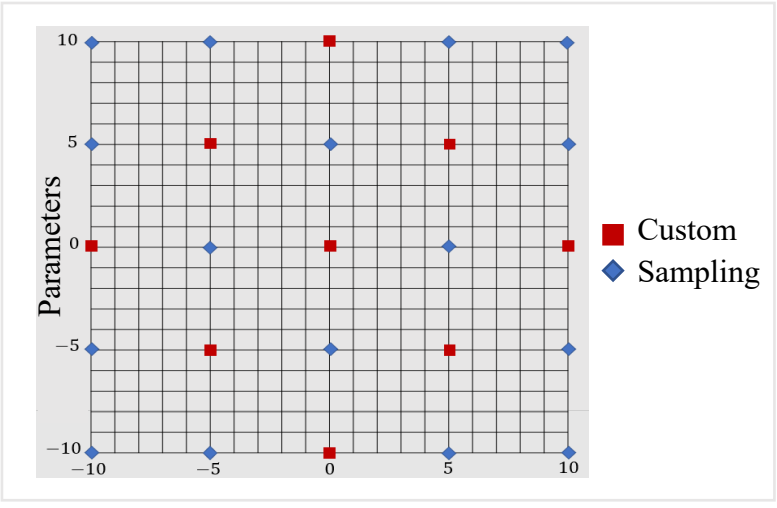

Figure 20: The Custom + Sampling design model with two input parameters

On the other hand, if the DoE is set Custom + Sampling method, the same capabilities are available for user as with the simple Custom sampling, the design points can be generated

automatically and changed if needed what increase the efficiency of the model. Design points also can be imported with CSV format files and can be used for testing as well as previous study points can be upload for the experiment. External data can be used in the mode of Custom design model. The Figure 20 illustrates the custom + sampling design model with two input parameters.

In ANSYS Workbench 2020 software, the user must enter desired positive number of design points. If the number of existing design points is larger than total number of samples, no new design points will be added to the table. For each combination of discrete input parameters, the total number of samples should be equal to the number of design points., It is also possible to generate manufacturable design points only if the user will choose this setup in the software. This will provide less error in the design process of the response surface.

5 Case study – General Steps in the Curved Plate Design Analysis

5.1 Software Application Process

In order to generate the model and obtain results of the curved plate design optimization the finite element design analysis software ANSYS Workbench 2020 was used. In a process of curved plate simulation, the ACP process in ANSYS Workbench 2020 was evaluated and shown with the flowchart in Figure 21. This chart defines the path in which the system will processed. The analysis provides several analysis systems in the process of curved plate design optimization, these are ACP pre/post process and static structural. Each system consists of different cells. ACP preprocess includes such cells as engineering data, geometry, model, setup and parameters. Static structural consists of model, setup, solution, results and parameters cells. ACP preprocess is connected to static structural and transfers the setup cell to model cell in order to include the setup values and possible setup changes of ACP preprocess in the model with the applied loads and boundary conditions. The ACP postprocess continues the ACP preprocess system including results cell. The ACP post process provides the ACP preprocess cells together with solution results from the static structural with considering results with the applied loads and boundary conditions. The main properties of the material can be found in the engineering data cell. The geometrical properties of the model can be established in the Geometry cell of the model. The model cell in ACP preprocess provides meshing of the geometry and helps to define the named selection of the model which is used for the failure criteria analysis. Setup of the ACP preprocess used in order to establish the thickness of the model with simulating appropriate number of material plies. Consideration of applied loads and boundary conditions of the model is possible in model cell of the static structural system. The deformation results after ACP preprocess setup and Static structural model cell are provided in solutions cell. Solution cell is transferred to the results of ACP postprocess. Using selected parameters in engineering data ACP postprocess results cell helps to evaluate the failure criteria in the named selection part of the model considering applied pressure and boundary conditions. ACP pre/post processes with the static structural system are connected and have common set of parameters which is used for the proper simulation of parameter correlation and response

surface analysis. The flowchart of the design optimization in ACP process is shown in the figure below and also includes the parameter correlation and response surface analysis steps.

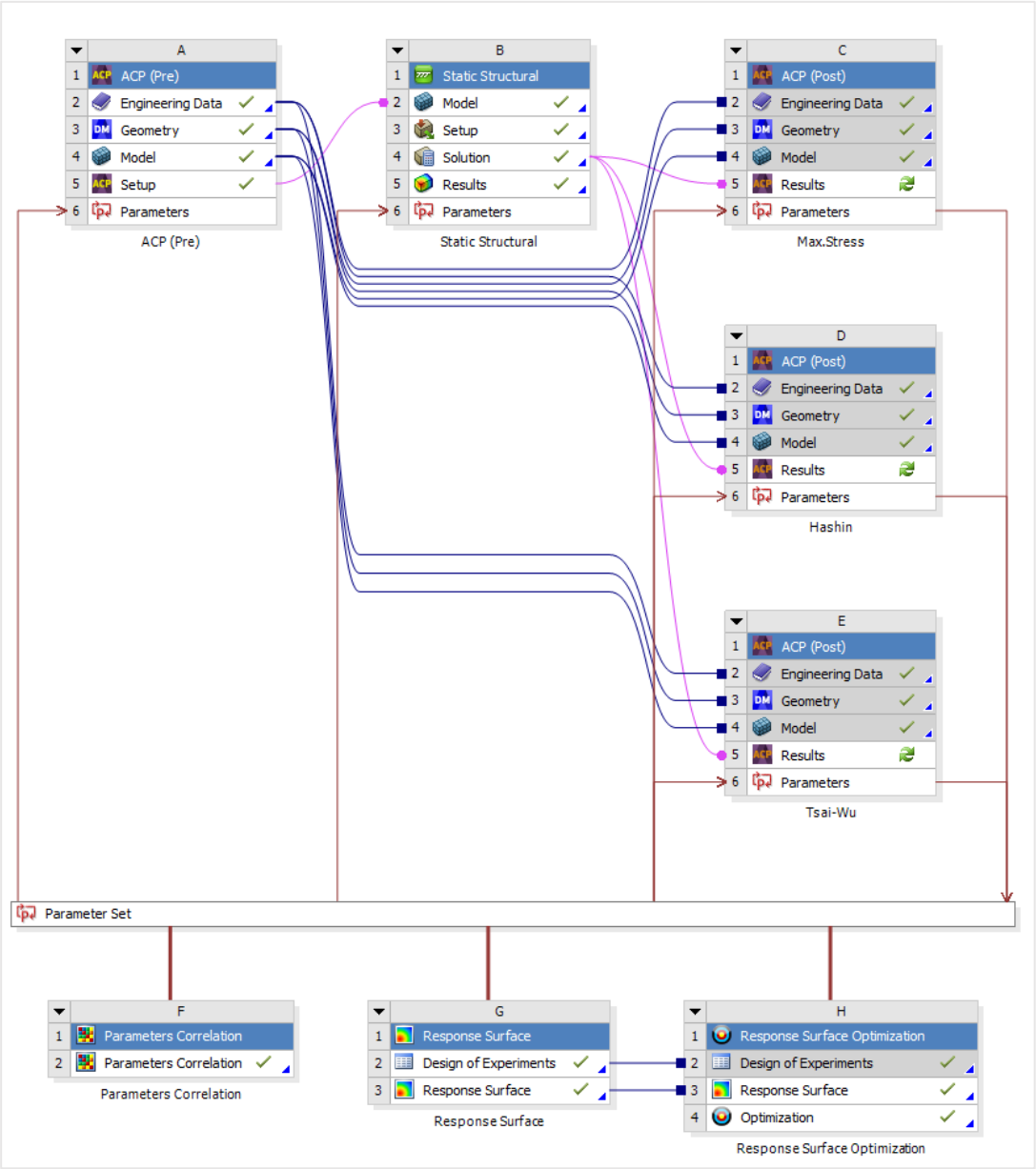

Figure 21: Flowchart of the curved plate design optimization process in ANSYS Workbench 2020

5.2 Geometry and General Material Properties

In this thesis, the curved plate with the defined number of stiffeners is considered and illustrated in Figure 22. The simple geometry of the curved plate is presented in the Figure 23. Main properties of the plate are listed in the Table 3 and 4. The staking sequence of the plies in plate is presented in the Figure 24.

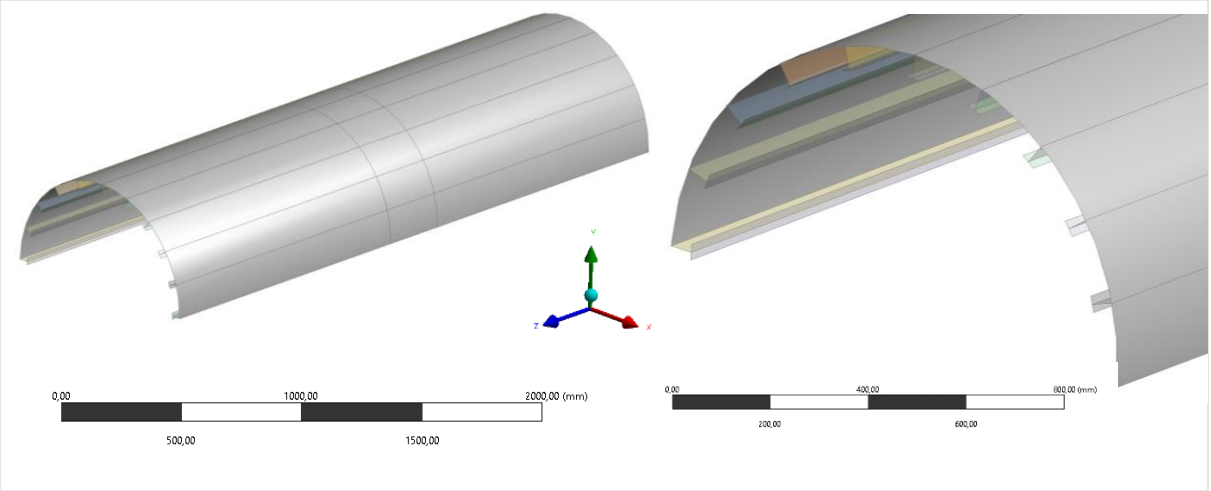

Figure 22: Curved plate with stiffeners used in ANSYS Workbench 2020

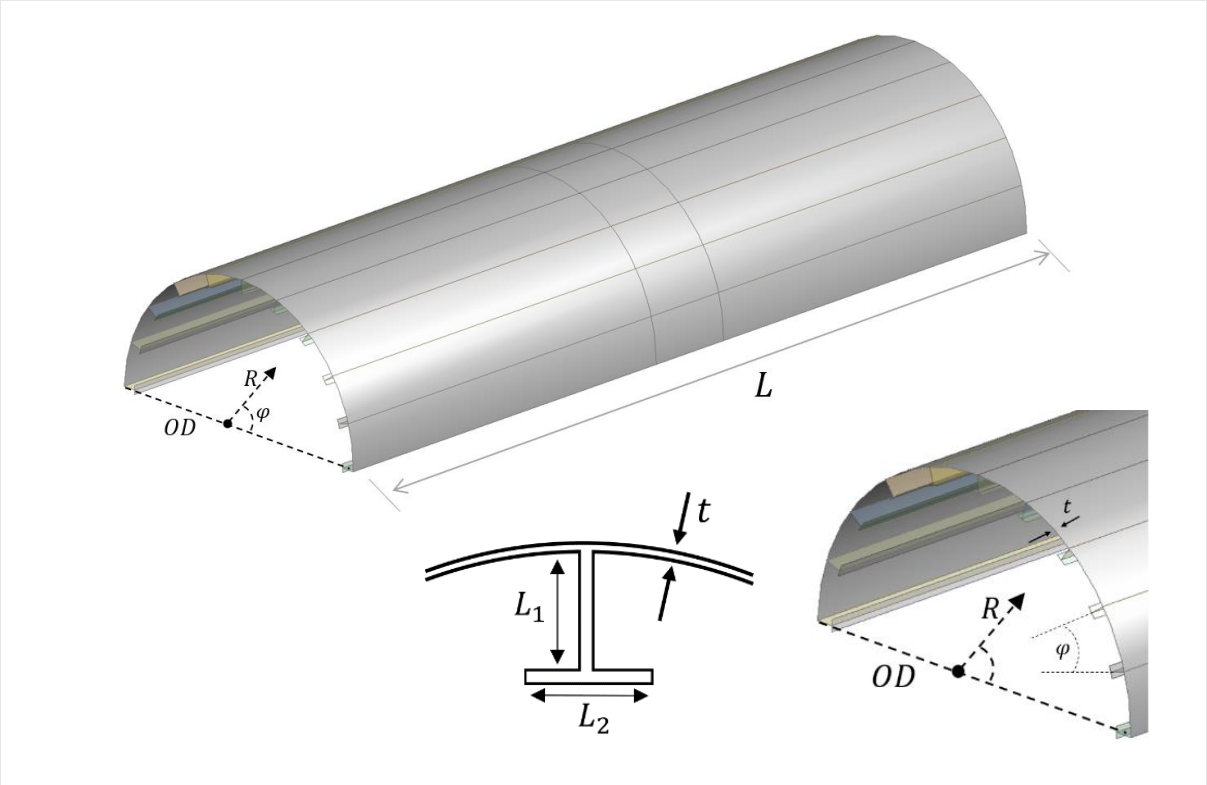

Figure 23: Geometry of the curved plate with stiffeners

Where: *OD* – length/diameter of the plate with stiffeners, considering its curvature,

L – length of the curved plate (6000 mm),

R – radius of curvature of the plate,

t – the plate thickness,

L_1 and L_2 – stiffener's flange and web lengths.

Table 3: General properties of the curved plate with the stiffeners

Property	Value	Unit	Symbol
Outer diameter	2000	mm	OD
Wall thickness	45	mm	t_{total}
Total number of plies	225	-	$Plies_{total}$
Thickness of one ply	0,2	mm	t
Length of the stiffener web (Length 1)	90	mm	L_1
Length of the stiffener flange (Length 2)	60	mm	L_2

Table 4: Material properties data (Epoxy Carbon UD (230 GPA) Prepreg)

Property	Value	Unit	Symbol
Shear modulus XY	4700	MPa	G_{12}
Shear modulus YZ	3100	MPa	G_{23}
Shear modulus XZ	4700	MPa	G_{13}
Young's modulus XY	121000	MPa	E_1
Young's modulus YZ	8600	MPa	E_2
Young's modulus XZ	8600	MPa	E_3
Poisson's ratio XY	0,27	-	ν_1
Poisson's ratio YZ	0,4	-	ν_2
Poisson's ratio XZ	0,27	-	ν_3
Tensile strength in X-direction	2231	MPa	σ_1^T
Tensile strength in Y-direction	29	MPa	σ_2^T
Tensile strength in Z-direction	29	MPa	σ_3^T
Compressive strength in X-direction	-1082	MPa	σ_1^C
Compressive strength in Y-direction	-100	MPa	σ_2^C
Compressive strength in Z-direction	-100	MPa	σ_3^C
Shear strength XY	60	MPa	τ_{12}^F
Shear strength YZ	32	MPa	τ_{23}^F
Shear strength XZ	60	MPa	τ_{13}^F
Tsai-Wu constant (Coupling coefficient XY)	-1	-	F_{12}
Tsai-Wu constants (Coupling coefficient YZ)	-1	-	F_{23}
Tsai-Wu constants (Coupling coefficient XZ)	-1	-	F_{13}

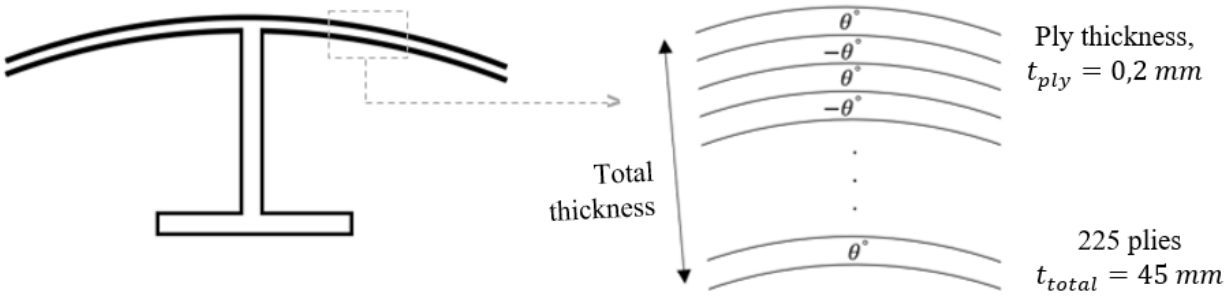

Figure 24: The staking sequence of the plies of curved plate $[(-45^{\circ}; 45^{\circ})_{225}]_T$

The Fiber orientation is ±45°. The curved plate thickness and its stiffeners thickness, the number of stiffeners and the distance between them as well as the diameter of the curved plate are design variables for the model considered in this thesis. The curved plate thickness and its stiffeners thickness are design variables which are used for further failure criteria analysis.

5.3 Mesh Refinement Study

A 6000 mm long curved plate with stiffeners is modeled in ANSYS Workbench 2020. The failure criteria analysis is calculated for the middle part of the curved plate as presented on the Figure 12. The finite element analysis is presented with the ANSYS Workbench 2020. The accuracy of the numerical computations depends on the mesh quality. For FEA, the mesh is presented by the system of algebraic equations which are used to estimate the values of the system/model numerically. For 2D model it is possible to use different mesh element types, examples are presented in Figure 25.

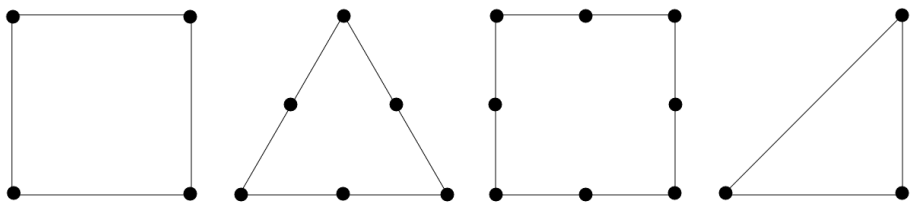

a) b) c) d)

Figure 25: a) 4 nodes, b) 6 nodes, c) 8 nodes, d) 3 nodes mesh element types in 2D

In order to gain the proper convergence test results, the optimal element size must be generated with the process of the mesh refinement. For the curved plate with stiffeners the refinement study is presented in the table below. Figure 26 and 27 illustrates the 30 mm and 60 mm elements size and meshing results respectively with the corresponding element sizes.

Table 5: Mesh refinement study for the curved plate model with stiffeners

Element size, mm	30	60	90	120	150
Number of elements	32733	9946	4645	3157	1720
Number of element nodes	33012	10095	4771	3268	2706

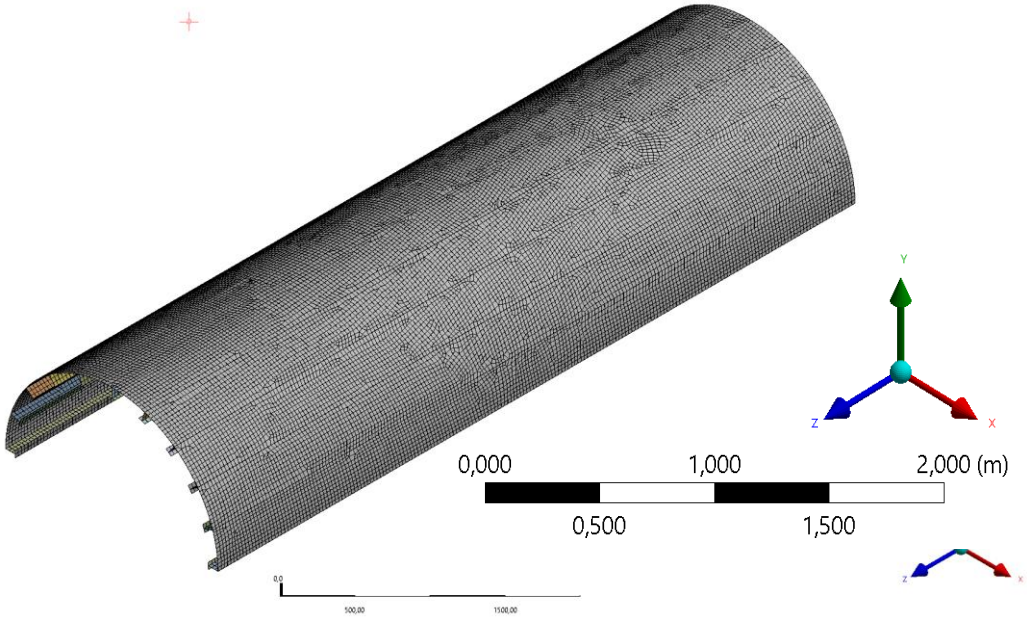

Figure 26: 30 mm element size mesh, 32733 elements with 33012 nodes

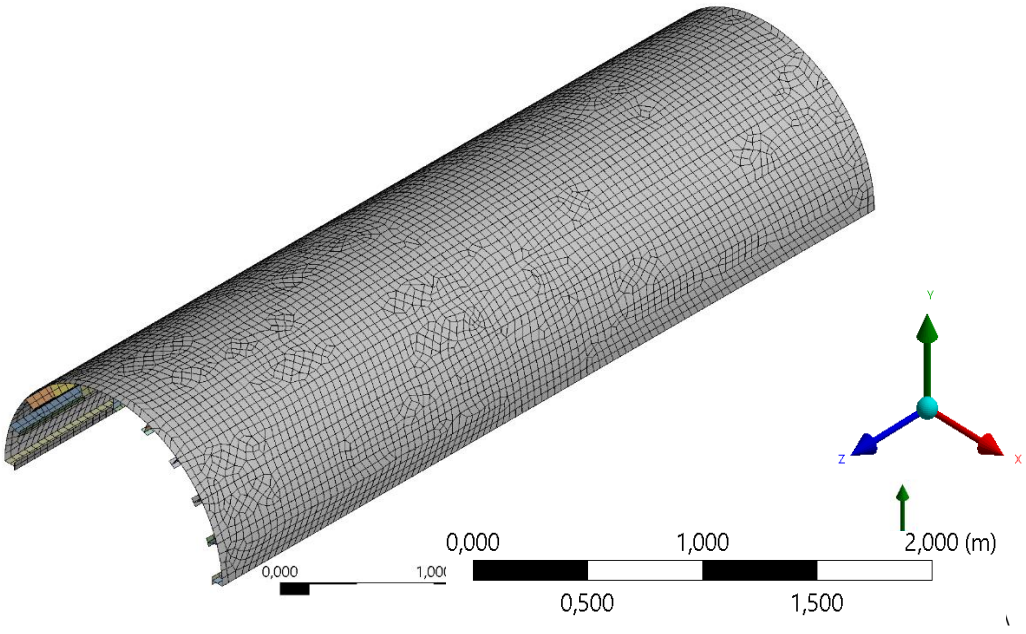

Figure 27: 60 mm element size mesh, 9946 elements with 10095 nodes

The 30 mm element size mesh with 32733 elements and 33012 nodes is used for the further analysis. The shell elements of different types are generated. The element with the 10 mm size is leading to have approximately 50 000 elements. The element size of 30 mm is more accurate and it is 3 times of the 60 mm element. The time to calculate converged result and obtain its acceptable efficiency will be longer for model with 30 mm element size but increase the accuracy of the results.

5.4 Loads and Boundary Conditions

Load values were applied to the model in Static structural in ANSYS Workbench 2020 and contain axial load and external pressure. The nominal loads are presented in the Table 6. The model has boundary condition as fixed support at one end and free end on the other side. Figure 28 presents loads, and boundary conditions applied to the model.

Table 6: Nominal loads applied to the model in ANSYS Workbench 2020

Load	Value	Units	Symbol
External pressure	50 000	Pa	P
Axial load	30	kN	F_a

Axial load (Load A) applied to the left edge of the curved plate and left edge of each stiffener. External pressure (Load B) is applied from above (red arrow) distributed evenly to the whole outer surface of the curved plate. Load C is presented with an end cap force acting in reverse direction to the load A to the left edge of the curved plate and stiffeners. The end cap force is presented with the formula:

$$F_{EndCap} = F_a^P + (F_a^S \times 11) \tag{42}$$

$$F_a^P = \frac{(OD - 2 \times t_{total}) \times \pi}{4} \times \frac{1}{2} \times P \tag{43}$$

Where: OD - outer diameter

F_a^P – axial force acting on the plate

t_{total} –thickness of the plate wall

$(F_a^s \times 11)$ – axial force acting on 11 stiffeners

F_a^s – axial load, acting on one stiffener

Fixed support (Load F) is applied on the right edge of the curved plate and stiffeners.

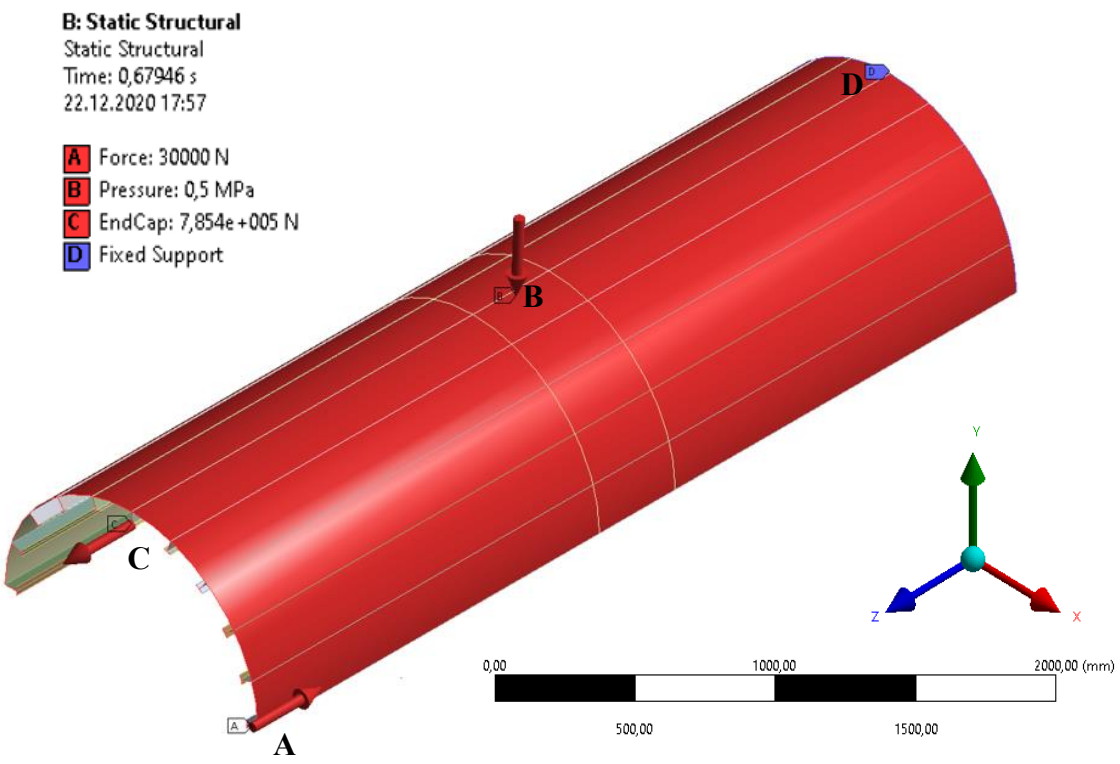

Figure 28: Loads and boundary conditions applied to the model

6 Corelation Study of the Base Case

6.1 Parameter Correlation and Determination study of the model

To find the relationship between the main parameters, the correlation ana determination matrixes were generated, using ANSYS Workbench 2020 from the Composite ACP pre/post process. Spearman correlation method was investigated with the sample size of 35. Values of correlation coefficients with the strongest relationship are close to 1 to -1 as well as values of coefficients close to zero indicates weak correlation. Main parameters of the correlation matrix are listed in the table below:

Table 7: Parameters used for parameter correlation

Ply thickness			
P1	Fabric1.thickness (ply thickness)		
Material properties			
P6	Young's Modulus X direction	P21	Tensile X direction
P7	Young's Modulus Y direction	P22	Tensile Y direction
P8	Young's Modulus Z direction	P23	Tensile Z direction
P9	Poisson's ratio XY	P24	Compressive X direction
P10	Poisson's ratio YZ	P25	Compressive Y direction
P11	Poisson's ratio XZ	P26	Compressive Z direction
P12	Shear modulus XY	P27	Shear XY
P13	Shear modulus YZ	P28	Shear YZ
P14	Shear modulus XZ	P29	Shear XZ
Tsai-Wu constants:		Geometry parameters:	
P15	Coupling coefficient XY	P18	OD, Diameter (curvature of the plate)
P16	Coupling coefficient YZ	P19	Length 1 (web length L_1)
P17	Coupling coefficient XZ	P20	Length 2 (flange length L_2)
Loads:		Failure criteria:	
P37	Force Magnitude	P33	Max. Stress
P45	Pressure Magnitude	P34	Hashin
P46	EndCap Magnitude	P44	Tsai-Wu

Correlation matrix with the sample size 35 is illustrated in the Figure 29. Sample size of 35 was chosen in the first try as the model is complicated. Sample size of N=120 was generated later and used in comparison to N=35. Other sample sizes matrixes are compared in the part 6.3 of this chapter. With the correlation coefficients values the main parameters which affect the failure criterion are defined.

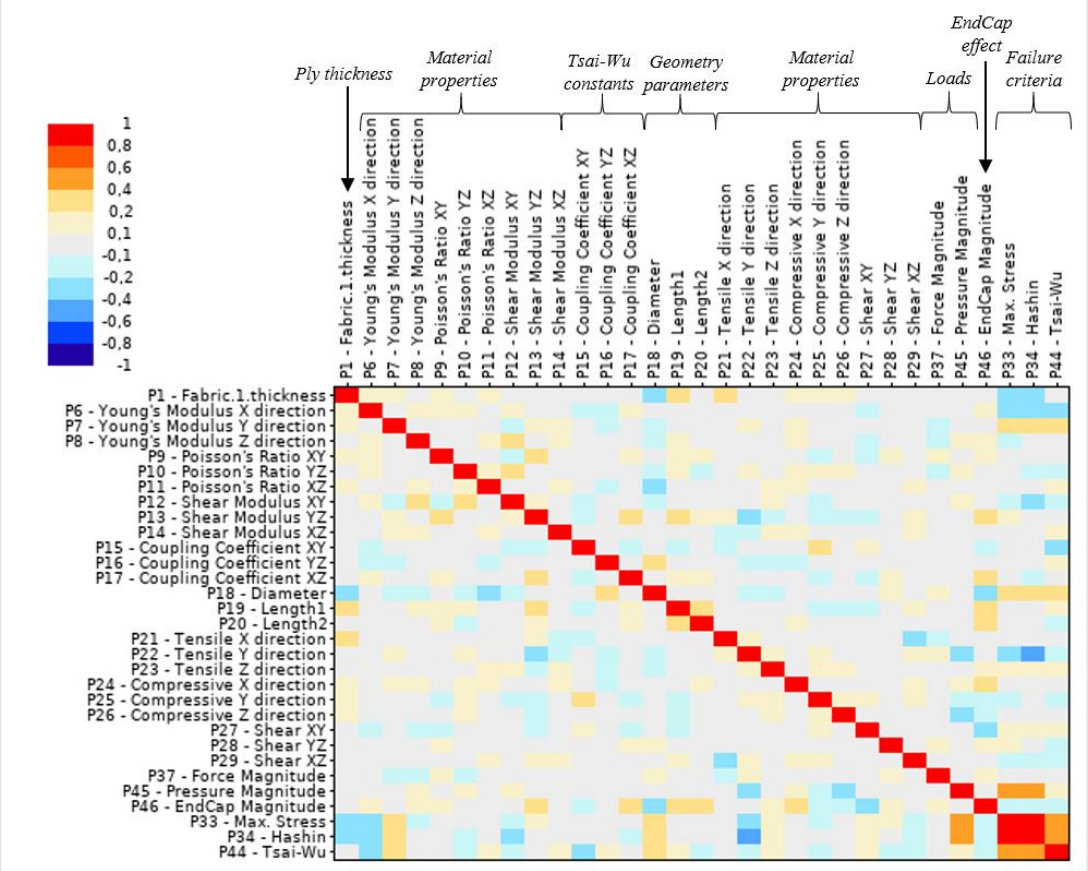

Figure 29: Parameter correlation, Spearman, N=35

There is a quite strong linear correlation between failure criteria. The coefficients are spread all around matrix so, to define main parameters correlation coefficient the detailed matrix was presented. The matrix with the highest values closer to -1 and 1 are illustrated on the Figure 30.

The correlation between main failure criterion is strong due to the high loads applied to each laminate. The coefficient of this relation is shown in Table 8 with the failure criteria correlation in the Table 9. With the matrix above it can be defined that, besides the failure criteria, tensile strength in Y direction, ply thickness, End Cap force magnitude and diameter of

the curved plate (its' curvature) have big influence on the model and its design. The ply thickness is defined in range of 0,18 to 0,2 mm, diameter is in the range of 1900 to 2000 mm.

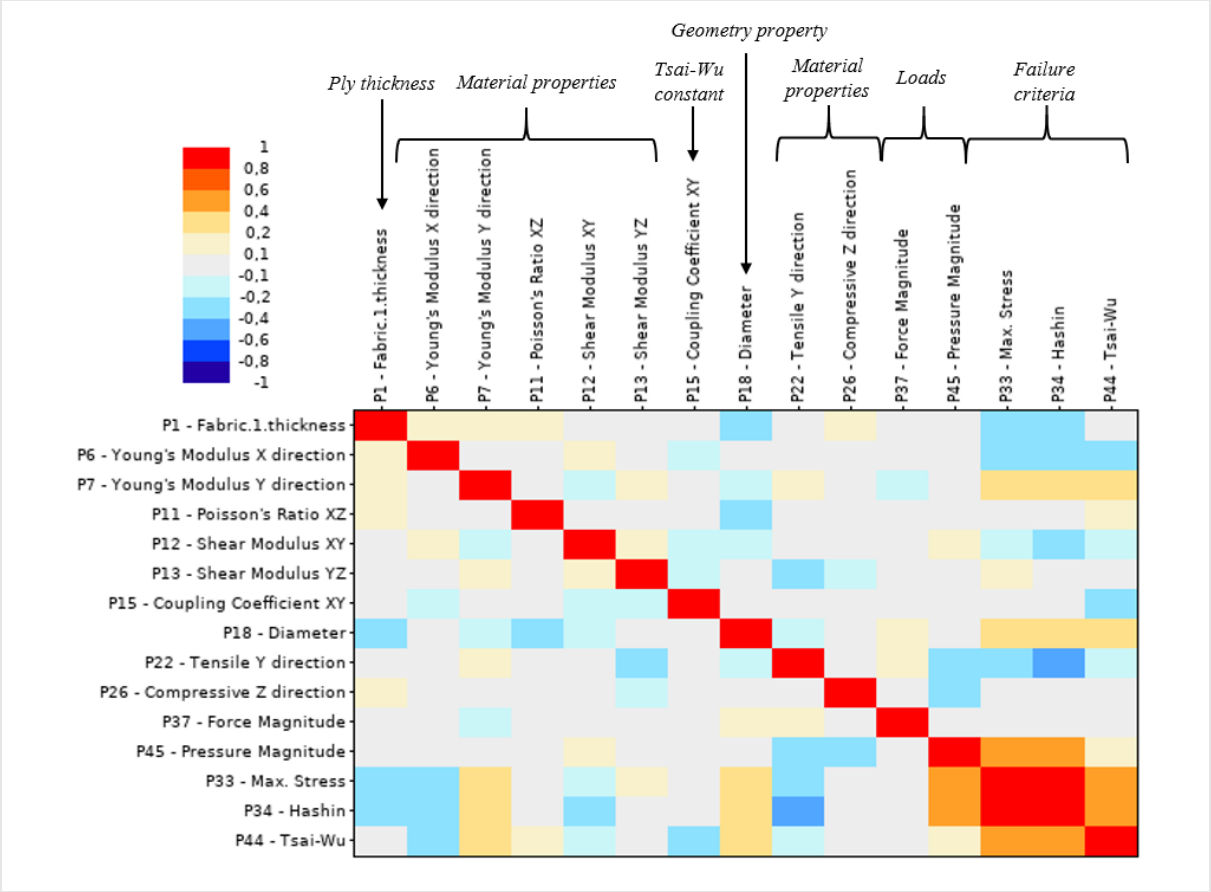

Figure 30: Detailed parameter correlation, spearman, N=35

Table 8: Parameters with quite significant values of correlation coefficients

Parameter	to	Parameter	Value
Fabric thickness	→	Diameter	-0,25317
Poisson ratio XZ	→	Diameter	-0,26325
Shear modulus YZ	→	Tensile Y direction	-0,20917
Pressure	→	Tensile Y direction	-0,25439
Pressure	→	Compressive Y direction	-0,21436

Table 9: Correlation coefficient values of the failure criteria

	Max Stress	Hashin	Tsai-Wu
Max Stress	1,0000	0,96761	0,58961
Hashin	0,96761	1,0000	0,56272
Tsai-Wu	0,58961	0,56272	1,0000

The coefficients' values in Table 8 indicates that the correlation between parameters is small but exists.

The Hashin failure criterion has the smallest correlation coefficient value with Tsai-Wu and Max. Stress criteria. At the same time, the relationships between failure criteria are significant. Max. Stress criteria correlates strong with Hashin. At the same time Tsai-Wu failure criterion indicates less strong but also significant correlation with other two criteria.

Table 10: Correlation coefficients for three failure criteria

	Max. Stress	Hashin
Fabric1. thickness	-2,7701	-0,26631
Young's modulus X direction	-0,33506	-0,29962
Young's modulus Y direction	0,22995	0,26295
Diameter	0,3861	0,33934
Tensile strength in Y direction	-0,38121	-0,45363

Hashin failure criterion also has a small correlation with shear modulus YZ with the coefficient of -0,26784.

Tsai-Wu failure criterion also correlates with the Young's modulus in X and Y direction parameters with the correlation coefficient values of -0,23422 and 0,22659 respectively as well as with the diameter and coupling coefficient XY parameters with the corresponding coefficient values of 0,36593 and -0,31215.

The sensitivities diagrams for Hashin and Max. Stress presented on the Figure 31 indicates that Diameter, pressure magnitude and tensile strength in Y direction are parameters that has the biggest influence on the model.

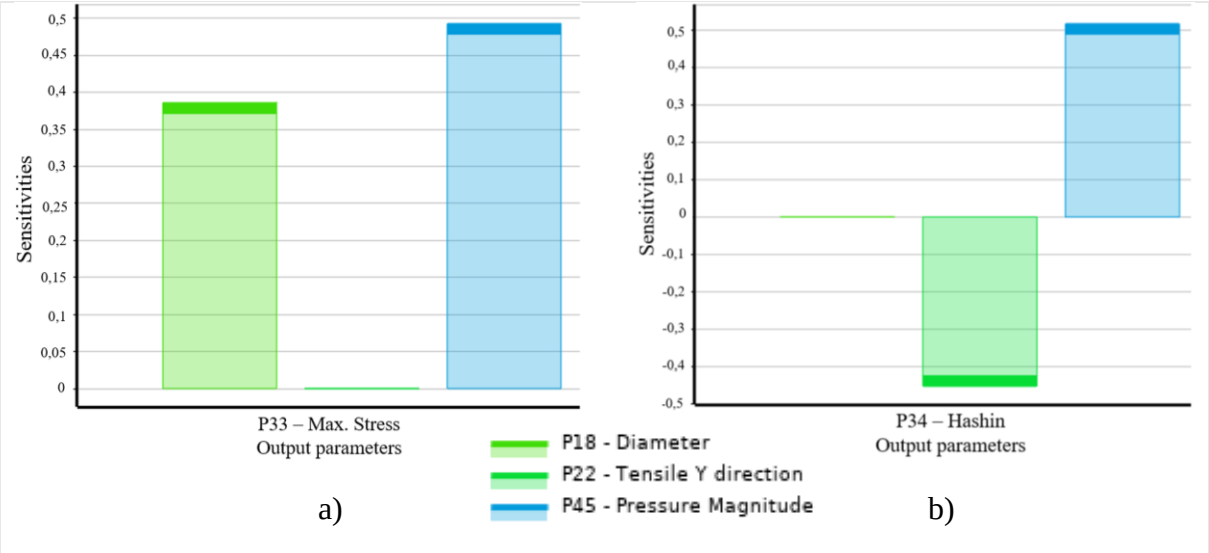

Figure 31: Sensitivities of a) Max. Stress, b) Hashin with the N=35, Spearman correlation

The strongest correlation relationships are presented with the relationship between pressure parameter and failure criteria. Max. Stress failure criterion correlates with the pressure parameter with the coefficient value of 0,51749 which indicated that correlation remains significant. Tsai-Wu has negligible correlation with Pressure (less than 0,20). Hashin failure criterion is the most sensitive to the changes in Pressure. The value of pressure parameter controls the tensile strength in Y direction. Hashin failure criterion has a significant correlation coefficient with Pressure and tensile strength in Y direction which have values of 0,51749 and -0,45363. This means that in case the Pressure parameter rises the Hashin value in increasing with simultaneous decreasing of the tensile strength in Y direction.

More precise information can be seen on the Figures 32 and 33 which illustrates the correlation matrix with the sample size 120. The correlation here shows main parameters which influence the failure criteria excluding correlation of other parameters. More detailed correlation matrix is illustrated in. Correlation parameters which affect Failure criteria are ply thickness and pressure magnitude. The diameter parameter is important for Hashin failure criterion. The Coupling coefficient XY is used in calculations for Tsai-Wu and has significant correlation coefficient of -0,63331with this failure criterion. Pressure magnitude and Tsai-Wu are also moderately correlated with the coefficient of 0,30726. The main correlation coefficients for Max. Stress and Hashin are presented in the Table 11.

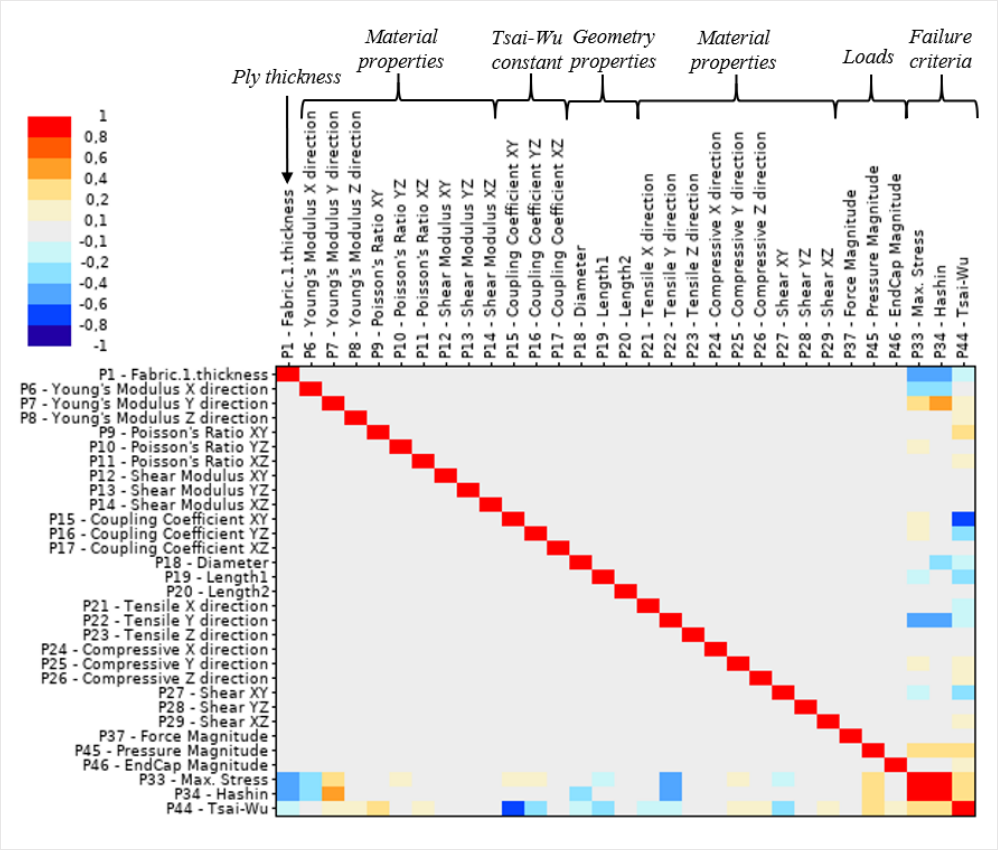

Figure 32: Parameter correlation, Spearman, N=120

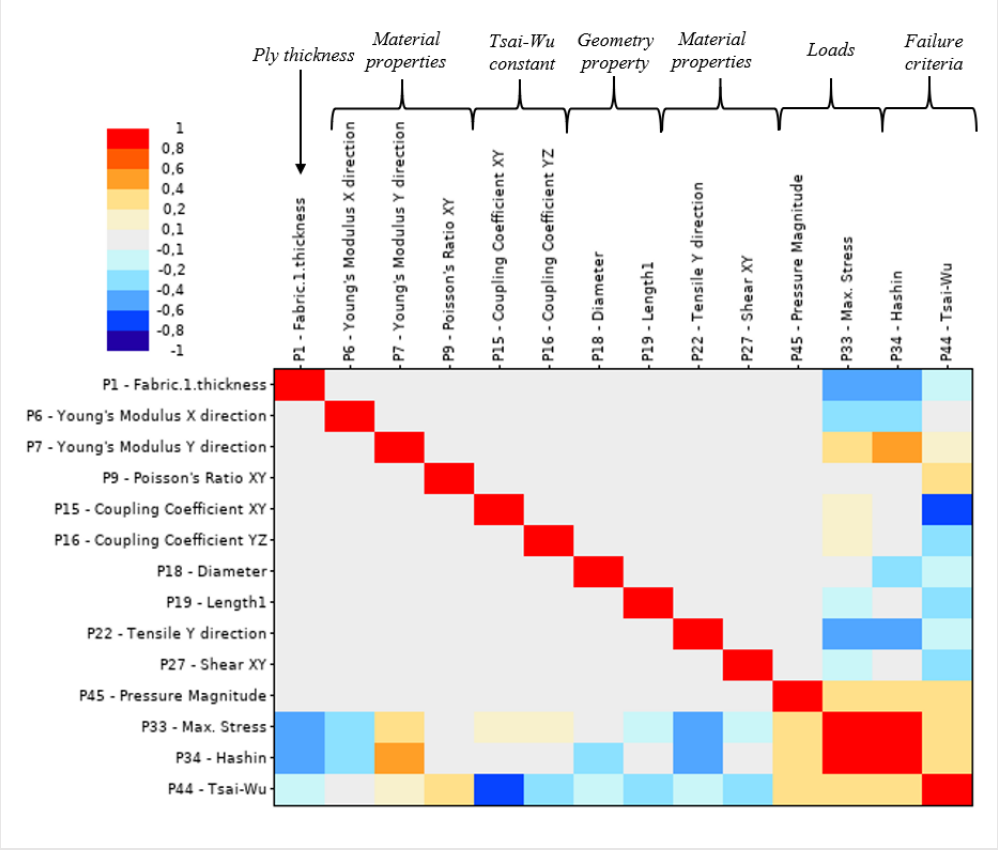

Figure 33: Detailed parameter correlation, Spearman, N=120

Table 11: Correlation coefficients for Max. Stress and Hashin

	Max. Stress	Hashin
Ply thickness	-0,55141	-0,44079
Young's modulus X direction	-0,23911	-0,27578
Young's modulus Y direction	0,36898	0,50833
Diameter	0,36776	0,3094
Tensile strength in Y direction	-0,4356	-0,47227

Correlation of Max. Stress and Hashin with Ply thickness and Tensile strength in Y direction is moderate while it is low with diameter and Young's modules in X and Y direction. The sensitiveness matrix indicates that ply thickness parameter is most important geometry parameter, which is used for failure criteria analysis, Figure 34:

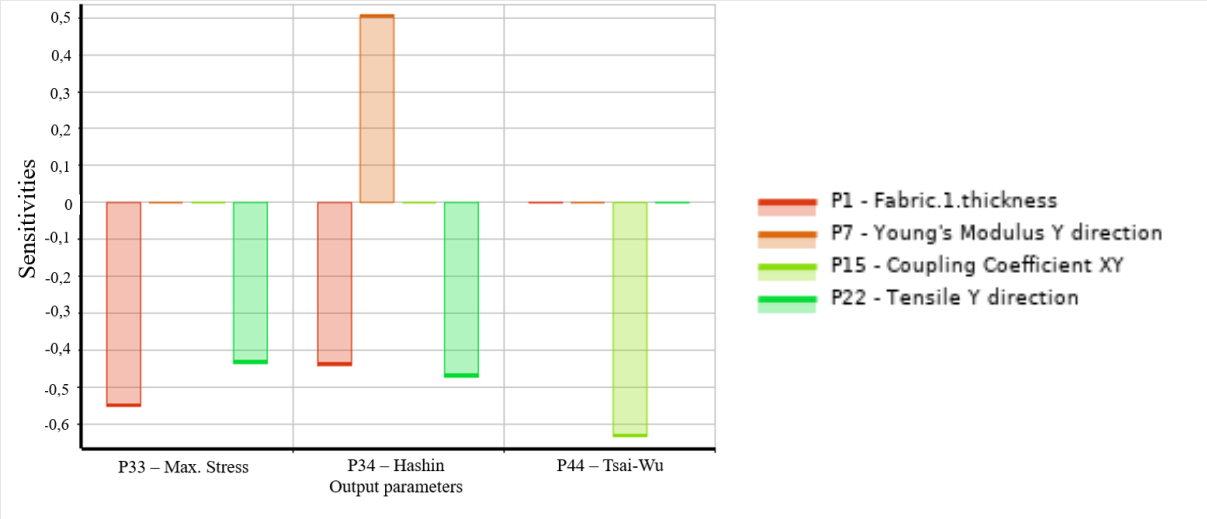

Figure 34: Sensitivities of Max. Stress, Hashin and Tsai-Wu with the N=120, spearman correlation

Figures 35 and 36 present determination matrixes for the model with the N=35, Spearman correlation. The determination coefficients (r^2) are useful as they determine the proportion of the variance of one parameter value that can be predicted from other value. Determination matrixes contain the coefficients which are measured and can be used to make predictions from the base model. The coefficients range from 1 (strongest correlation-red) to 0 (weakest) and express the strength of linear dependencies between two parameters (variation of one parameter y to the total variation of the parameters). Linear relationship between two parameters (determination coefficient) is presented with the regression equation for parameters:

$$r^2 = \frac{Sum\ of\ squares\ regression}{sum\ of\ squares\ total} = \frac{\sum(y^* - \bar{y})^2}{\sum(y - \bar{y})^2} = 1 - \frac{\sum(y - y^*)^2}{\sum(y - \bar{y})^2} \qquad (44)$$

The application of regression function can be seen in figures of determination matrixes:

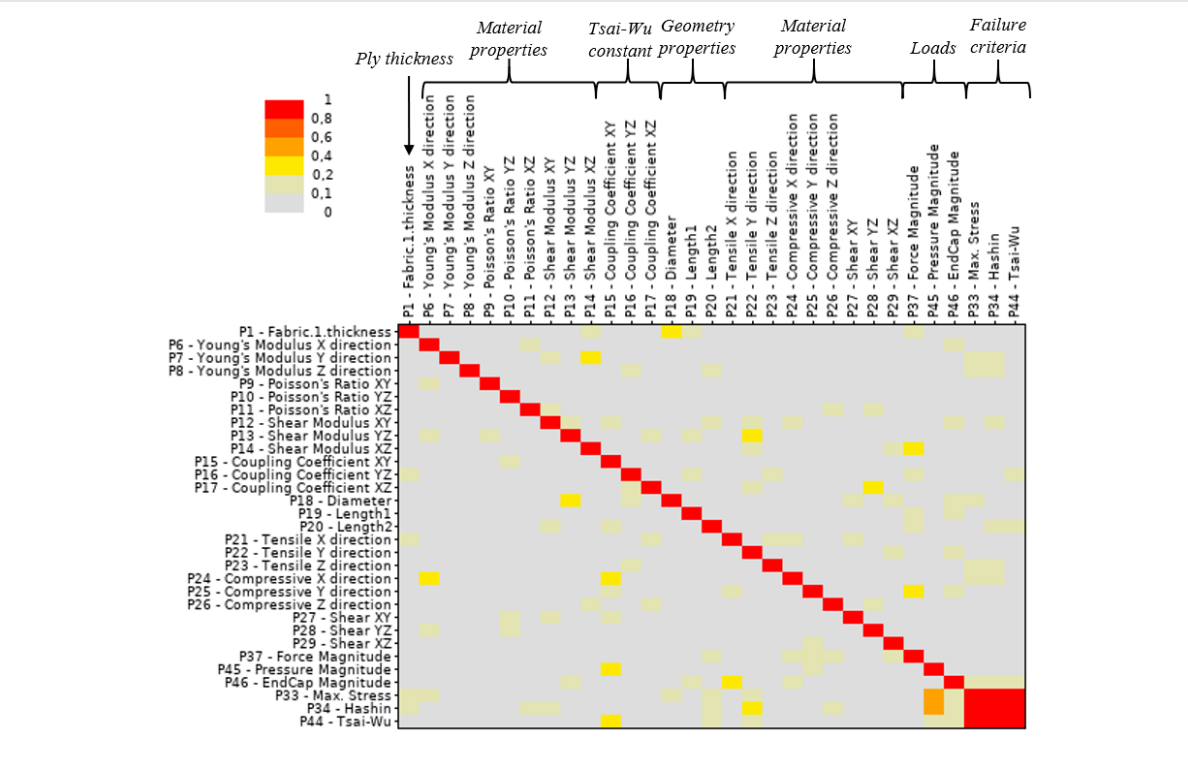

Figure 35: Determination matrix for the model, N=35, Spearman correlation

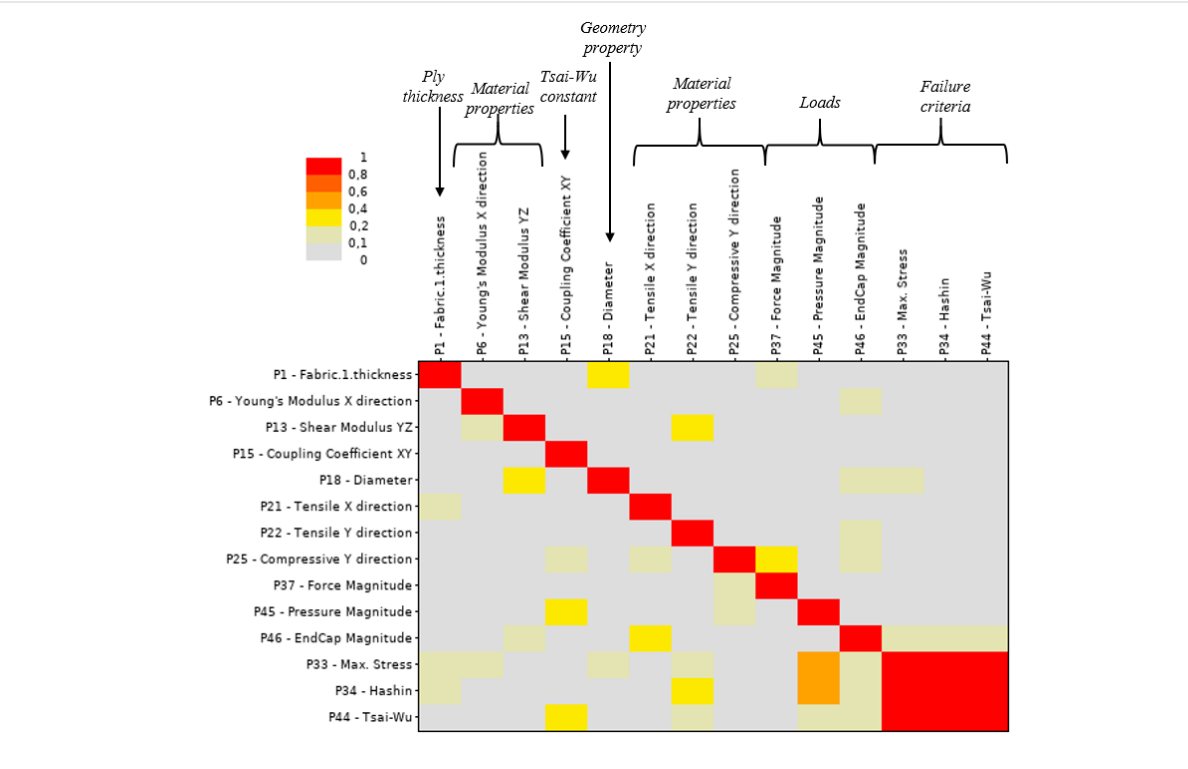

Figure 36: Detailed determination matrix, N=35, Spearman correlation

Parameter set is the same as for correlation matrixes. The determination matrix clearly shows the parameters with the highest determination coefficients. Determination coefficients are showing the % of data which is closest to the best fit line which can be reflected in scatter diagrams. The Figure 36 shows that the variation can be calculated and expressed with the linear relationship between diameter and shear modulus as well as relationship between Endcap magnitude and tensile strength in Y direction. Endcap, at the same time depends on the pressure magnitude parameter. The diameter is affected by shear modulus YZ. The Determination matrix shows that approximately 24 % of the total variation in the diameter can be explained by the linear relationship between shear modulus YZ and diameter (which can be calculate with the regression function). The same can be said about correlation of End Cap and tensile strength in X direction. The pressure perimeter relationship with coupling coefficient XY provides only 22 % of variation in pressure which can express the correlation between pressure and coupling coefficient XY.

The determination coefficients of the failure criteria relationships have high percentages (89-98%). Approximately 41% of the total variation in pressure magnitude is possible to explain with linear relationship between this applied pressure parameter value and Max. Stress failure criterion or Hashin failure criterion (both show ≈ 41% or r^2 is 0,41) So, 59% of total variation data can remain unexplained which leads to significant correlation between pressure and failure criteria.

Considering the correlation and determination matrixes above and matrixes presented on the Figures 37-38 in the sample size study, it was found that the Pressure magnitude, fabric1.thickness and diameter parameters influence the model most.

Determination matrix for N=120 is almost same and presented in the Figures 37 and 38. In The case of larger sample size, the values of determination coefficient for failure criteria parameters are higher. It is shown that approximately 29-32% of the total variation in ply thickness is possible to explain with linear relationship between ply thickness parameter value and Max. Stress failure criterion or Hashin failure criterion (both show ≈ 29-32% or r^2 is 0,29-0,32)

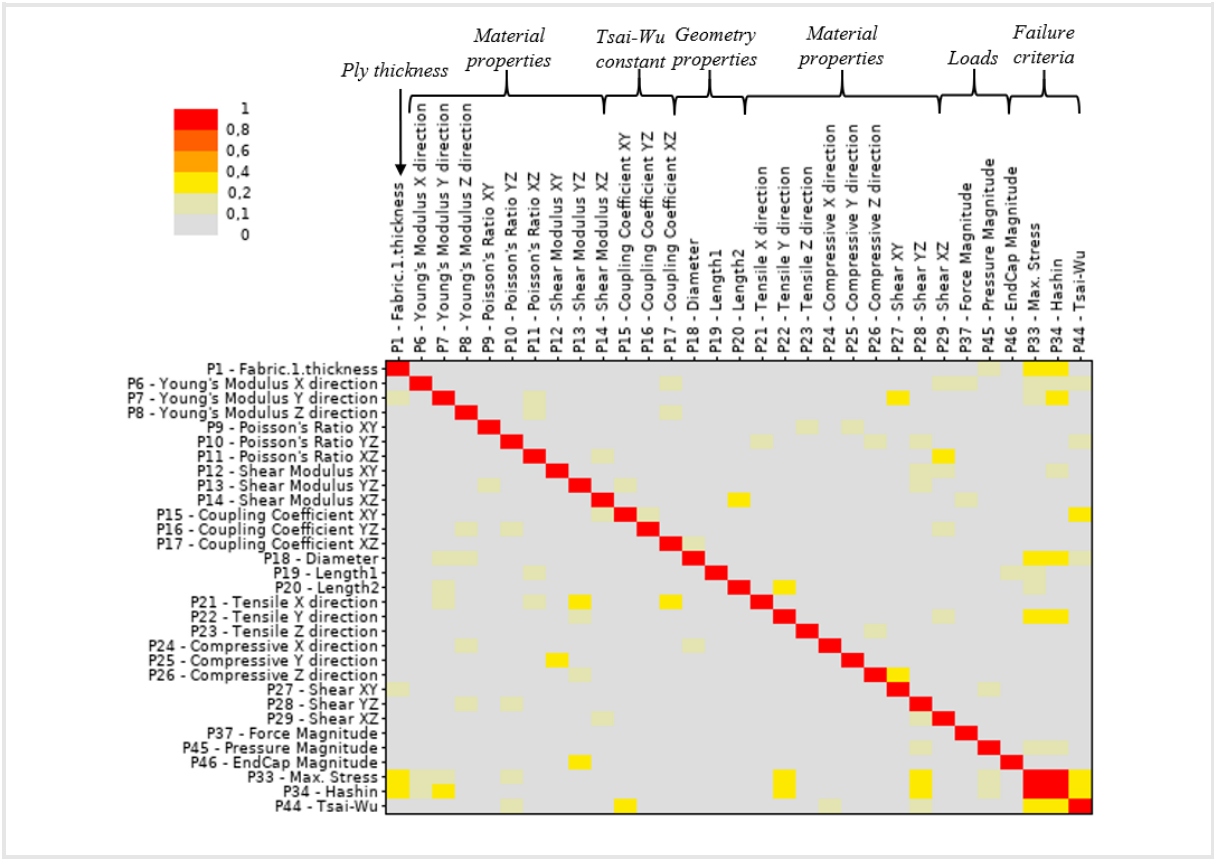

Figure 37: Determination matrix for the model, N=120, Spearman correlation

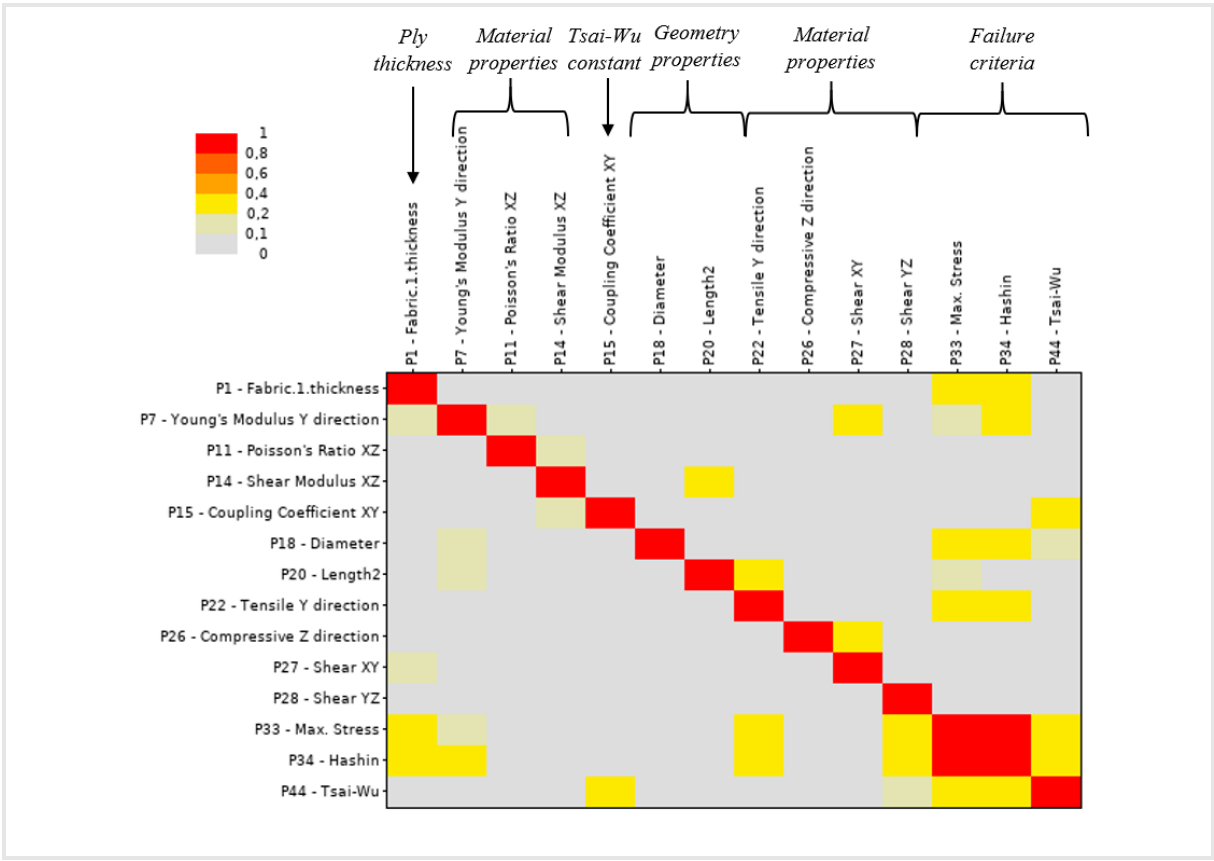

Figure 38: Detailed determination matrix, N=120, Spearman correlation

6.2 Scatter Diagrams

The scatter diagrams are presented in the figures below for sample sizes of 35 and 120. Diagrams illustrate the plots of input and output data of certain variables (x-input, y-output) with the correlation of these variables. As a result, the quadratic and linear curves are obtained with the generation of the parameter correlation. With the strong correlation, the points will fall closer to the linear and quadratic lines which leads to easier and better explanation of the variation, defined with the determination matrixes and coefficients. Scatter diagrams identify positive and negative correlations between the parameters and express their sensitivity in relation to each other.

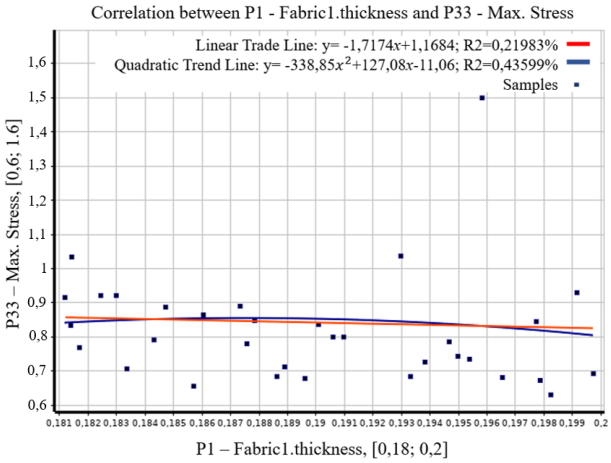

a) Fabric1.thickness vs. Max. Stress, N=35

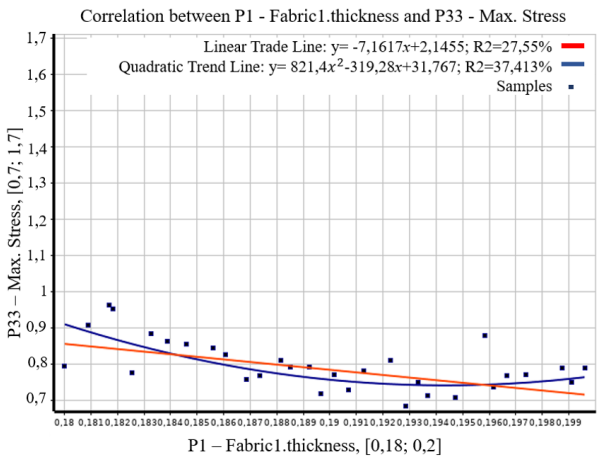

b) Fabric1.thickness vs. Max. Stress, N=120

Figure 39: Correlation scatter diagram, Fabric1.thickness vs. Max. Stress for a) N=35 and b) N=120, Spearman correlation

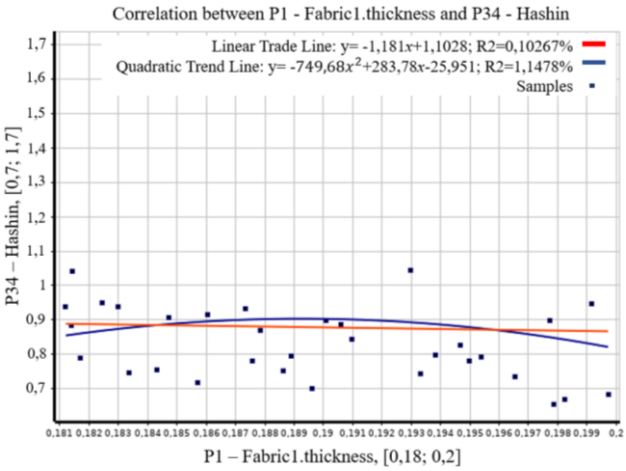

a) Fabric1.thickness vs. Hashin, N=35,

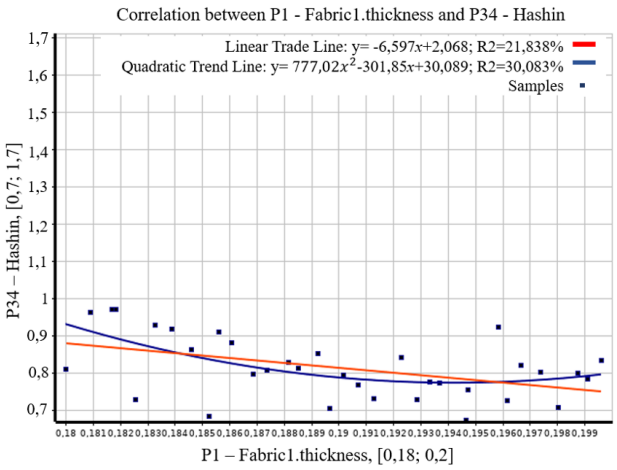

b) Fabric1.thickness vs. Hashin, N=120.

Figure 40: Correlation scatter diagram, Fabric1.thickness vs. Hashin for a) N=35 and b) N=120, Spearman correlation

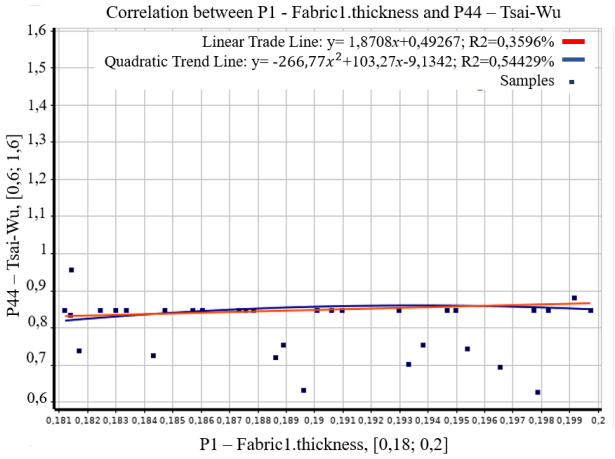

a) Fabric1.thickness vs. Tsai-Wu, N=35,

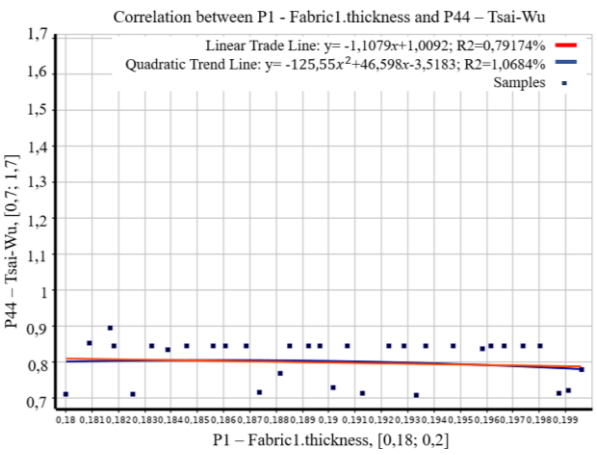

b) Fabric1.thickness vs. Tsai-Wu, N=120,

Figure 41: Correlation scatter diagram, Fabric1.thickness vs. Tsai-Wu for a) N=35 and b) N=120, Spearman correlation

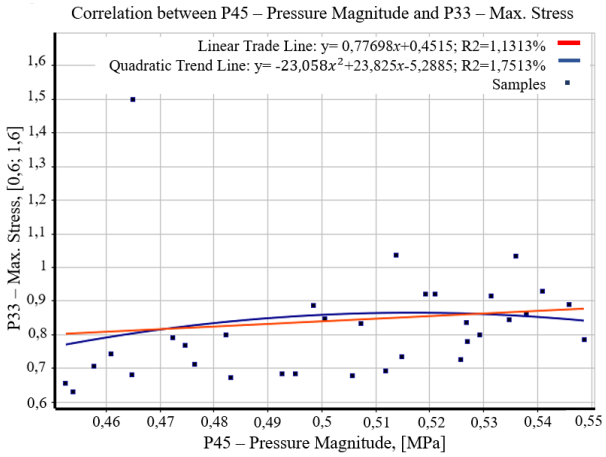

a) Pressure magnitude vs. Max. Stress, N=35

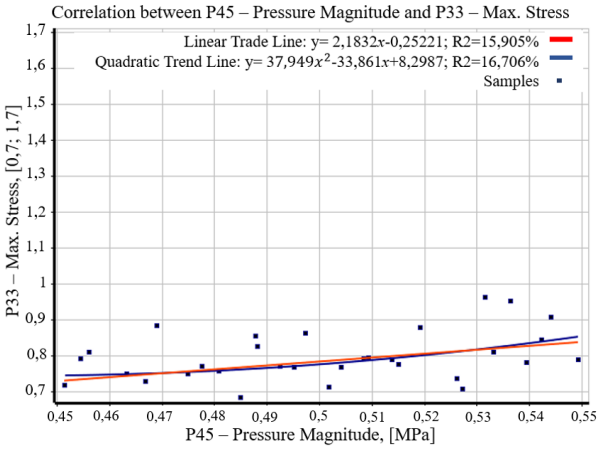

b) Pressure magnitude vs. Max. Stress, N=120,

Figure 42: Correlation scatter diagram, Pressure magnitude vs. Max. Stress for a) N=35 and b) N=120, Spearman correlation

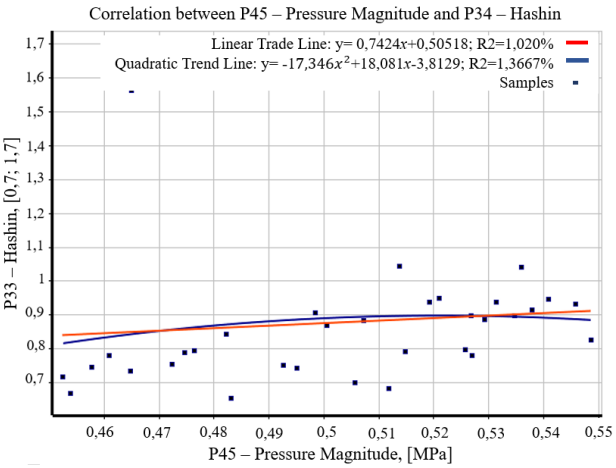

a) Pressure magnitude vs. Hashin, N=35

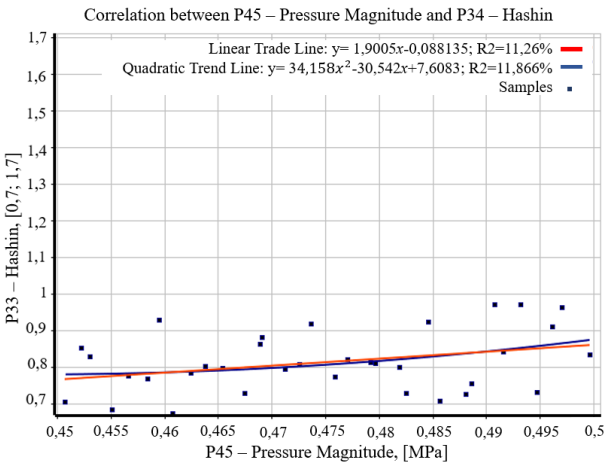

b) Pressure magnitude vs. Hashin, N=120

Figure 43: Correlation scatter diagram, Pressure magnitude vs. Hashin for a) N=35 and b) N=120, Spearman correlation

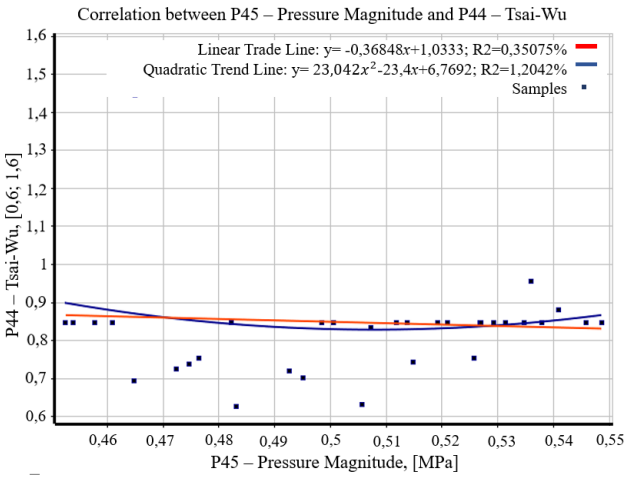

a) Pressure magnitude vs. Tsai-Wu, N=35

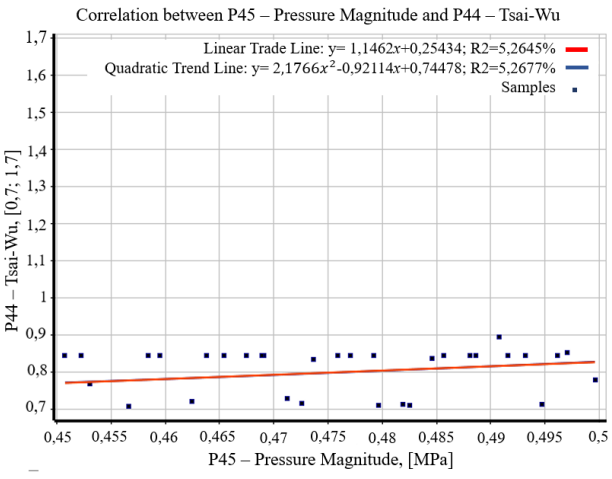

b) Pressure magnitude vs. Tsai-Wu, N=120

Figure 44: Correlation scatter diagram, Pressure magnitude vs. Tsai-Wu for a) N=35 and b) N=120, Spearman correlation

As it is shown above in the correlation matrixes, the ply thickness of curved plate, diameter of curvature and pressure parameters correlated most to the failure criteria and have the highest correlation coefficients. These parameters are considered in scatter diagrams and presented in the Figures 39 to 44. As can be seen from the diagrams, the scatter is large for all three parameters for N=35. With the application of N=120 the scatter diagram is small, so the parameter correlation is stronger. Points are closer to the linear and quadratic lines which means that the larger sample size shows give better explanation of the variations of the parameters and their stronger correlation.

For both ample sizes, Ply thickness and diameter scatter diagram for Tsai-Wu the importance of these two parameters as the point reach the curves but the scatter is still large for other cases. Parameters of pressure magnitude, ply thickness and diameter are important for failure criteria calculations and can be more precise for the scatter diagram generation in case the other important parameters were added to the study of the model (i.e., stacking sequence of plies and direction of the fiber).

6.3 Sample Size Study

The Pearson and Spearman correlation matrixes with different sample size are presented in the Figure 45.

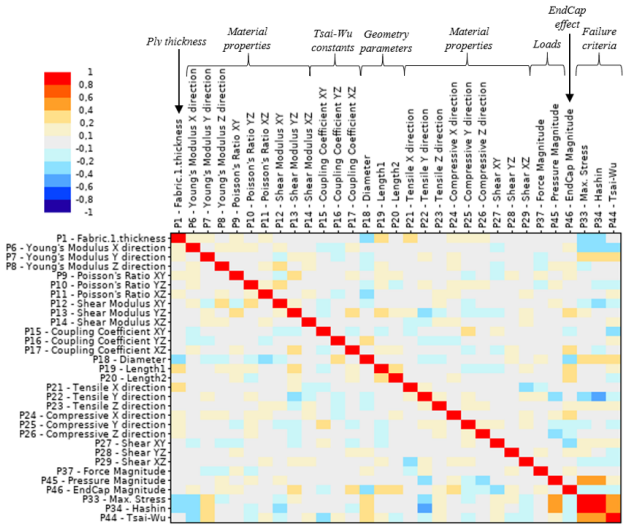

a) Spearman correlation N=35

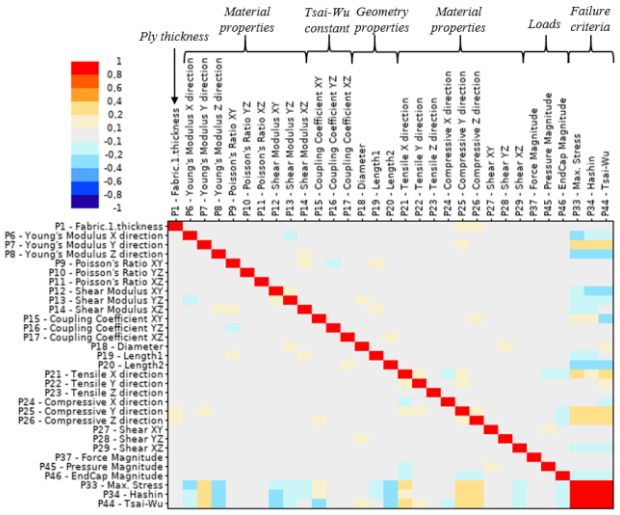

b) Pearson correlation N=35

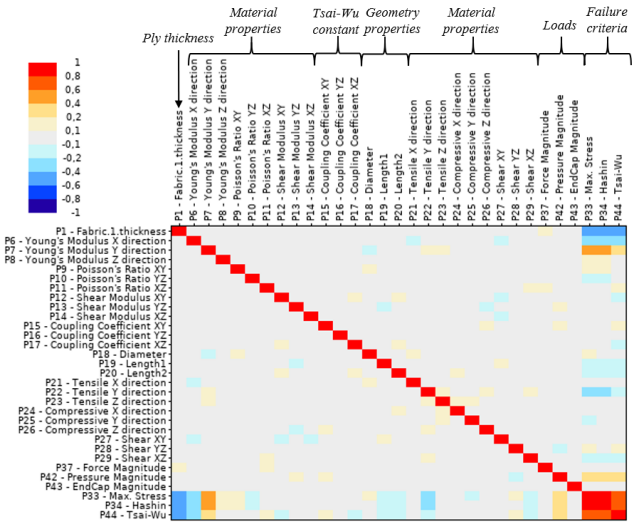

c) Spearman correlation N=60

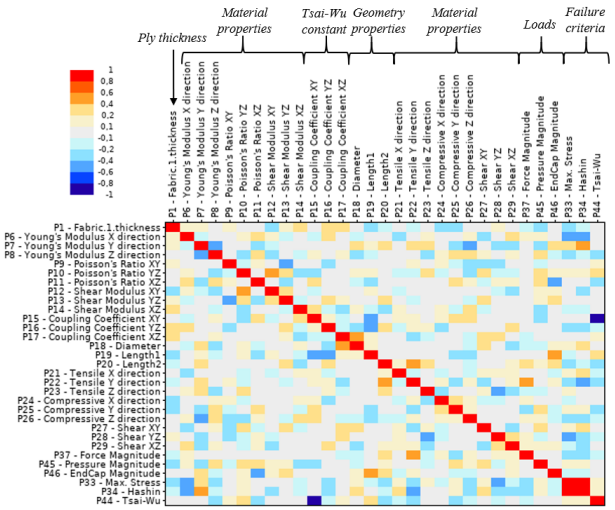

d) Pearson correlation N=60

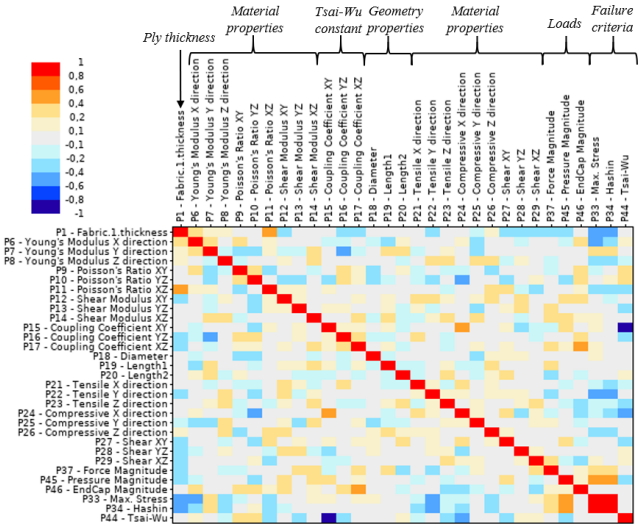

e) Spearman correlation N=90

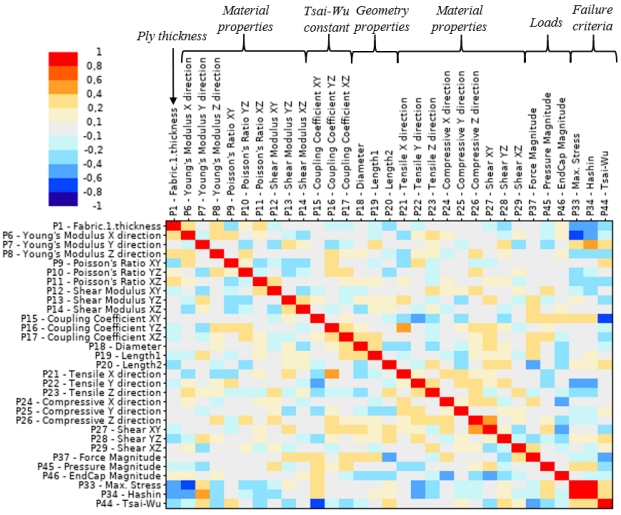

f) Pearson correlation N=90

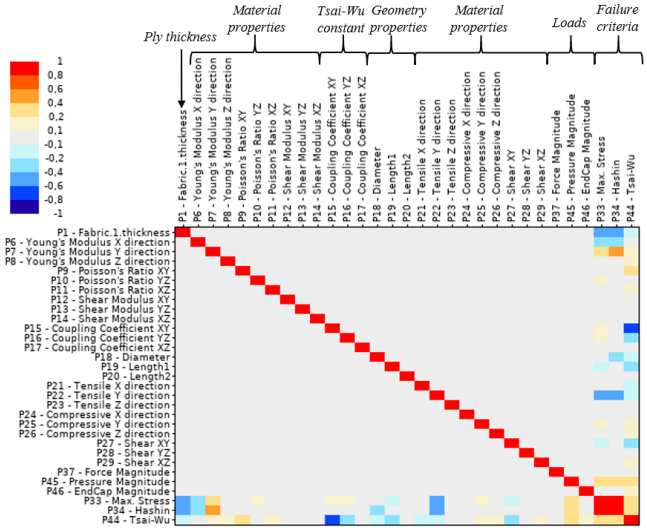

g) Spearman correlation N=120

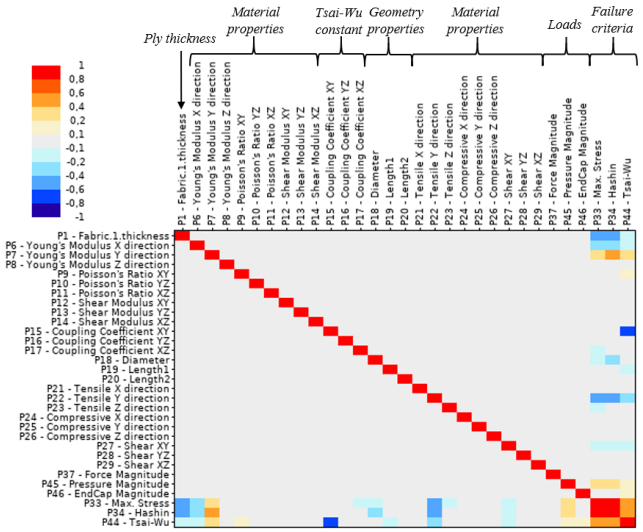

h) Pearson correlation N=120

Figure 45: Linear correlation matrices with N=35: a), b); N=60: c) d); N=90: e) f); N=120: g) h) for Spearman and Person correlation

The number of the samples (N) influences the correlation significantly and shows more precise results with the increasing of the sample size. It can be seen, both Pearson and Spearman correlations with the same number of samples provide almost similar results in correlation matrixes. However, the correlation with the N=120 shows more detailed correlation and scatter diagram result than the correlation with less sample size. For case of 34 and 60 sample size the scatter is larger than the scatter of 120 and 90 samples. Pearson correlation for 60 and 90 sample size are more detailed than Spearman, but for 120 sample size leads to similar correlation matrix of both types. The most important parameters get higher values of correlation coefficients as their weight become more obvious with increasing of sample size. Besides that, some parameters of Tsai-Wu constants, material and geometry properties obtain small correlation coefficients, so, they become lighter and decay with the increase of the sample size. Thus, the matrix is considered to become “converged”. As it is seen from the figures above, the most accurate and reasonable correlation matrix is one with the sample size of 120.

7 Response Surface Study

7.1 Design of Experiments and Response Surface Parameters

The response surface is generated in order to find the optimum values for the design of the model using ANSYS 2020 Response surface tool with the design of experiment response surface cells. Further optimization of response surface was done. Five types of central composite design of DoE type response surface and one custom + sampling response surface were generated.

The Spearman correlation type with the sample size of 35 and 120 was used to find the coefficients of correlation between the failure criteria and important input parameters. To generate the response surface, 15 parameters with the highest correlation coefficients were chosen from the response surface parameter set in ANSYS Workbench 2020. Higher correlated response surface parameters are listed in the Table 12.

Table 12: Parameters with biggest influence on the model design used in Response surface simulation

Name of parameter	Symbol	Range of parameter value		Unit
		Lower limit	Upper limit	
Fabric1.thickness	t	0,18	0,2	Mm
Youngs modulus in X direction	E_1	108900	133100	MPa
Youngs modulus in Y direction	E_2	7740	9460	MPa
Poisons Ratio XZ	ν_{13}	0,243	0,297	-
Shear modulus XY	G_{12}	4230	5170	MPa
Coupling coefficient XY	F_{12}	-1,1	-0,9	-
Diameter (plate curvature D)	OD	1900	2000	Mm
Length1	L_1	81	99	Mm
Length 2	L_2	54	66	Mm
Tensile strength in Y direction	σ_2^T	26,1	31,9	MPa
Compressive strength in Z direction	σ_3^C	-110	-90	MPa
Shear XY	τ_{12}	54	66	MPa
Force Magnitude	F	0,27	0,33	MN
Pressure magnitude	P	0,45	0,5	MPa
End Cap Magnitude	F_{EndCap}	70685,8	86393,8	MN

For parameters which are used for response surface simulation, the upper and lower limit of each parameter is established (see Table 12). The range include the parameters' value which will define the failure criteria values with no errors. The appropriate range for values of the parameters guarantees the accuracy of the response surface results.

The number of design of experiments samples were defined automatically with ANSYS Workbench 2020 and equal to 287. This number depends on the number of input parameters which are selected for the response surface simulation. The design of experiments (DoE) samples was generated with 15 selected parameters. Different input parameters number with DoE size is presented in the Table 13 below. The accuracy of the response surface results increases with the larger number of input parameters. The minimum correlation coefficient will increase with decreasing number of input parameters.

Table 13: Different Number of Input Parameters and the DoE size

Number of Input Parameters	DoE size, Number of Sample Points
10	149
15	287
20	551

The prediction of failure criteria values and preventing the model from failure can be done easily with logical increasing of the thickness with the same or reduced pressure value. This will create both less stress and larger number of laminates which will make analysis more complicated and time consuming but will decrease the possible error and will increase the safety of the model. The goal is to find the exact combination of parameter values which will give the lowest possible failure for the design model. The response surface study is investigated for this purpose and presented below. The ply thickness and pressure magnitude parameters range are selected to be changed to improve the efficiency of the response surface.

7.2 Response Surface Simulation

The DoE helps to predict the behaviour between the samples. Difficulties to find the optimum decision rise with the increasing for the input parameters. The purpose of the response surface is to interpolate the values of the parameters in their multiple dimensions.

7.2.1 Central Composite Design Response Surface

Generating the response surface, the minimum and maximum values for failure criteria were found as output parameters. They are presented in the Table 14. The parameters in design of experiment are indicated in the Table 14 with the ranges. Auto defined design type tool in CCD helps to optimize the DoE based on the number of input parameter.

Table 14: Minimum and maximum failure criteria values in Design of Experiments of 2nd order polynomial response surface

	Max. Stress	Hashin	Tsai-Wu
Max value	0,84253	0,88647	0,84588
Min value	0,61203	0,66594	0,62807

For the CCD response surfaces, the values from the outputs can be shown in the chart of the design points vs. parameters. Design point values for the output minimum and maximum failure criteria for simple 2nd order polynomial response surface are shown in the Figures 46 and 47:

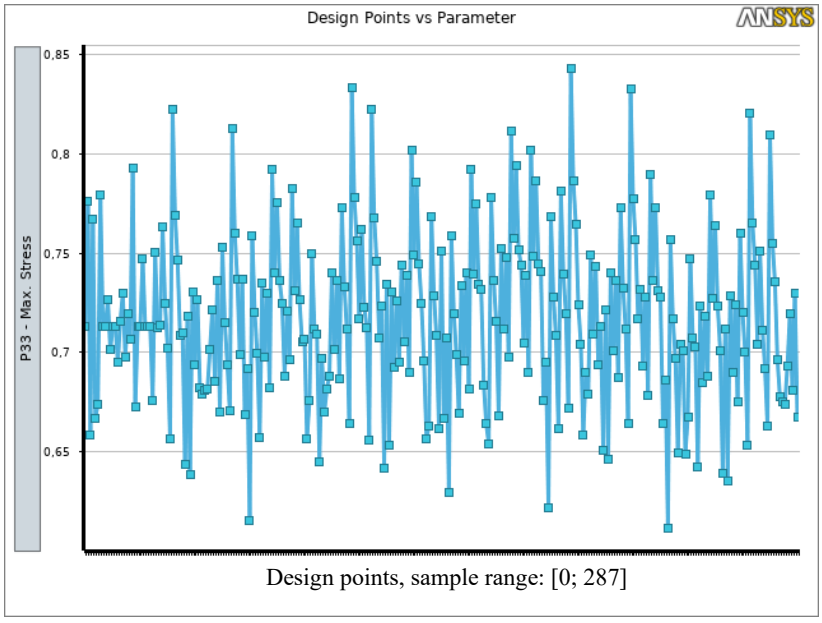

Figure 46: Design point values for the output minimum and maximum failure criteria for simple 2nd order polynomial response surface for Max. Stress failure criterion for the samples range: [0; 287]

The x-axis represents the design points of the range from 0 to 287 and the y-axis is Max. Stress values. The maximum and minimum values from the Figure 46 are presented in the Figure 47 below.

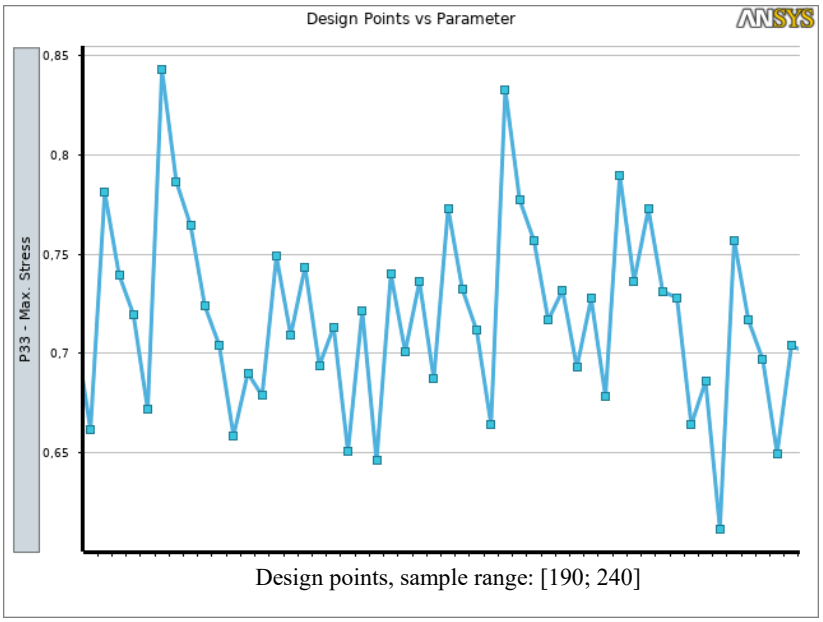

Figure 47: Design points for the output minimum and maximum failure criteria for simple 2nd order polynomial response surface for Max. Stress failure criterion in the samples range: [190; 240]

The maximum value for Max. Stress failure criterion in the design points range is 0,84253 (design point (DP) 196) and the minimum is 0,61203 (design point 235). The value of Max. Stress with minimum values should be considered for the design. Considering the combination of the main parameters which can influence the design and the failure criteria most (pressure, diameter, ply thickness) the further conclusion can be made. Smaller diameter value and higher-pressure value were chosen for the Max. Stress failure criterion with value of 0,84253. On the other hand, larger diameter and smaller pressure value was chosen for the Max. Stress failure criterion with value of 0,61203. With the considering of other input parameters the result can be even more complex. Even if there is one combination which is optimal for the requirements, there can be more possible combinations which also meets the optimal failure criteria results.

On the Figure 47 can be seen that approximately half of the design points have Max. Stress failure criterion values under 0,7 and ¼ with less than 0,6.

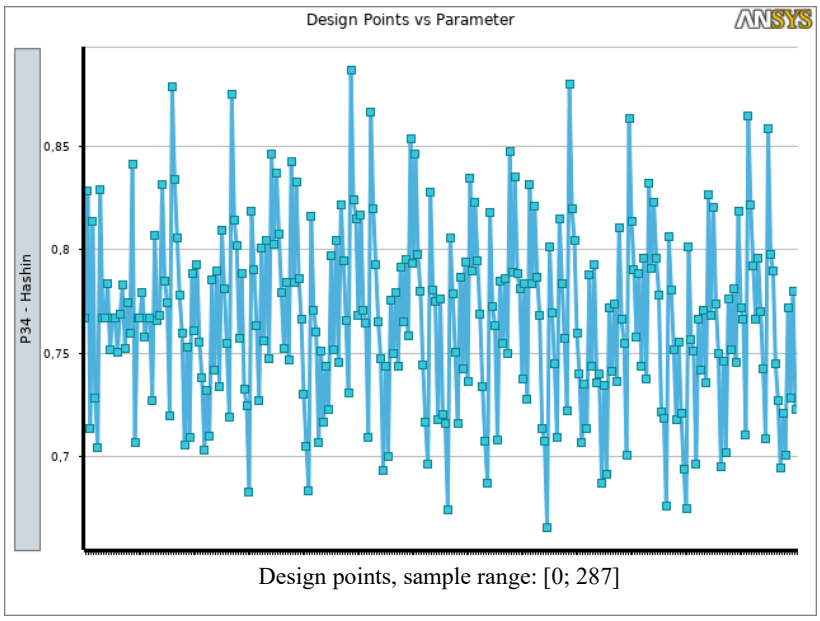

Figure 48: Design point values for the output minimum and maximum failure criteria for simple 2nd order polynomial response surface for Hashin failure criterion for the samples range: [0; 287]

The y-axis in Figure 48 represents the Hashin maximum and minimum failure criterion values: 0,88647 (Design point 108) and 0,66594 (Design point 187) respectively.

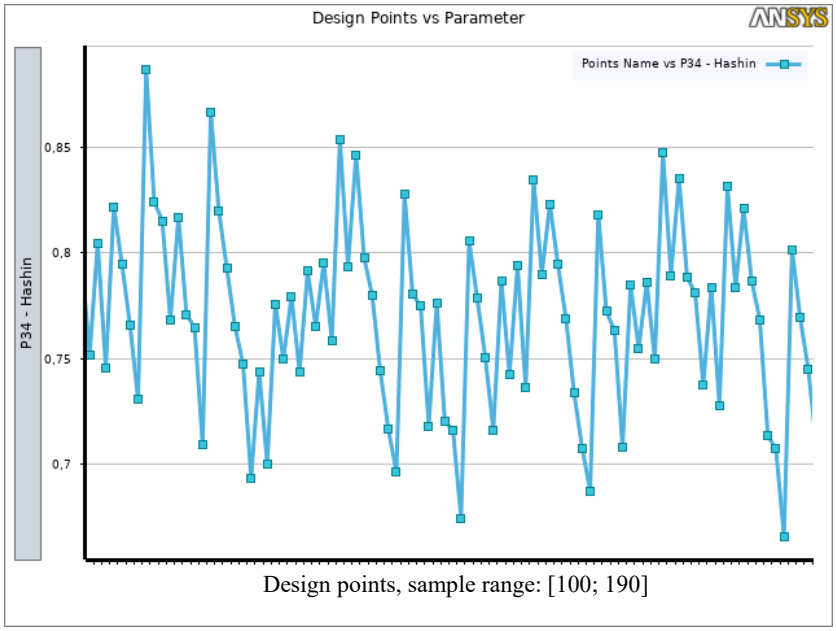

Figure 49: Design points for the output minimum and maximum failure criteria for simple 2nd order polynomial response surface for Hashin failure criterion in the samples range: [100; 190]

In combination with the pressure magnitude and ply thickness parameters, the following should be considered simultaneously: with the increasing of pressure parameter and decreasing of the ply thickness, the value of Hashin failure criteria will increase. Parameters with the lowest failure values should be considered for the design.

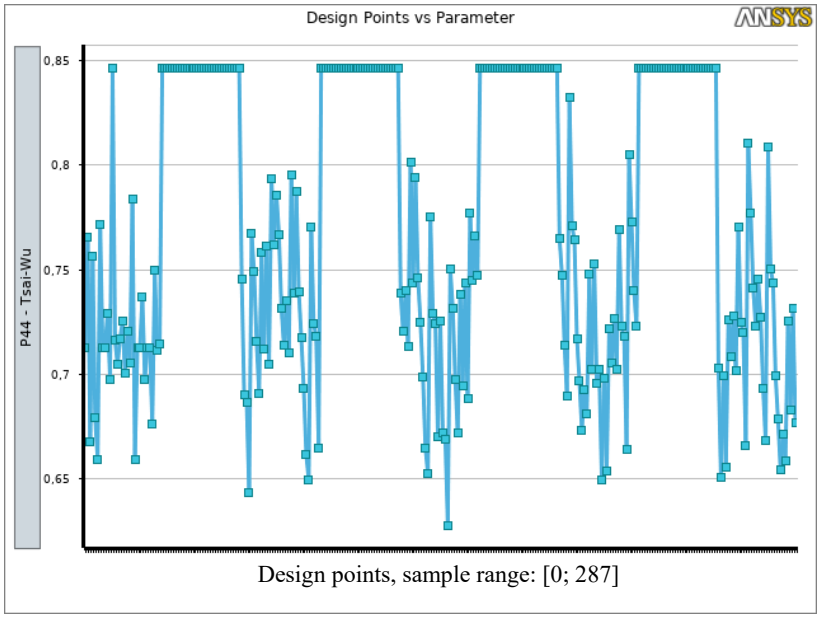

Figure 50: Design point values for the output minimum and maximum failure criteria for simple 2nd order polynomial response surface for Tsai-Wu failure criterion for the samples range: [0; 287]

Figures 50 and 51 are presenting the Tsai-Wu failure criterion results with the generated design points. Y-axis is Tsai-Wu failure criterion values in this case.

The minimum value has the design point number 147 which is equal to 0,62807. Several design points reach maximum value which is equal to 0,84588 and leads to increased failure probability. The value of 0,84588 belong to 126 design points (almost a half of all design points). The behaviour of the failure values due to change in pressure and ply thickness is the same as in Hashin and Max. Stress failure criteria.

The design points with the lowest failure criteria values should be used for the design of the model. The same values and design points vs. parameters charts were generated in other studied response surface types: Kriging, Non-parametric regression, Neural Network, Generic Aggregation.

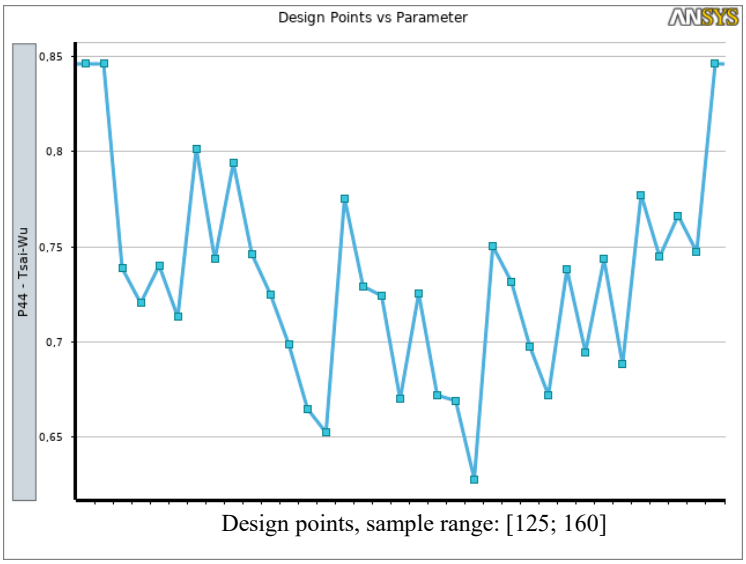

Figure 51: Design points for the output minimum and maximum failure criteria for simple 2nd order polynomial response surface for Tsai-Wu failure criterion in the samples range: [125; 160]

The response surface cell is used after DoE. In this part, the behaviour of the failure criteria is shown within the influence of pressure magnitude or ply thickness changes. Figure 52 illustrates the standard response surface 2nd order polynomials type with chosen manual refinement. Number of initial samples is 100 with the 3 start points. The failure criteria values are increasing when the ply thickness is decreasing. The reverse behaviour is with the pressure magnitude. The values of failure criteria will increase with the increasing of the pressure magnitude.

In general, the behaviour for all three failure criteria with the change of the pressure and ply thickness remain the same. Non-parametric regression response surface cell of ANSYS Workbench 20.0 results of the failure criteria and main parameters has parabolic form but follow the same pattern.

For the same type of CCD response surface, the goodness of fit matrix is established. It is calculated for DoE points and can also be calculated for verification points to check how accurately the response surface can predict the design points. For the comparison, the goodness of fit matrix for the Generic Aggregation was generated (Figures 53 and 54),

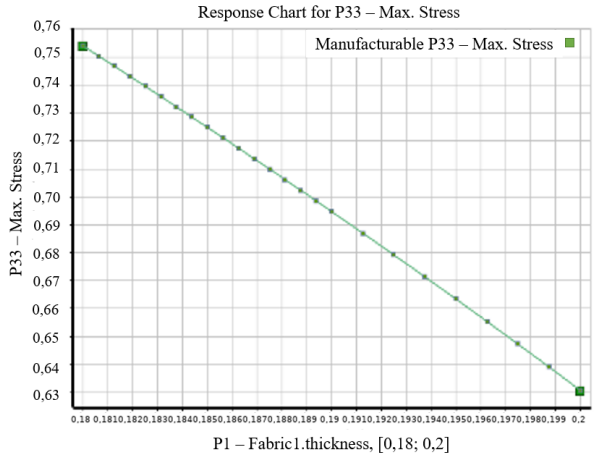

a) Max. Stress vs. Fabric.1 thickness

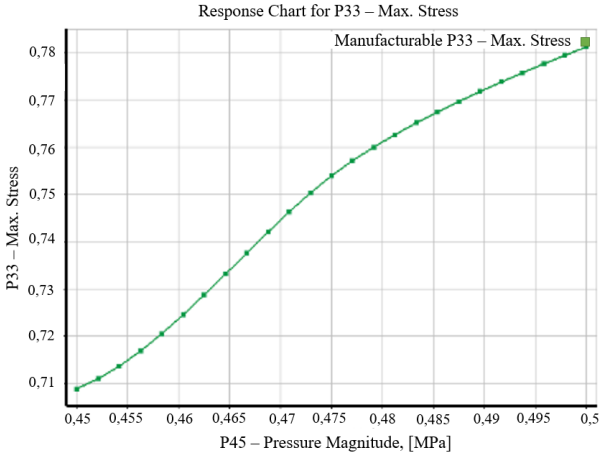

b) Max. Stress vs. Pressure magnitude

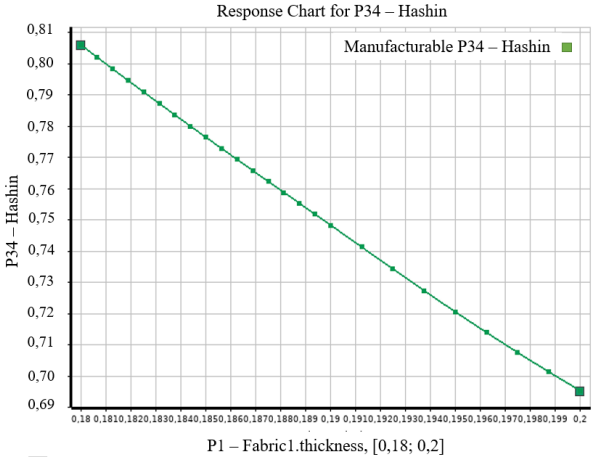

c) Hashin vs. Fabric.1 thickness

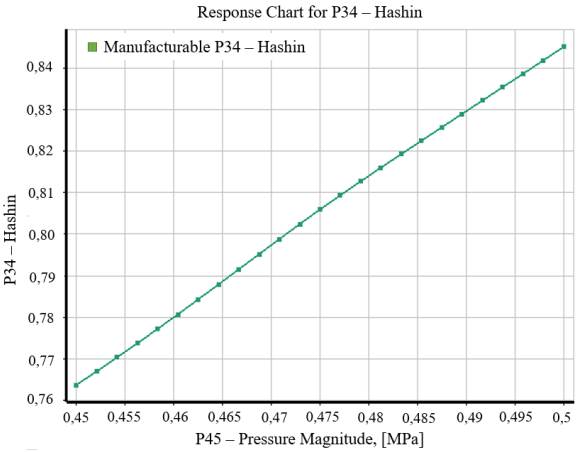

d) Hashin vs. Pressure magnitude

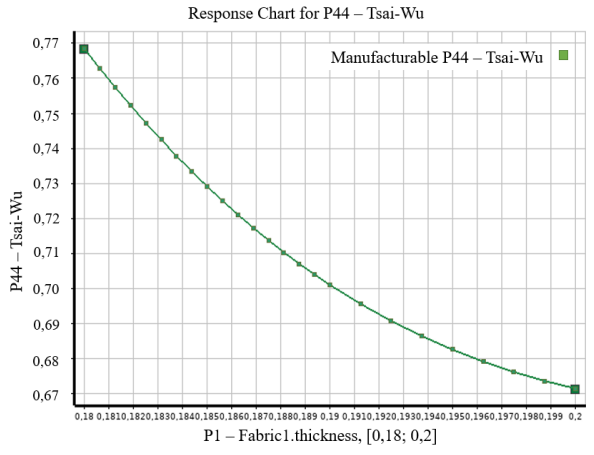

e) Tsai-Wu vs. Fabric.1 thickness

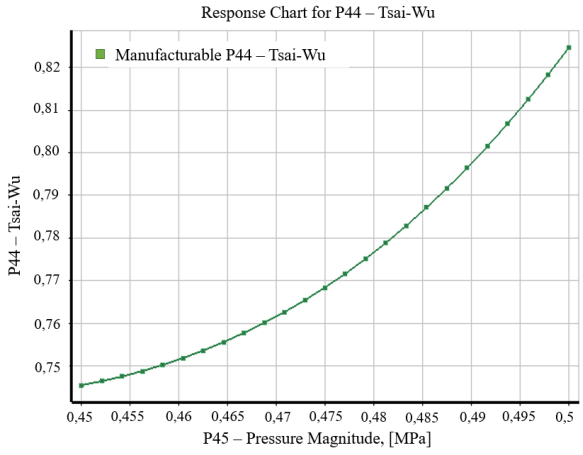

f) Tsai-Wu vs. Pressure magnitude

Figure 52: The behaviour of the a), b) Max. Stress, c), d) Hashin and e), f) Tsai-Wu failure criteria under the influence of pressure magnitude and ply thickness changes (2nd order response surface)

As was said above, the examples of the predicted vs. observed charts which shows goodness of fit data for one or more outputs for studied 2nd order polynomial and Generic aggregation response surfaces (RS) are presented below:

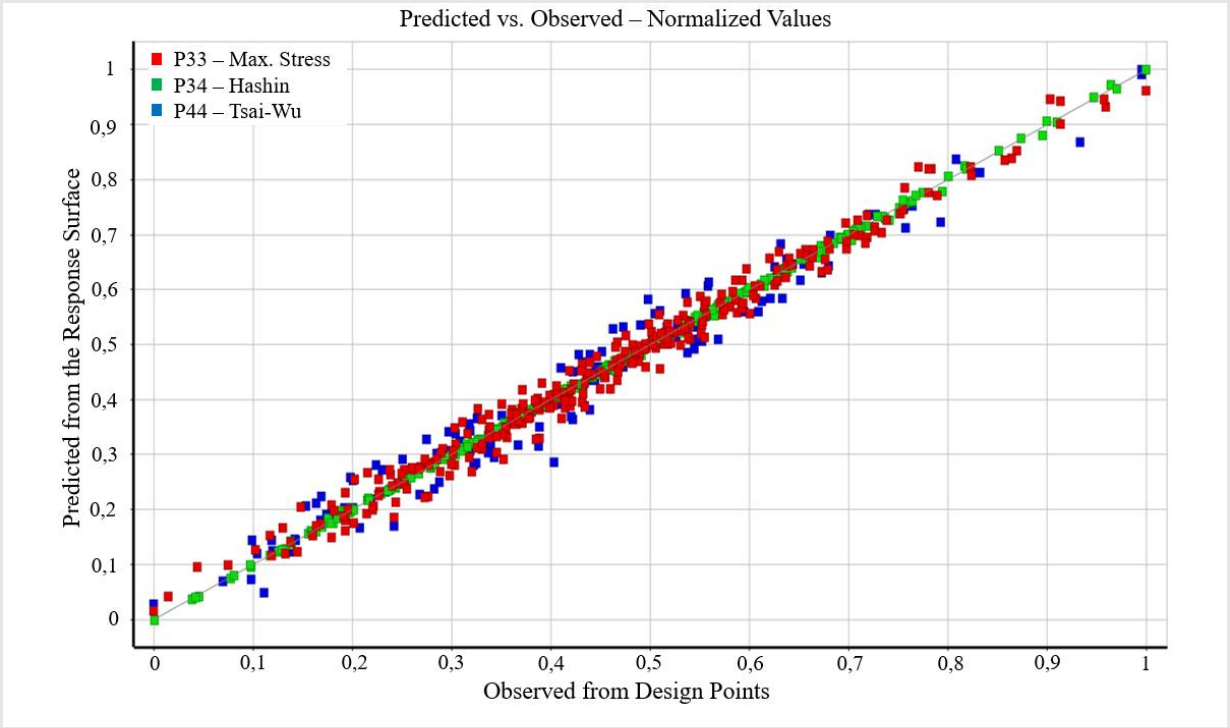

Figure 53: Goodness of fit chart for 2nd order polynomial RS

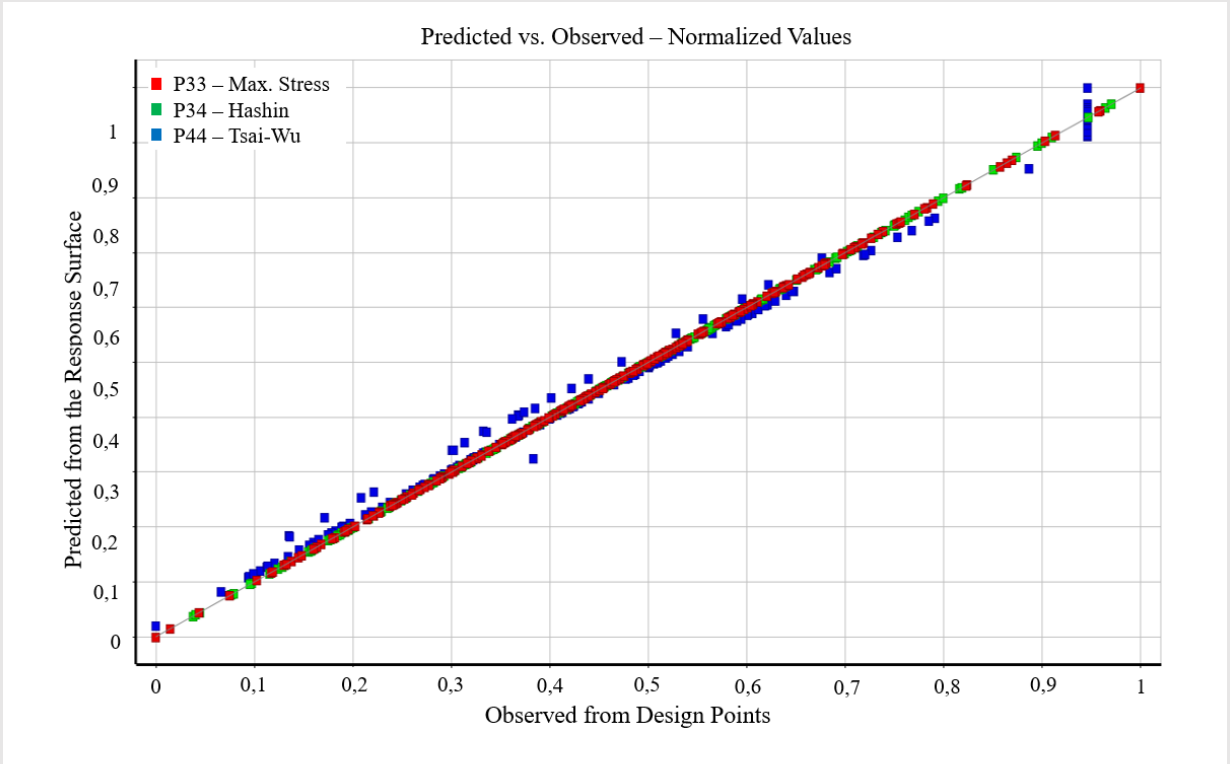

Figure 54: Goodness of fit chart for Generic Aggregation RS

Each rectangular point includes the input and output values. All the points fall on or near the line which means that the response surface can predict values for most of the design points withing its range. The response surface is a well fit for the DoE points. Table 15 below contains data of goodness of fit chart of the 2nd order polynomial and Generic Aggregation. Each of the criteria is calculated regarding the two outputs. The values of determination coefficient for Kriging reaches 1 for each failure criteria with the almost negligible error. Non-parametric regression and Neural Network response surfaces determination coefficients for Tsai-Wu were determined as 0,99681 and 0,99768 respectively with the 3, 3% relative average absolute error for both.

Table 15: Goodness of fit chart data of the 2nd order polynomial and Generic Aggregation

Simple 2nd order polynomial response surface		
Failure criterion	Coef. of determination	Relative Average absolute error, %
Max. Stress	0,98371	10,099
Hashin	0,99963	1,354
Tsai-Wu	0,99361	4,7021
Best value	1	0
Generic Aggregation		
Failure criterion	Coef. of determination	Relative Average absolute error, %
Max. Stress	0,98998	0,0001
Hashin	0,99837	0,0001
Tsai-Wu	0,99681	4,2169
Best value	1	0

The values close to the best one shows how closely the parameter comes to the ideal value for each criterion. The best match of parameters has the closest value to the best value. There are also two different sensitivity results available for the response surfaces- the local sensitivity curves chart and the local sensitivity chart. These charts are local in the sense that they show the sensitivity values local to the current response point.

The local sensitivity curves chart uses multiple curves shows the local sensitivities. The

show the effect of selected input parameters on the output parameters as well as the impact on the other input parameters. As examples, the local sensitivity charts for studied 2nd order polynomial and Generic aggregation response surfaces are presented in Figures 55 and 56.

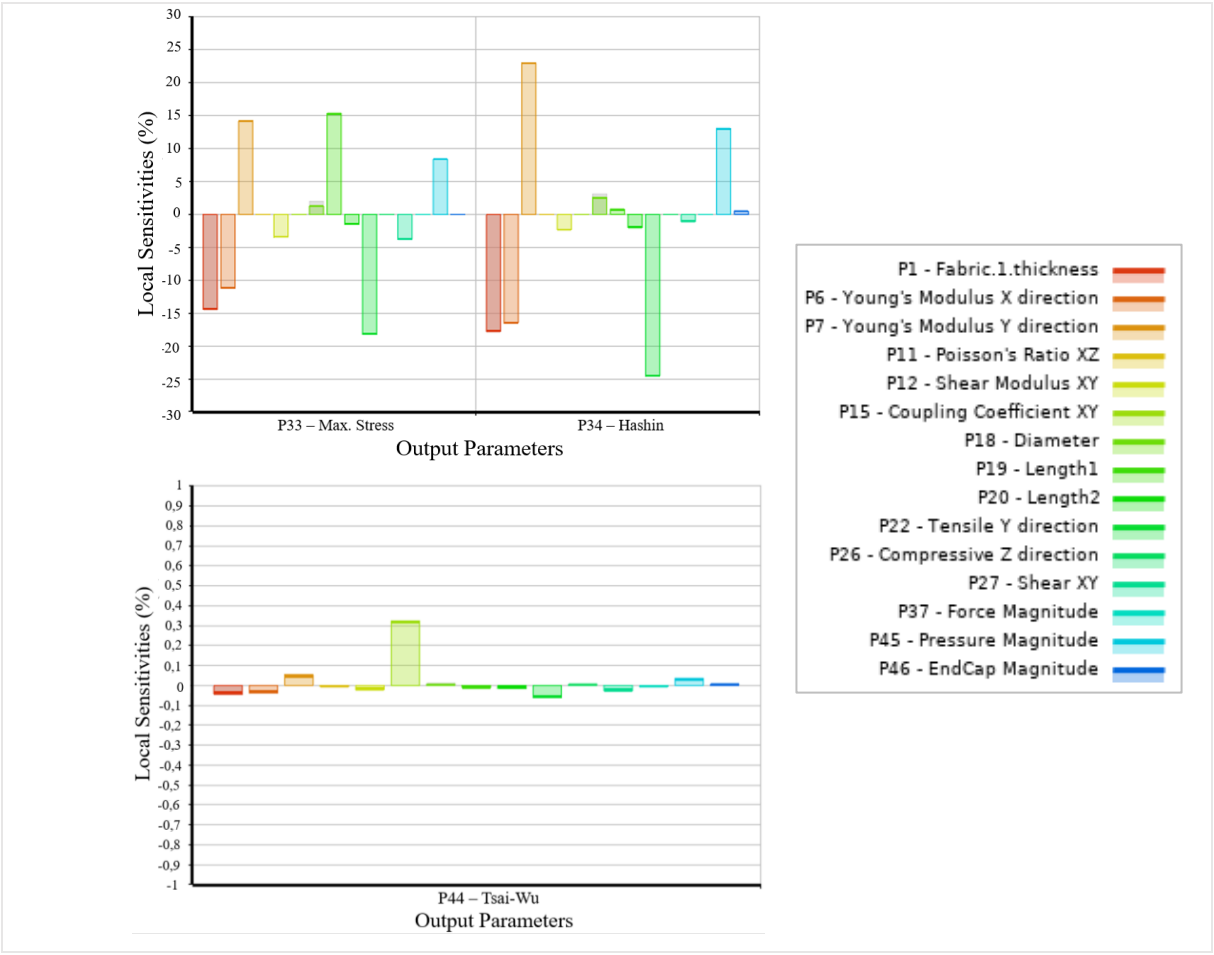

Figure 55: Local sensitivity charts for studied 2nd order polynomial response surface

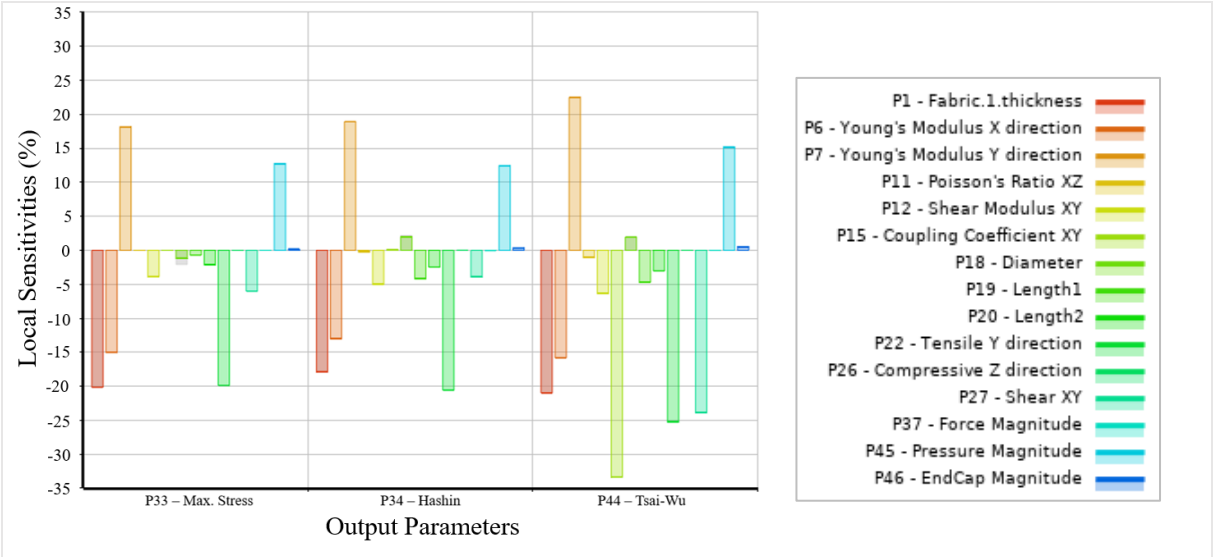

Figure 56: Local sensitivity charts for studied Generic Aggregation response surface

Local sensitivity charts show the sensitivity across the range with each input represented in different colors. Sensitivities are shown for the tree different failure criteria. For the Max. Stress failure criteria, the Ply thickness, Youngs modulus in Y direction and tensile in Y direction are negatively correlated with the load impact. Youngs modulus in Y direction has almost the same impact as Ply thickness on the Max. Stress failure criteria result. Tensile strength in Y direction bar is almost twice lower than the Youngs modulus in Y direction bar for the optimal Max. Stress failure criterion. Youngs modulus in X direction is positively correlated and has an impact on the Max. Stress failure criterion but inversely. When the ply thickness decreasing and the pressure magnitude increasing, the rise of the Max. Stress can be observed. Length 2 of the stiffener as well as the diameter has very low impact on the criterion. Almost the same situation is happening with the Tsai-Wu and Hashin failure criteria. The material parameters which influence the failure criterion much are Youngs modulus in X and Y direction as well as tensile strength in Y direction. The load and geometry parameters which influence the failure criteria most are ply thickness, the diameter of curvature of the plate itself, lengths of the attached stiffeners and pressure magnitude applied to the plate.

The min-max part in the response surface gives the results of the minimum and maximum values for 3 candidate points usually generated in ANSYS. The results from all five CCD response surfaces (RS) can be seen below in Table 16 and 17. Generic Aggregation in the table 16 contains the Maximum predicted error in the failure criteria calculations. The minimum and maximum values are shown in bold.

Table 16: Minimum-maximum failure criteria values of Generic Aggregation RS

Generic Aggregation							
Candidate points ➡	Calculated minimum			Calculated Maximum			Max. Predicted error
	1	2	3	1	2	3	
Max. Stress	**0,47347**	0,48736	0,49031	**1,0568**	1,0502	1,0143	0,067841
Hashin	0,46838	**0,44903**	0,50168	1,0772	**1,0866**	1,0516	0,007135
Tsai-Wu	0,81922	0,70723	**0,51152**	0,78375	0,7518	**0,94072**	0,068852

Table 17: Minimum-maximum failure criteria values of different response surfaces

Simple 2nd order polynomial response surface						
Candidate points ➡	1	2	3	1	2	3
Failure criterion	Calculated minimum			Calculated Maximum		
Max. Stress	**0,38262**	0,61285	1,0089	**1,2364**	1,0804	0,51617
Hashin	0,54871	**0,50848**	1,0864	1,1131	**1,1304**	0,50957
Tsai-Wu	0,66536	3,2057	**0.17213**	1,223	1,2989	**1,1946**
Kriging						
Failure criterion	Calculated minimum			Calculated Maximum		
Max. Stress	**0,39062**	0,49698	0,52648	**1,3389**	1,0838	0,72366
Hashin	0,54344	**0,50912**	0,54154	1,0986	**1,1749**	0,55523
Tsai-Wu	1,6753	0,92678	**0,27498**	1,2371	1,4026	**1,6901**
Non-Parametric Regression						
Failure criterion	Calculated minimum			Calculated Maximum		
Max. Stress	**0,62747**	0,6324	0,6525	**0,83063**	0,83063	0,66063
Hashin	0,68445	**0,67456**	0,70112	0,86111	**0,86864**	0,70778
Tsai-Wu	0,76283	0,74999	**0,6441**	0,85779	0,85411	**0,93648**
Neural Network						
Failure criterion	Calculated minimum			Calculated Maximum		
Max. Stress	**0,53881**	0,55426	0,60617	**0,91488**	0,91391	0,90062
Hashin	0,58042	**0,56346**	0,59397	0,97327	**0,99123**	0,98949
Tsai-Wu	0,84077	0,83924	**0,50505**	0,74136	0,6918	**1,1807**

Considering the results above, the response surface with the appropriate candidate points with failure criteria values are defined in the Table 16 and 17. The optimal response points with parameters values and appropriate failure criteria values, that can be used in the design are presented in the Table 18.

Table 18: Failure criteria values for defined optimal response point with parameters

		Max. Stress	Hashin	Tsai-Wu
2nd order polynomial		0,75611	0,80821	0,77002
Kriging		0,77226	0,81315	0,80299
Non-parametric regression		0,75166	0,8033	0,79315
Neural Network		0,76477	0,82669	0,76186
For each sub-type of CCD response surface	Fabric1.thickness		0,18	Mm
	Youngs modulus in X direction		121000	MPa
	Youngs modulus in Y direction		8600	MPa
	Poisons Ratio XZ		0,27	-
	Shear modulus XY		4700	MPa
	Coupling coefficient XY		-1	-
	Diameter (plate curvature D)		1900	Mm
	Length 1 (L_1)		90	Mm
	Length 2 (L_2)		60	Mm
	Tensile strength in Y direction		29	MPa
	Compressive strength in Z direction		-100	MPa
	Shear XY		60	MPa
	Force Magnitude		30000	MN
	Pressure magnitude		0,475	MPa
	End Cap Magnitude		0,7854	MN

The Generic Aggregation (GA) response surface results are shown separately in the Figure 19. The results suggest three candidate point for the design with the different values of failure criteria. The optimization of the response surface was investigated for the response surface with values off diameter (maximum 2000 mm) and ply thickness (maximum 0,2 mm). Apart from three candidate points, the response point in GA can be considered as optimal point for the design of the plate with stiffeners.

Table 19: Optimal response points with parameters and Failure criteria values for Generic Aggregation response surface

Response surface / Parameter	Candidate points			**Response point of GARS**	Unit
	1	2	3		
Ply thickness	0,2	0,2	0,18	0,18	Mm
Young's Modulus in X direction	129970	121440	125000	121000	MPa
Young's Modulus in Y direction	9208	8607	86715	8600	MPa
Poisson's Ratio XZ	0,2882	0,27048	0,8662	0,27	-
Shear Modulus XY	5133,7	4456,2	4738,6	4700	MPa
Coupling coefficient XY	-0,91327	-0,9733	-0,97417	-1	-
Diameter	2000	2000	2000	1900	Mm
Length 1 (L_1)	98,324	91,674	92,946	90	Mm
Length 2 (L_2)	64,742	62,822	65,787	60	Mm
Tensile strength in Y direction	31,898	26,947	30,409	29	MPa
Compressive strength in Z direction	-91,712	-91,343	-90,412	-100	MPa
Shear XY	65,177	59,221	56,939	60	MPa
Force	32937	31813	27508	30000	MN
Pressure	0,5	0,5	0,5	0,475	MPa
End Cap	0,84476	0,73541	0,7428	0,7854	MN
Max. Stress	0,64685	0,73806	0,77241	0,77093	-
Hashin	0,65701	0,80294	0,82071	0,8145	-
Tsai-Wu	0,71908	0,73592	0,7662	0,76324	-

7.2.2 Custom + Sampling Response surface

For the Custom + Sampling response surface type (C+S RS) the design points with the failure criteria are presented in the figures 57, 58 and 59. The x-axis contains the sample points with numbers interval from 1 to 287. Y-axis is failure criteria values. Table 18 shows the maximum and minimum values of the failure criteria.

The Figure 57 illustrates that design point 12 with the value of 1,0648 and design point 35 with the value 0,50252 are respectively the maximum and minimum values of the Max. Stress failure criterion. Design point 35 should be considered for the design as it has the lowest possible value of failure criterion which minimize the risk of failure in the model. This point has the parameters with the higher ply thickness value and less pressure magnitude value which are available in the predefined ranges. The Figure 57 shows that approximately 6 points with the low failure criterion values can be considered as safe ones for the design of the model. However, sample with the lowest failure criterion value should be used.

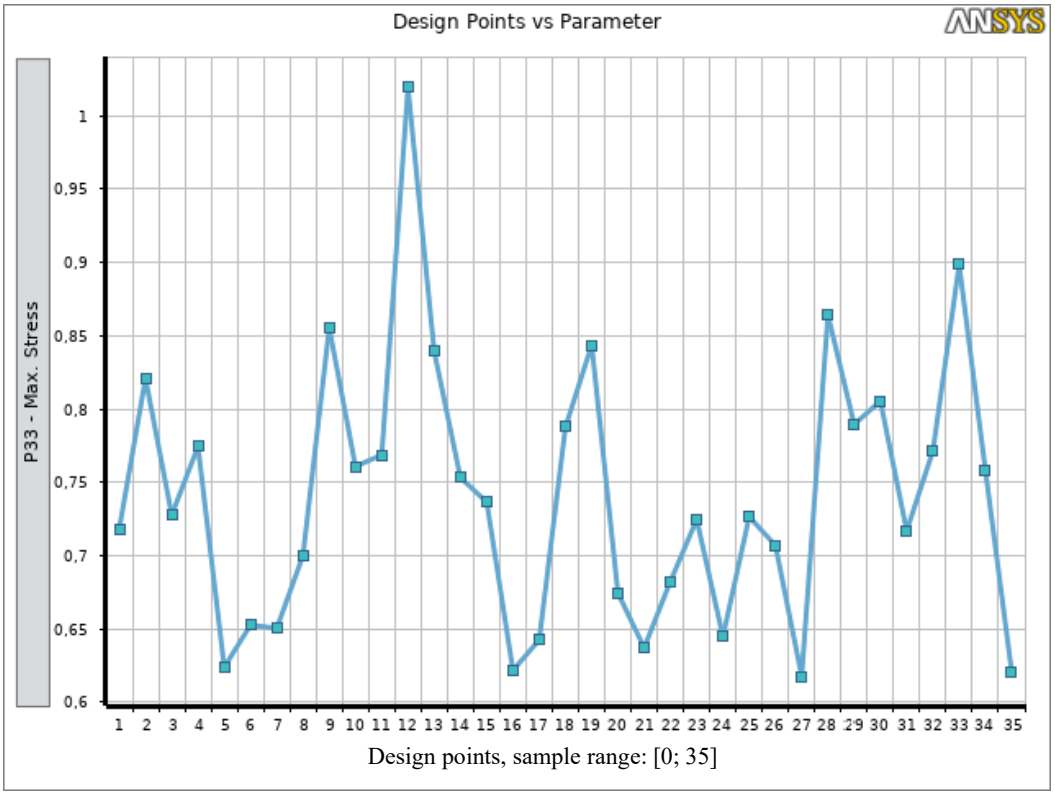

Figure 57: Design point values for the output minimum and maximum failure criteria for Custom + Sampling response surface for Max. Stress failure criterion for the samples range: [0; 35]

The Figure 58 illustrates the Hashin maximum and minimum failure criterion values. As well as for Max. Stress failure criterion, the design point 12 has the highest value of 1,1273 (maximum) and the design 35 has the lowest value of 0,4429 (minimum). This proves that point 12 has values which lead to the failure in the model. This can be improved with decreasing the pressure magnitude value and increasing of the ply thickness. However, the sample with the lowest failure criterion value should be considered for the design.

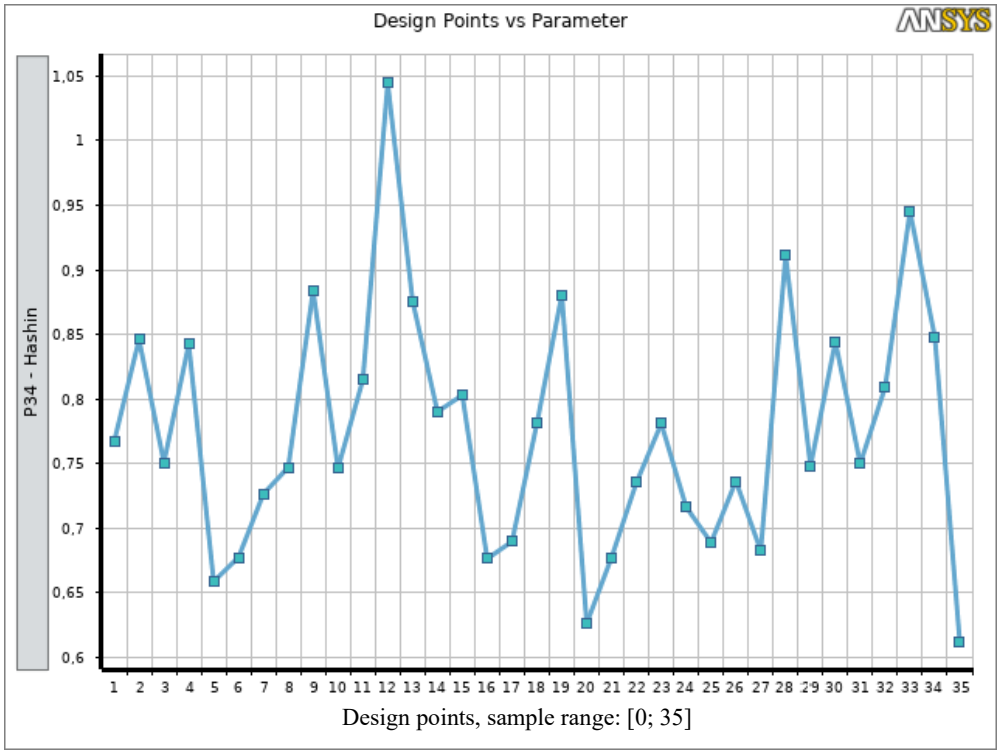

Figure 58: Design point values for the output minimum and maximum failure criteria for Custom + Sampling response surface for Hashin failure criterion for the samples range: [0; 35]

The Figure 59 shows the Tsai-Wu failure criterion values with the design points. Many of the design points have highest value of the Tsai-Wu failure criterion in the possible range. Point 35 remain the optimal one with the lowest failure criterion value of 0,51572.

As it can be seen from the Figure 59, the highest value of the failure criterion is 0,8866 and does not reach 1 as in cases with Hashin and Max. Stress failure criteria.

This means that the Tsai-Wu maximum do not reach the point of model collapse, but the value of possible failure remains high and indicates possible risk. From the Figure 59 can be seen that approximately 4 points can be considered as safe ones for the design as they have the

low failure criterion values. However, the design point 35 remains more optimal for the design.

As it was with CCD below, the response surface cell was used after DoE points were generated. This part of the response surface analysis allows us to see the behaviour of the failure criteria with the change of the pressure magnitude and ply thickness which is the same as in the response surfaces studied in the Chapter 7 of this thesis.

The minimum-maximum calculated results for the Custom + Sampling response surface are presented in the table 20.

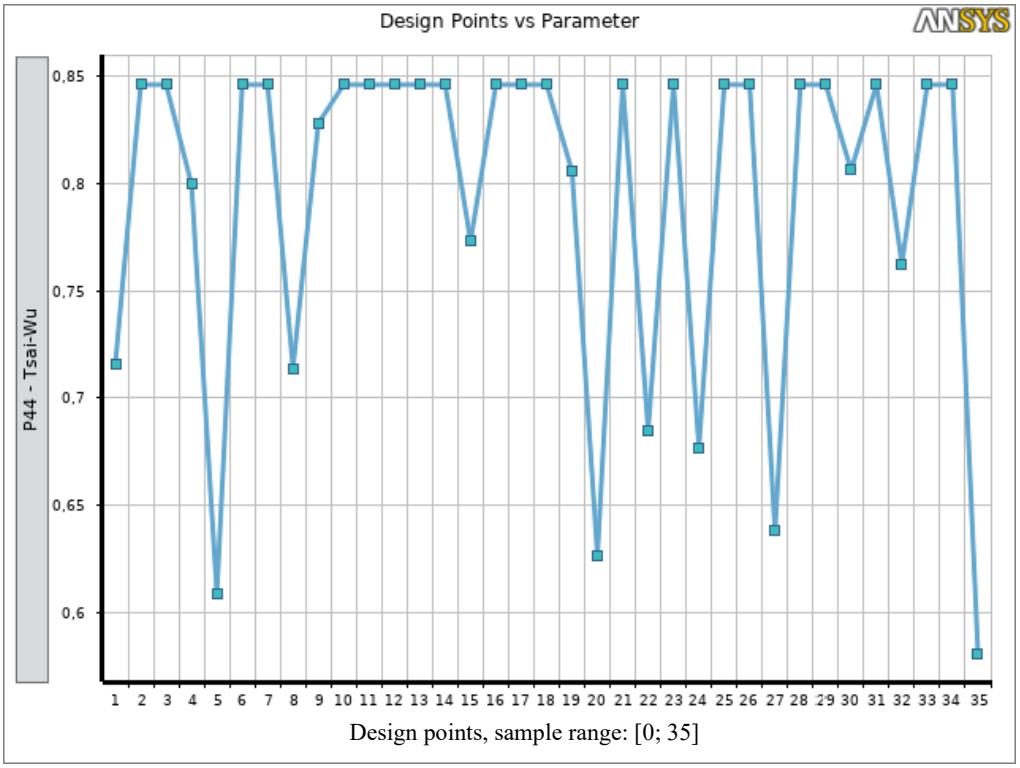

Figure 59: Design point values for the output minimum and maximum failure criteria for Custom + Sampling response surface for Tsai-Wu failure criterion for the samples range: [0; 35]

Table 20: Maximum and minimum values of the failure criteria for the Custom + Sampling response surface

Failure criterion	Calculated minimum	Calculated Maximum	Maximum predicted error, %
Max. Stress	0,50252	1,0648	0,043305
Hashin	0,4429	1,1273	0,021119
Tsai-Wu	0,51527	0,8866	0,11685

The sensitivity study for the Custom + Sampling response surface is presented with the local sensitivity charts in Figure 60.

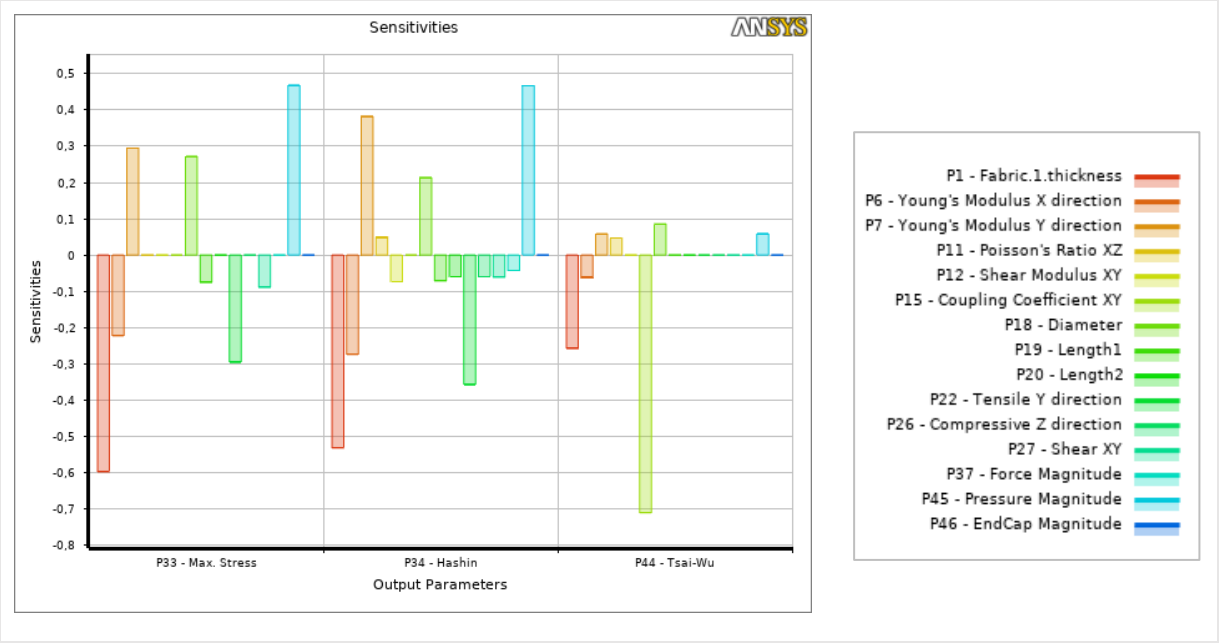

Figure 60: Sensitivity chart for the Custom + Sampling response surface

Considering the input parameters for the Custom + Sampling response surface, the local sensitivity charts for tree different failure criteria show that for the Max. Stress and Hashin failure criteria, the ply thickness, Youngs modulus in X direction are negatively correlated with the load impact. Tensile strength in Y direction bar is twice lower than the ply thickness bar for the Max. Stress and Hashin failure criterion and is inversed to the ply thickness and Elastic modulus in X direction, thus has positive correlation values. The same is shown for Length 1 of the stiffener and pressure magnitude.

For the Tsai-Wu Youngs modulus in Y direction and ply thickness parameters has smaller correlation value but also negatively correlated as Hashin and Max. Stress. The Tsai-Wu failure criterion has the largest sensitiveness to the change of coupling coefficient value in XY. Pressure magnitude is also important for Tsai-Wu failure criterion.

Custom + Sampling type of the response surface in ANSYS Workbench 2020 has the response surface optimization in order to find design point for best design. It allows to establish a range of values for the main parameters. Three parameters got the constraints: ply thickness (≤ 0,2), diameter (≤ 2000mm) and pressure magnitude (≤0,5 MPa). Considering constraints and using the method of screening (approach of sorting the results due to the defined objectives and

constraints), the response surface optimization process generated three candidate points that can be optimal for the safe design of the model. Except that, the candidate point in Custom + Sampling response surface can be considered as optimal point for the design of the model.

Main parameters and failure criterion values of the candidate points can be seen in the Table 21.

Table 21: Candidate points with the optimal values for further application in design

Response surface / Parameter	Candidate points			**Response point of C+S RS**	Unit
	1	2	3		
Ply thickness	0,18	0,18	0,18	0,18	Mm
Young's Modulus in X direction	108900	121000	114900	1,21e+11	MPa
Young's Modulus in Y direction	7740,2	8313,5	8886,8	8,6e+09	MPa
Poisson's Ratio XZ	0,24301	0,26381	0,26461	0,27	-
Shear Modulus XY	4230,1	4364,4	4498,7	4,7e+09	MPa
Coupling coefficient XY	-1,1	-1,0818	-1,0636	-1	-
Diameter (OD)	1900	1900	1900	1900	Mm
Length 1 (L_1)	81,002	82,061	83,119	90	Mm
Length 2 (L_2)	54,001	54,633	55,264	60	Mm
Tensile strength in Y direction	26,101	26,353	26,605	2,9e+07	MPa
Compressive strength in Z direction	-110	-109,31	-108,62	-1e+08	MPa
Shear XY	54,001	54,288	54,775	6e+07	MPa
Force	27001	27163	27325	30000	MN
Pressure	0,45	0,45	0,45	0,475	MPa
End Cap	0,7068	0,71053	0,71418	7,854e+05	MN
Max. Stress	0,81007	0,79589	0,82557	0,71841	-
Hashin	0,86107	0,84866	0,90455	0,76714	-
Tsai-Wu	0,85617	0,86591	0,83956	0,71608	-

8 Conclusion and Future Work

8.1 Conclusion

This thesis shows an effective way to use the design optimisation methods such as correlation and response surface to generate the optimal parameters values for the design of the curved plate with stiffeners. The parameters which can affect the model were studied in order to increase the response surface accuracy, thus, predict possible failure for each finite element of the plate model. Main steps of predicting the failure criteria values using response surface methodology is presented in the flowchart below (Figure 61).

First, the input parameters for the curved plate with stiffeners such as material properties, geometry properties (dimensions of the model) and ply stacking sequence are defined. These parameters are set up in order to create the finite element model of the plate with stiffeners which is used in the ACP process in ANSYS software, where the failure criteria can be defined, applied to the model and calculated for each individual finite element of the plate and stiffeners. The input parameters values were adjusted in order to let the failure criteria stay in a certain range with the maximum value of 0,88~0,90. As the upper boundary for the failure criteria is 1, the maximum and minimum values indicate if the failure is possible or not.

Second, with created parameter set, the correlation and determination matrices are calculated. The matrixes were calculated with the different sample size (35, 60, 90, 120 samples). Correlation matrixes with the 35 samples were considered for further calculation as well as compared to the correlation with the 120 samples. Parameters with the largest correlation coefficients, thus, stronger co-relation were selected for further Response Surface simulation. As studied in the Section 6 of the thesis, parameters with the coefficient of correlation higher than 0,2 were used for the response surface analysis.

The Figure 61 shows that with the selected parameters two types of the response surface was modelled. The 287 samples were generated in the response surface analysis.

In Chapter 7, the diameter parameter for the response surface is in range of 1900 to 2000 mm and ply thickness is in range of 0,18 to 0,20 mm. Predicted relative error in both response surfaces is below 10%.

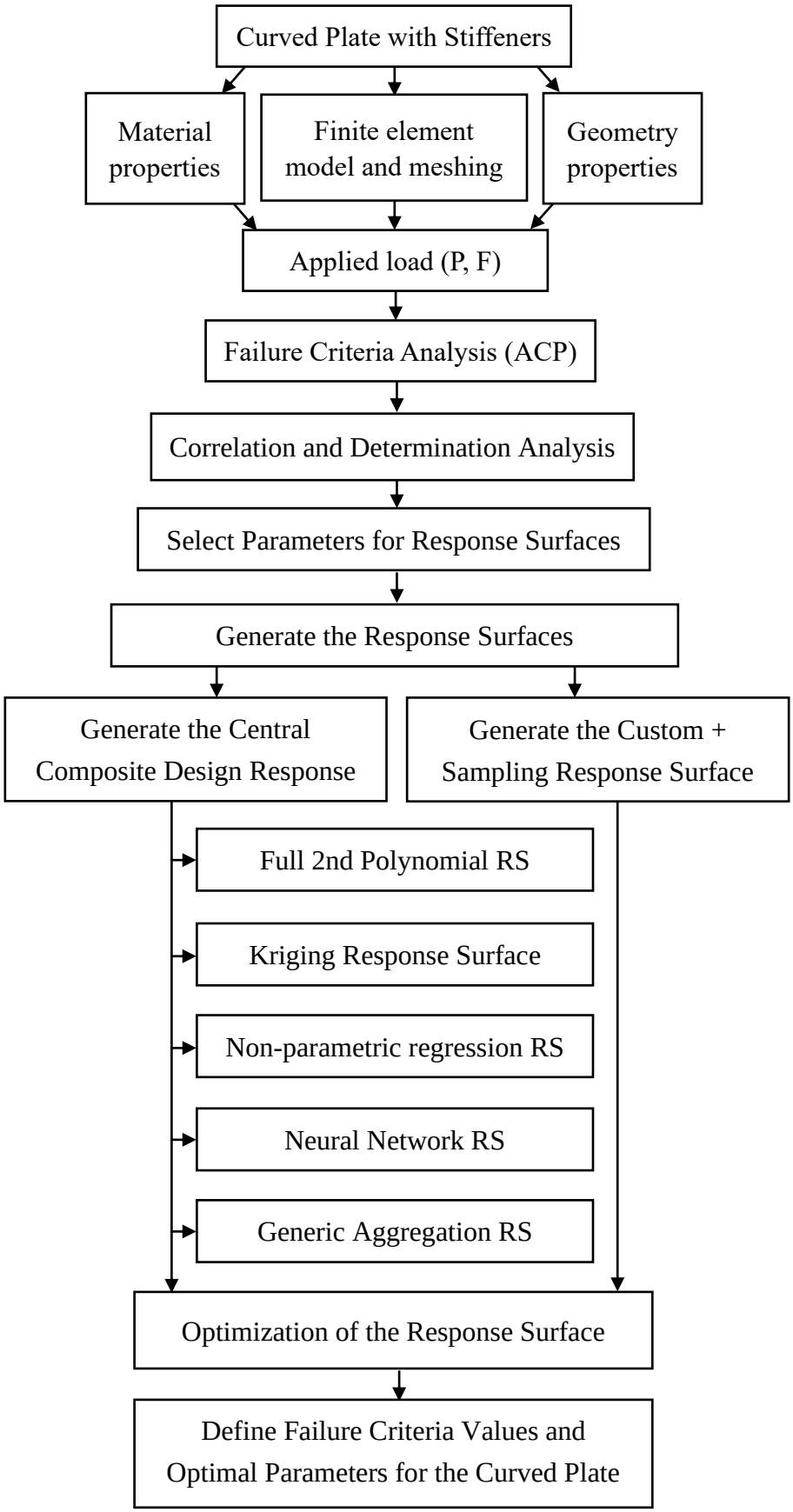

Figure 61: Main steps of predicting the failure criteria values with the response surface methodology

The Central Composite Design response surface suggest 5 different response surfaces sub-types with compared results and several candidate points with the same values which can be used as optimal design of the model, presented in the Table 16. The Custom + Sampling response surface suggest the optimization of the response surface with the applied boundary conditions. It provides the candidate point with the maximized properties of the diameter (2000 mm), ply thickness (0,2 mm) and applied pressure (0,5 MPa). The candidate points with the reliable properties for the design defined with the Custom + Sampling response surface is shown in the Table 18.

With the established pressure and thickness of the plate and stiffeners, the response surface analysis gives the most appropriate design points with the optimal parameters for the model simulation and design with the lowest probability of failure to occur. These values are presented in the Tables 18, 19 and 21 (response points column) in the Chapter 7 of this thesis.

8.2 Future Work

Response The response surface analysis is efficient in use to find the optimal design parameters for the model considering large sample size and small failure criteria values. The wider study of the changes in the model and its better optimization due to different circumstances and factors can include following topics for further work:

1. Application of the bending and torsion on the curved plate to find critical values of these loads in combination with the minimization of the weight of the model.
2. Effect of the plate and stiffeners geometry changes, number of stiffeners and distance between them, the effect of the plate curvature changes. Increasing the number of the stiffeners leads to improvement in the reliability and safety of the model. The decreasing of the distance between stiffeners decreases the pressure impact significantly. The effect of the ply thickness change in a combination with the change in the applied pressure suggests the increasing or decreasing of laminate thickness with corresponding increasing and decreasing of the pressure.
3. Consideration of the other material instead of Carbon Fibre Composite 230GPa which can be used in curved plate design.

4. Stacking sequence effect which suggests different fibre directions in the laminate which can change the strength of the material within each ply due to loads transformations.
5. Calculation of the safety factor which can be used in order to adjust the failure criteria, calculated during the response surface analysis.
6. Performing of the six-sigma analysis in ANSYS Workbench 2020 to study the parameter uncertainties influence on the model with the defined material properties and geometry (number of the stiffeners and distance between them, curvature of the plate), applied loads and boundary conditions. The parameters for six-sigma can remain same as for response surface analysis.
7. Effect of the dynamic loads. The combination of the loads applied to the model and studied in this thesis is simplified as constants. In fact, the loads which can be applied to the curved plate in real environment can be more complicated and can change with the time. In order to find the dynamic loads impact, the time interval can be established, and the failure criteria will be calculated during certain period of time. The loads will also change with the time so the actual results will be more realistic.

References

[1] B. Jia, X. Yu, Q. Yan, “A new sampling strategy for Kriging-based response surface method and its application in structural reliability”. *Advanced in Structural Engineering*, vol. 20, no. 4, pp. 564-581, 2016. [Online]. Available: doi:10.1177/1369433216658485

[2] T. Simpson, T. Mauery, J. Korte. “Comparison of response surface and Kriging models for multidisciplinary design optimization”, presented at 7th AIAA/NASA/USAF/ISSMO symposium on multidisciplinary analysis and optimization. Reston, USA, 1998.

[3] S. Gupta, C. Manohar, “An improved response surface method for the determination of failure probability and importance measures”. *Structural Safety*, vol. 26, no. 2, pp. 123-139, 2004. [Online]. Available: doi:10.1016/S0167-4730(03)00021-3

[4] A.K. Noor, W.S. Burton, “Assessment of shear deformation theories for multilayer composite plates”. *Applied Mechanics Review*, vol. 42, nr. 1, pp. 1–13, 1989. [Online]. Available: doi:10.1115/1.3152418

[5] A.K. Noor, W.S. Burton, “Assessment of computational models for multilayer composite shells”. *Applied Mechanics Review*, vol. 43, no. 4, pp. 67–97, 1990. [Online]. Available: doi:10.1115/1.3119162

[6] A.K. Noor, “Mechanics of anisotropic plates and shells—a new look at an old subject”. *Computers & Structures*, vol. 44, pp. 499–514, 1992. [Online]. Available: doi:10.1016/0045-7949(92)90383-B

[7] J.N. Reddy, C.M. Wang, “An overview of the relationships between solutions of the classical and shear deformation plate theories”, *Composites Science and Technology,* vol. 60, pp. 2327–2335, 2000. [Online]. Available: doi:10.18400/tekderg.396672

[8] J.N. Reddy, “The Classical Laminated plate theory”, in *Mechanics of laminated composite plates and shells: theory and analysis*. 2nd edition. Boca Raton, USA: CRC Press, 2003, pp. 568-578.

[9] O.A. Bauchau, J. I. Craig. “Kirchhoff plate theory” in *Structural Analysis,* New York, USA:

Springer, 2009, pp. 819-914.

[10] R.Hazimeh, G.Challita, K. Khalil, R. Othman, “Experimental investigation of the influence of substrates’ fibers orientations on the impact response of composite double-lap joints”, *Composite Structures*, vol. 134, pp. 82-89, 2015. [Online]. Available: doi: 10.1016/j.compstruct.2015.08.040

[11] L.H. Strait, M.L. Karasek, M.F. Amateau, “Effects of stacking sequence on the impact resistance of carbon fibre reinforced thermoplastic toughened epoxy laminates”, *Journal of Composite Materials*, Vol. 26, No. 12, pp.1725-1740, 1992. [Online]. Available: doi:10.1177/002199839202601202

[12] G. Hassan, M. F. Aly, I. Goda, “Finite element prediction of flexural and torsional frequencies of laminated composite beams”, Department of Industrial Engineering, Faculty of Engineering, Fayoum University, Fayoum, Egypt, p 1-17, 2012. [Online]. Available: https://paginas.fe.up.pt/~icnmmcs/abstracts/394.pdf

[13] J. R. Vinson, R. L. Sierakowski, “Strength and Failure Theories”, in *Behaviour of structures composed of composite materials*, 1st edition. Dordrecht, Netherlands: Springer, 1987, pp. 209-238.

[14] S. Li, “The Maximum Stress Failure Criterion and the Maximum Strain Failure Criterion: Their Unification and Rationalization”, *Journal of Composite Science*, vol. 4, no. 4, p. 157-161, 2000. [Online]. Available: doi: 10.3390/jcs4040157

[15] S. Li, E. Sitnikova, Y. Liang, A-S. Kaddour, “The Tsai-Wu failure criterion rationalised in the context of UD composites”, *Composites Part A: Applied Science and Manufacturing*, vol. 102, pp. 207-217, 2017. [Online]. Available: doi: 10.1016/j.compositesa.2017.08.007

[16] I.I. Gol’denblat and V. A. Kopnov, “Strength of Glass Reinforced Plastic in the Complex Stress State,” Polymer Mechanics, vol. 1, no. 2, pp. 54-59, 1966. [Online]. Available: doi:10.1007/BF00860685

[17] F.L. Chaht, M. Mokhtari, H. Benzaama, “Using a Hashin Criteria to predict the Damage of composite notched plate under traction and torsion behaviour”, *Frattura ed Integrità*

Structural, vol. 13 no. 50, pp. 331-341, 2019. [Online]. Available: doi: 10.3221/IGF-ESIS.50.28.

[18] J. Wang and W. K. Chiu, "Prediction of Matrix Failure in Fibre Reinforced Polymer Composites", *Journal of Engineering,* pp. 1-9, 2013, art. no. 973026. [Online]. Available: doi: 10.1155/2013/973026

[19] G.R. Kress, "Examination of Hashin's failure criteria for the second World-Wide Failure" Exercise. *Journal of Composite Materials*, vol. 46, no. 19-20, pp. 2539-2561, 2012. [Online]. Available: doi:10.1177/0021998312449892

[20] Z. Hashin, "Failure criteria for unidirectional fibre composites", *ASME Journal of Applied Mechanics*, vol. 47, no. 2, pp 329-334, 1980. [Online]. Available: doi:10.1115/1.3153664

[21] *DNVGL-CG-0127 - CLASS GUIDELINE*: "Finite element analysis", Norway: DNV GL AS, 2016. [Online]. Available: https://rules.dnvgl.com/docs/pdf/DNVGL/CG/2016-02/DNVGL-CG-0127.pdf

[22] J.N. Reddy, *An Introduction to the Finite Element Method*, 3rd Edition, New York, USA: McGraw-Hill Education, 2006.

[23] J. Chakrabarty, *Applied Plasticity*, 2nd Edition, New York, USA: Springer, 2010.

[24] R.L. Spilker, "Hybrid-stress eight-node elements for thin and thick multilayer laminated plates", *International Journal for Numerical Methods in Engineering*, vol.18, pp. 801-828, 1982. [Online]. Available: doi:10.1002/nme.1620180602

[25] A.K. Noor and W.S. Burton, "Assessment of shear deformation theories for multi-layered composite plates", *Applied Mechanics Reviews*, vol. 42, no. 1, pp. 1-13, 1989. [Online]. Available: doi:10.1115/1.3152418

[26] J.N. Reddy, "On refined computational models of composite laminates", International *Journal of Numerical Methods in Engineering*, vol. 27, pp. 361-382, 1989. [Online]. Available: doi: 10.1002/nme.1620270210

[27] S.V. Hoa and W. Feng "Application of A Global/Local Finite Element Model to Composite Laminates", *Science and Engineering of Composite materials*, vol. 5, no. 3-4, p 151-

168, 1996. [Online]. Available: doi: 10.1515/SECM.1996.5.3-4.151

[28] P. Schober, C. Boer, L. Schwarte, “Correlation Coefficients: Appropriate Use and Interpretation”, *Anaesthesia & Analgesia*, vol. 126, no. 5, p 1763-1768, 2018. [Online]. Available: doi: 10.1213/ANE.0000000000002864

[29] W. Pirie, “Spearman Rank Correlation Coefficient” in *Encyclopedia of Statistical Sciences*, 2nd edition. New Jersey, USA: John Wiley & Sons, Inc. 2006. [Online]. Available: doi: 10.1002/0471667196.ess2499.pub2

[30] S. Kotz, C.B. Read, N. Balakrishnan, B. Vidakovic, N.L. Johnson, *Encyclopedia of Statistical Sciences*, 2nd Edition. New Jersey, USA: John Wiley & Sons, Inc., 2006. [Online]. Available: doi: 10.1002/0471667196

[31] J.-M. Dufour, “Coefficients of determination”, Department of Economics, McGill University, Montreal, Canada, pp 1-14, 2011. [Online]. Available: https://monde.cirano.qc.ca/~dufourj/Web_Site/ResE/Dufour_1983_R2_W.pdf

[32] Z. Dabao, “A Coefficient of Determination for Generalized Linear Models”, *The American Statistician*, vol. 71, pp. 1-18, 2016. [Online]. Available: doi: 10.1080/00031305.2016.1256839

[33] G.E.P. Box and K.B. Wilson. “On the experimental attainment of optimum conditions (with discussion)”, *Journal of the Royal Statistical Society. Series B(Methodological)*, vol. 13, no. 1, pp. 1-45, 1951. [Online]. Available: doi:10.1111/j.2517-6161.1951.tb00067.x

[34] A. Khuri, S. Mukhopadhyay, “Response Surface Methodology”, *Wiley Interdisciplinary Reviews: Computational Statistics*, vol 2, no. 2 , pp. 128 – 149, 2010. [Online]. Available: doi:10.1002/wics.73

[35] J. Huh, “Reliability analysis of nonlinear structural systems using response surface method”, *KSCE Journal of Civil Engineering*, vol. 4, no. 3, pp. 135–143, 2000. [Online]. Available: doi:10.1007/BF02830867

[36] R.H. Myers, and D.C. Montgomery, *Response Surface Methodology: Product and Process Optimization Using Designed Experiments*. 2nd Edition. New York, USA: John Wiley

& Sons, 2002.

[37] D.C. Montgomery, “Guidelines for Designing Experiments” in *Design and Analysis of Experiments*, 9th Edition, New York, USA: John Wiley & Sons, 2017, pp. 17-19.

[38] J.P. Davim, “Modeling strategies: First-order model: MLR” in *Computational Methods and Production Engineering Research and Development,* 1st edition. Cambridge, UK: Woodhead Publishing, 2017, pp. 57-58.

[39] R.H. Myers, D. C. Montgomery, C. M. Anderson-Cook, *Response Surface Methodology: Process and Product Optimization Using Designed Experiments*, 4th Edition. New York, USA: John Wiley & Sons, 2016.

[40] J. Sacks, W.J. Welch, T.J. Mitchell, H.P. Wynn, “Design and analysis of computer experiments”. *Statistical Science*, vol. 4 no. 4, pp. 409-435, 1989. [Online]. Available: doi:10.1214/ss/1177012420

[41] C. Lu, Y-W. Feng, R. P. Liem, C-W. Fei, “Improved Kriging with extremum response surface method for structural dynamic reliability and sensitivity analyses”, *Aerospace Science and Technology*, vol. 76, pp 164-175, 2018. [Online]. Available: doi:10.1016/j.ast.2018.02.012.

[42] T.W. Simpson, T.M. Mauery, J.J. Korte, F. Mistree “Kriging metamodels for global approximation in simulation-based multidisciplinary design optimization”, *AIAA Journal,* vol. 39, no. 12, pp. 2233-2241, 2001. [Online]. Available: doi: 10.2514/2.1234

[43] W. Zhao, Z. Qiu, “An efficient response surface method and its application to structural reliability and reliability-based optimization”, *Finite Elements in Analysis and Design*, vol. 67, pp. 34–42, 2013.

[44] T. Hastie, R. Tibshirani, J. Friedman, “Neural Networks” in *The Elements of Statistical Learning: Data Mining, Inference and Prediction,* 2nd edition. New York, USA :Springer, 2009, pp. 389-415.

[45] S.D. Balkin, D. Lin, “A neural network approach to response surface methodology”, *Communications in Statistics - Theory and Methods Journal*, vol. 29, pp. 2215 – 2227, 2000.